Doctoral Thesis ETH No. 16914

Multifunctional Titanium Dental Implant Surface Based on Biochemically Modified Molecular Assembly Systems

A dissertation submitted to the

SWISS FEDERAL INSTITUTE OF TECHNOLOGY ZURICH

for the degree of

Doctor of Sciences

presented by

Martin Schuler

Dipl.Werkstoff-Ing. ETH

born May 18$^{\text{th}}$, 1973

citizen of Davos GR, Switzerland

accepted on the recommendation of

Prof. Dr. Marcus Textor, examiner

Prof. Dr. Donald M. Brunette, co-examiner

Prof. Dr. Viola Vogel, co-examiner

Dr. Marco Wieland, co-examiner

Dr. Samuele Tosatti, co-examiner

Zürich, November 1$^{\text{st}}$, 2006

For Karim

Abstract

The success of a titanium dental implant depends on its strong anchorage to the surrounding bone to withstand the continuous cyclic loading that occurs during mastication. Several factors, such as surgical technique, implant design, surface topography and surface (bio)chemistry are known to influence cellular processes and tissue formation at the implant-body interface during healing. In particular, surface topography and surface (bio)chemistry may exert significant effects on these processes. Thus, an improved osseointegration capacity of the implant is envisaged through topographical and/or (bio)chemical surface modification.

We modified the surface (bio)chemistry of smooth and rough (SLA; particle-blasted and acid-etched) titanium surfaces using the non-fouling polycationic co-polymer poly(L-lysine)-*graft*-poly(ethylene glycol) (PLL-*g*-PEG) known to impart protein resistance to negatively charged surfaces (e.g., titanium dioxide). Cell-interactive peptides with the RGD, KRSR and FHRRIKA motives were covalently grafted to a fraction of the PEG-chains. The functional co-polymers with and without peptide functionalities were assembled in a one-step assembly process in aqueous solution on negatively charged titanium oxide surfaces. The rationale behind this approach was to be able to study the interaction of single or multiple types of bioligands at quantitatively controlled surface densities with cells *in vitro*, without the interference produced by non-specific protein (serum) adsorption.

We investigated cell adhesion and spreading patterns of porcine epithelial cells, 3T3 fibroblasts and rat calvarial osteoblasts on RGD-modified smooth and SLA titanium surfaces. Our findings demonstrated that surface topography and (bio)chemistry directly influenced the attachment and morphology of all cell types tested after 24 hours in culture. In general, an increase in cell number and fraction of spread cells was observed on bioactive substrates (containing the cell-adhesive RGD-peptide sequence) when compared to bio-inactive surfaces, i.e., unfunctionalized PLL-*g*-PEG and RDG-functionalized (scrambled peptide) surfaces. More 3T3 fibroblasts were present on smooth than on rough topographies, whereas more rat calvarial osteoblasts attached to rough than to smooth surfaces. Porcine epithelial cell attachment did not follow any regular pattern. Footprint areas for all cell types were significantly reduced on rough compared to smooth surfaces. Rat calvarial

osteoblast attachment and footprint areas increased with increasing RGD-peptide surface density. However, no synergy between RGD-peptide surface density and surface topography was observed for either the attachment or footprint area of rat calvarial osteblasts.

The novel consensus heparin-binding peptides sequences KRSR and FHRIKKA were also immobilized via PLL-g-PEG chemistry to SLA titanium surfaces and tested for their ability to support rat calvarial osteoblast and human gingival fibroblast proliferation after 7 days in culture. Cell-binding peptide sequence RGD in combination with KRSR or FHRRIKA was used to examine a possible enhanced effect on rat calvarial osteoblast attachment and proliferation. In addition, freshly harvested bone chips from newborn rat calvariae were placed onto similar functionally modified rough titanium substrates and the size and pattern of osteoblast outgrowths were studied. Our findings demonstrated that the difference in rat calvarial osteoblast and human gingival fibroblast attachment was influenced mostly by surface topography rather than by the presence of the KRSR- and FHRRIKA-peptides. In contrast to rat calvarial osteoblast cell lines, outgrowths of osteoblasts from fragments of rat calvariae attached to pure heparin-binding peptides KRSR and FHRRIKA coated surfaces. In comparison with the control surfaces K<u>S</u>SR, <u>RFHARIK</u> and PEG, osteoblast outgrowths from rat calvarial bone chips covered a significantly larger area on RGD-, KRSR- and FHRRIKA-containing surfaces after 8 days and also migrated in an isotropic way unlike cells on the bio-inactive substrates. Furthermore, the stimulatory effect of RGD on both rat calvarial osteoblast attachment and migration pattern could be enhanced when applied in combination with KRSR.

MG63 osteoblast-like cells on PLL-g-PEG coatings showed increased ALP activity as well as increased osteocalcin, total TGF-β1 and prostaglandin E$_2$ production compared to cells on unmodified SLA titanium after 8 days in culture. However, the introduction of the KRSR-peptide at different concentrations did not show any further up (or down) regulation of these markers. Additionally, MG63 osteoblast-like cells did not show any increased attachment or synergistic effect on osteoblast markers on RGD/KRSR surfaces in comparison to PEGylated control surfaces (e.g., RGD/K<u>S</u>SR).

For designing a dental implant surface to serve patients that have an impaired bone forming or wound healing capacity, as those suffering from osteoporosis or diabetes, a surface modification using peptides only, is probably not sufficient. A surface with a therapeutic effect by additional functionalities such as growth factors might

be required to rapidly stimulate the formation of the desired tissue at the interface. Therefore, two new surface modification strategies using PLL-g-PEG chemistry were developed within this thesis: first, TG-modified (Transglutaminase substrate site) vascular endothelial growth factor (VEGF) was coupled to PLL-g-PEG coated titanium surfaces through the transglutaminase factor XIII. Coupling of VEGF to the PEG was demonstrated by SDS-page gel and Western blot analysis as well as by the optical waveguide lightmode spectroscopy (OWLS) technique. Second, model drug delivery carriers (polystyrene microspheres) were coated with PLL-g-PEG/PEG-TG and coupled to PLL-g-PEG/PEG-Lyspep (cleavable Lys-containing peptide sequence) modified titanium surfaces. Successful coupling and immobilization of drug delivery carriers was shown on patterned surfaces produced by the molecular assembly patterning by lift-off (MAPL) technique.

In conclusion, the results of this thesis demonstrate that cell attachment to titanium surfaces can be facilitated through incorporation of cell binding peptide, such as RGD onto a PLL-g-PEG system that resists non-specific protein adsorption. Moreover, other peptides, such as KRSR and FHRRIKA, can be grafted onto the PLL-g-PEG system and modify cell migration and attachment for primary rat osteoblasts. Preliminary results have also shown that growth factors or drug delivery carriers can also be attached to PLL-g-PEG, thus demonstrating that in principle it should be possible to provide cells on the titanium surface with suitable attachment factors, growth factors, and other components to enhance osseointegration.

Kurzfassung

Der Erfolg eines Zahnimplantates aus Titan ist abhängig von einer starken Veran-
kerung im umgebenden Knochengewebe, um den während des Kauvorgangs kon-
tinuierlichen zyklischen Belastungen zu widerstehen. Viele Faktoren beeinflussen
die zellulären Prozesse und die Gewebeentwicklung an der Grenzfläche zwischen
Implantat und Körper während des Einheilens: Operationstechnik, Implantatde-
sign, Oberflächentopographie und Oberflächen(bio)chemie sind die wichtigsten da-
von. Vor allem Oberflächentopographie und Oberflächen(bio)chemie haben einen
grossen Einfluss, und deshalb kann eine verbesserte Osseointegrationskapazität des
Implantats durch topographische und/oder (bio)chemische Oberflächenmodifikation
erreicht werden.

Wir modifizierten die (Bio)chemie von glatten und rauhen (SLA; partikel-gestrahlten
und säure-geätzten) Titanoberflächen mittels des "non-fouling" polykationischen
Copolymers Poly(L-Lysin)-*pfropf*-Poly(Ethylen) Glykol. Dieses Polymer adsorbiert
spontan auf negativ geladenen Oberflächen wie Titandioxid und verleiht dadurch
einen hohen Grad an Resistenz gegen unspezifische Proteinadsorption. Zellinterak-
tive Peptidesequenzen wie RGD, KRSR und FHRRIKA wurden kovalent an einen
Bruchteil der PEG-Ketten gebunden. Die funktionsfähigen Copolymere mit und oh-
ne Peptidfunktionalisierung wurden in einem Schritt in wässriger Lösung auf nega-
tiv geladenen Titandioxidoberflächen adsorbiert. Das Grundprinzip dieses Ansatzes
liegt in der Möglichkeit, die Interaktion von einzelnen oder mehreren Bioligandtypen
(mit quantitativ kontrollierter Oberflächendichte) mit Zellen *in vitro* zu studieren
und das ohne störenden Einfluss von unspezifisch adsorbierten (Serum)proteinen.

Wir untersuchten Zelladhäsion und -ausbreitungsmuster von Schweineepithelzel-
len, 3T3 Fibroblasten und Rattenkalvarialosteoblasten auf RGD-modifizierten glat-
ten und SLA Titanoberflächen. Unsere Ergebnisse demonstrierten, dass die Ober-
flächentopographie und die Oberflächen(bio)chemie das Anhaften und die Morpho-
logie aller getesteten Zelltypen nach 24 h in Kultur beeinflussten. Allgemein wurde
eine Erhöhung der Zellanzahl und mehr ausgespreizte Zellen auf bioaktiven (mit
zell-adhäsivem RGD-Peptid) im Vergleich zu bio-inaktiven (i.e., unfunktionalisierten
PLL-*g*-PEG und RDG-funktionalisierten) Oberflächen gefunden. Mehr 3T3 Fibro-
blasten waren präsent auf glatten als auf rauhen Topographien, während mehr Rat-

tenkalvarialosteoblasten auf rauhen als auf glatten Oberflächen gefunden wurden. Schweineepithelzellen zeigten kein reguläres Muster. Die Fläche der Fussabdrücke aller Zelltypen war auf rauhen Oberflächen signifikant kleiner als auf glatten Oberflächen. Die Zellanzahl und die Fläche der Fussabdrücke von Rattenkalvarialosteoblasten nahm mit steigender RGD-Peptidoberflächendichte zu. Jedoch wurde keine Synergie zwischen RGD-Peptidoberflächendichte und Oberflächentopographie beobachtet, weder für die Zellanhaftung noch für die Grösse der Fussabdrücke von Rattenkalvarialosteoblasten.

Die neuartigen, mutmasslichen heparin-bindenden Peptidsekuenzen KRSR und FHRRIKA wurden auch mittels PLL-g-PEG-Chemie auf SLA Titanoberflächen immobilisiert. Die Proliferation von Rattenkalvarialosteoblasten und menschlichen Zahnfleischfibroblasten nach 7 Tagen in Kultur wurde getestet. Die zell-bindende RGD-Peptidsequenz wurde in Kombination mit KRSR und FHRRIKA benützt, um einen möglichen synergetischen Effekt auf Rattenkalvarialosteoblastproliferation zu untersuchen. Zusätzlich wurden frisch geerntete Knochenchips aus Kalvarialknochen von neugeborenen Ratten auf gleich modifizierte rauhe Titanoberflächen gelegt und die Grösse und das Muster der ausgewachsenen Osteoblasten studiert. Unsere Resultate demonstrierten, dass der Unterschied im Anhaften von Rattenkalvarialosteoblasten und menschlichen Zahnfleischfibroblasten stärker durch die Oberflächenrauhigkeit als durch die Präsenz von KRSR- und FHRRIKA-Peptiden beinflusst wurde.

Im Gegensatz zu Osteoblasten aus Zelllinien hafteten Osteoblasten, welche aus Kalvarialknochenfragmenten auswuchsen, auf reinen mit heparin-bindenden KRSR- und FHRRIKA-Peptiden beschichteten Oberflächen. Im Vergleich zu den mit KSSR, RFHARIK und PEG beschichteten Kontrolloberflächen bedeckten Osteoblastauswüchse von Rattenkalvarialknochen auf RGD-, KRSR- und FHRRIKA-Oberflächen eine signifikant grössere Fläche nach 8 Tagen und migrierten isotropisch im Gegensatz zu Zellen auf bio-inaktiven Substraten. Ausserdem konnte der stimulierende Effekt von RGD in Kombination mit KRSR erhöht werden, was durch erhöhte Rattenkalvarialosteoblastanhaftung und ausgedehntere Migrationsmuster demonstriert wurde.

MG63 osteoblast-ähnliche Zellen zeigten erhöhte ALP-Aktivität als auch erhöhte Osteokalzin-, totale TGF-β1- und Prostaglandin E$_2$-werte auf PLL-g-PEG-Beschichtungen im Vergleich mit Zellen auf unmodifizierten SLA Titanoberflächen nach 8 Tagen in Kultur. Allerdings konnte keine Auf- oder Abregulierung dieser

Zellmarker durch die Immobilisation von KRSR-Peptiden in verschiedenen Konzentrationen festgestellt werden. Auch wurde durch die Präsentation von gemischten RGD/KRSR-Oberflächen im Vergleich zu PEGylierten Kontrolloberflächen (e.g., RGD/KSSR) weder eine erhöhte Zellanhaftung von MG63 Zellen, noch ein etwaiger synergetischer Effekt auf Osteoblastmarker gefunden.

Für das Design einer neuartigen Zahnimplantatoberfläche, um Patienten mit beeinträchtiger Knochenausprägung oder Wundheilungskapazität zu bedienen, ist eine Oberflächenmodifikation durch Peptide möglicherweise nicht ausreichend. Eine Oberfläche mit einem therapeutischen Effekt, der durch zusätzliche Funktionalisierung wie beispielsweise Wachstumsfaktoren erreicht werden könnte, dürfte notwendig sein, um eine rasche Ausbildung des gewünschten Gewebes an der Grenzfläche zu gewährleisten. Daher wurden zwei neue Oberflächenmodifikationsstrategien durch PLL-g-PEG-Chemie innerhalb dieser Arbeit entwickelt: erstens wurde TG-modifizierter (Transglutaminase) vaskulärer Endothelialwachstumsfaktor (VEGF) an PLL-g-PEG beschichtete Titanoberflächen durch den Transglutaminasefaktor XIII gebunden. Die Kopplung von VEGF zu PEG wurde durch SDS-page Gel und Western Blot Analyse sowie durch Optical Waveguide Lightmode Spectroscopy (OWLS) Technik demonstriert. Zweitens, wurden Testträger für Medikamenttransport (engl.: drug delivery carrier) mit PLL-g-PEG/PEG-TG beschichtet und an PLL-g-PEG/PEG-Lyspeptid (spaltbare Lysin-enthaltende Peptidsequenz) modifizierte Titanoberflächen gekoppelt. Eine erfolgreiche Kopplung und die Immobilisierung von den drug delivery carriern wurde mittels gerasterten Oberflächen, welche durch die Molecular Assembly Patterning by Lift-off Technik (MAPL) produziert wurden, gezeigt.

Zusammengefasst demonstrierten die Resultate dieser Arbeit, dass durch zellbindende RGD-Peptide mittels PLL-g-PEG-Chemie eine Zellanhaftung an Titanoberflächen vereinfacht werden kann und zugleich die Oberfläche resistant gegen unspezifische Proteinadsorption ist. Ausserdem können auch andere Peptidsequenzen wie KRSR und FHRRIKA an PLL-g-PEG-Polymere gebunden werden und dadurch Zellmigration und Zellanhaftung für primäre Rattenosteoblasten modifiziert werden. Vorläufige Resultate haben ausserdem gezeigt, dass Wachstumsfaktoren oder drug delivery carrier auch an PLL-g-PEG gekoppelt werden können und es dadurch prinzipiell möglich sein wird, geeignete Faktoren, Wachstumsfaktoren und andere Komponenten auf einer Titanoberfläche den Zellen anzubieten, und damit die Osseointegration zu verbessern.

Acknowledgements

Along my thesis I met many interesting people and I would like to express them my sincerest thanks.

First of all, I am very grateful to Prof. Dr. Marcus Textor for giving me confidence and valuable guidance throughout my thesis, as well as freedom and self-determination; and for let me travel around the globe making my thesis a very interesting and productive experience.

I do thank Prof. Dr. Nicholas D. Spencer for providing me the opportunity to perform my thesis in the LSST research group and for his always interesting and concise comments during group meetings.

A great thanks to Dr. Samuele Tosatti, my direct supervisor, who always supported me in any kind of situation, his valuable help and many, many ideas in how to improve my experiments and thesis. I also thank him for letting me go my own way and still bringing me back to the more or less straight path of my work.

Many thanks to Dr. Diana Trentin for introducing me to the world of drug delivery systems and improving my knowledge in general aspects of cell biology. I would also like to thank her four numerous scientific and non-scientific discussions and for very valuable help in proof-reading my papers and thesis.

Many thanks to Prof. Dr. Janos Vörös for always having time even on short notice for numerous scientific discussions with very valuable suggestions and comments.

Dr. Stefan Zürcher, Dr. Salvatore Chessari and Dr. Firat Durmaz are thanked for many fruitful discussions concerning the synthesis of PLL-g-PEG and for giving me chemical tips, tricks and support in the laboratory.

A great thanks to Esther Stähli for always taking care about administrative issues, for providing help in dealing with the ETH bureaucracy and for numerous

discussions. Many thanks also to Brigitta de Chapeaurouge and Josephine Baer for administrative help. Tomas Bartos is thanked for dealing with IT-questions and for always providing support when dealing with PC-companies and warranty-issues. I would like to thank also Martin Elsener for producing PTFE-templates for the replica technique and Jaroslav Vanicek for dealing with electronics.

All the LSST members are thanked for sharing an interesting and collaborative time together. In particular, Dr. Martin Halter is thanked for numerous support in IT-related questions, for many discussions about how to deal with a PhD and also for discussions outside science. A great thanks goes to Dr. Tobias Künzler for developing together highly innovative experiments, for countless discussions about cells on surfaces and for performing sports over lunch-time. Dr. Marc Dusseiller is thanked for cell biology related discussions and critical thinking about science, Dr. Christoph Huwiler for discussing all kind of sport-related topics, Dr. Laurent Feuz for discussing icehockey-issues, Dr. Stéphanie Pasche for help in PLL-g-PEG synthesis, Brigitte Städler and Dr. Guoliang Zhen for OWLS trouble-shooting, Vincent Zoulalian for teaching French, Thomas Blättler for providing MAPL substrates, Martina Baumann for working together with KRSR, Orane Guillaume-Gentil for working together with cells, Lydia Feller for cultural discussions, Katrin Barth and Barbora Malisova for cutting Si-wafers, Doris Spori for collaborating with epoxy replicas, Mirjam Ochsner for spin-coating, Mathias Rodenstein for proof-reading the German abstract, Fabian Anderegg for dealing with pipetts, Dr. Fabiano Assi for IT-help in Schlieren and having fun in Australia, Dr. Andrea König, Dr. Jost Lussi and Dr. Didier Falconnet for discussions about cells and surfaces, Dr. Michelle Grandin for Canadian discussions, Dr. Géraldine Coullerez for organizing the lab, Dr. Rupert Konradi for ELM-issues and Dr. Erik Reimhult for giving tips about how to deal with a newborn.

I would like to thank also my students Peter Worbs, David Klang, Daniel Vonwil, Petros Kokkinos and Anita Bardill for their excellent work and collaboration. A big thanks goes to all my Hilfsassistenten Victoria Maurer, Matthias Wirz and Rafael Gentsch that performed many valuable jobs and experiments during my thesis.

Many thanks to Christian Brunner for excellent support in all mac-related matters and support in the clean room.

about North America and Vancouver, and for always giving me support during my thesis. I also thank him for taking over the job as co-examiner. Dr. Michael de Wild is thanked for excellent support from Straumann-side, for providing SLA titanium samples and other materials in a very efficient and unbureaucratic way and for numerous interesting and fruitful discussions beyond science and newborn-related issues. I would like also to thank Heiner Bieli for helping to feel home in the lab in Basel, Dr. Aart Molenberg for NMR-expertise and Adrian Zumbach for great support in writing the patent application.

Many thanks to all the people I met from the AO Research Institute, in particular to Christoph Sprecher for countless discussions about science and beyond in the lab, on the phone or while skiing. I would also like to thank him for his ability to put everything into another perspective and look at it in a pragmatic and critical way to find creative solutions. Dr. Geoff Richards is thanked for providing access to his scanning electron microscopy unit and valuable discussions and Dr. Stefan Milz for scientific discussions and for providing access to the fluorescence microscopes. Dr. Llinos Harris and Raj Maddikkeri are thanked for excellent collaboration within the bacteria studies.

Prof. Dr. Barbara B. Boyan, Prof. Dr. Zvika Schwartz and Brian Bell from Georgia Tech University in Atlanta are thanked for working together within the CTI/ITI project.

Prof. Dr. Daniel Buser and Dr. Nina Broggini from University of Berne are thanked for great collaboration regarding the animal studies.

Prof. Dr. Viola Vogel is thanked for her commitment as a co-examiner.

I would like to thank all my friends I met during all the years at ETH, in particular Chrigeli, Trara, Π, Mäxxxu and Tobiforever for having a great time together while learning and enjoying student life.

A great thanks goes also to Dr. Michael Portmann for his countless fruitful discussions about science and beyond, for providing mental support and for spending a great time together with our families, Karin, Silvana, Florian, Ursina, Karim and

Ethan.

Finally, I would like to thank my parents and my two sisters for their constant love, support and care from childhood until now. And last but not least my greatest and deepest thanks goes to my own little family, to Karim and Ethan (also known as Nemo), for making my life a very happy, funny, interesting and challenging one, for your endless love, care and patience as well as guidance in statistics, lots of understanding during my thesis writing and proof-reading of my thesis! Thank you so much!!

Contents

1

Scope of my Thesis Work

1.1 Background and Motivation

The work and objectives of my thesis were motivated by the important need for
new titanium dental implant surfaces that have the potential of improving the de-
vice performance, further reducing the time between implantation and restoration
of the patient's dentition and providing a safer treatment for patients suffering from
today's critical contraindications such as diabetes and osteoporosis.

The surface properties of a titanium dental implant are known to have a strong influ-
ence on the mechanism and the time required for osseointegration [1]. In particular,
surface topography and surface (bio)chemistry may significantly affect this process.
Thus, an improved osseointegration capacity of the implant is envisaged through
topographical and/or (bio)chemical surface modification. The fabrication of struc-
tured titanium surfaces used in bone-contact applications with defined macro, micro-
and nano-topographies has resulted in the past in reduced healing time and faster
integration in the host tissue. Although most of the development of novel structured
titanium surfaces occurred in the past (i.e., 70ies and 80ies of the last century), only
few new techniques have been developed since. Among the new surfaces produced
in the past 15 years, the so-called SLA dental implant surface [2] (particle-blasted
and acid-etched fabricated by Institut Straumann AG, Switzerland; Figure 1.1) has
been a particularly successful development because it demonstrated enhanced bone
apposition [3], based on histomorphometric evaluation in animal studies and higher
removal torque values in biomechanical testing [4].

On the other hand, a new trend in surface engineering has been the use of biologi-
cally inspired surfaces with the potential to induce cell-selective responses, increase
resistance against bacteria attachment, reduce the risk of inflammation and improve
the long-term performance of the implant. Since amount and type of biomolecules,
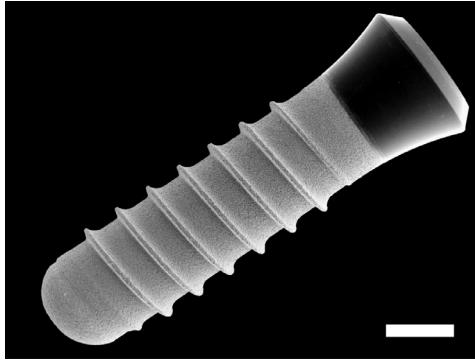
Figure 1.1: Scanning electron micrograph of a titanium dental implant with SLA (particle-blasted and acid-etched) surface topography (courtesy of Institut Straumann AG, Basel, CH). Scale bar corresponds to 2000 μm.

in particular proteins, adsorbed upon exposure to blood and other body fluids are considered as a non-specific response of the body to the artificial implant material [5], an approach for bio-active surfaces can also be motivated by the desire of eliminating or substantially reducing non-specific protein adsorption and thus reducing adverse, undesirable host responses. Adding bioligands to non-fouling surfaces is a common approach to achieve a more specific interaction with different cells and tissues. One way to create such a non-fouling surface [6] is by means of the monomolecular poly(L-lysine)-*graft*-poly(ethylene glycol) (PLL-*g*-PEG) assembly system (Figure 1.2) [7–9].

The poly(L-lysine) backbone of this graft-polymer spontaneously adsorbs onto negatively charged metal oxide surfaces, as titanium dioxide, and the poly(ethylene glycol) chains are exposed to the fluid as a brush resulting in adsorbed protein masses as low as 5 ng/cm^2 [9, 10]. Furthermore, biomolecules (e.g., peptides) can be covalently linked to a fraction of the PEG-chains [11], allowing an interaction with cells and tissues (Figure 1.3).

A frequently used peptide sequence is RGD (arginine-glycine-aspartic acid) [12] that is recognized by nearly half of the over 20 known α/β integrins [13], a family of receptors present in most cell types. Another group of cell-interacting moieties are heparin-binding peptides such as KRSR (lysine-arginine-serine-lysine)[14] and FHRRIKA (phenylalanine-histidine-arginine-arginine-isoleucine-lysine-alanine) [15]. Both sequences are present in the ECM of osteoblasts and, therefore, are of potential interest for bone-related applications.
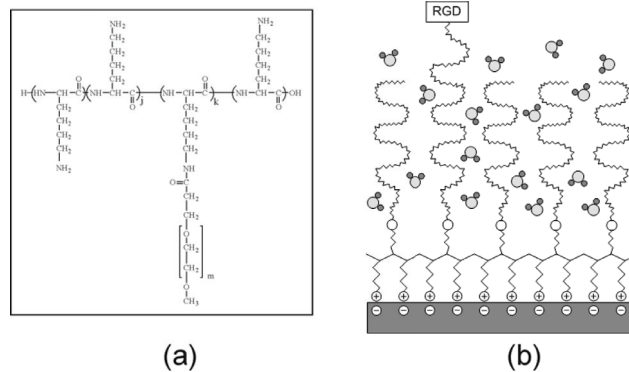
Figure 1.2: (a) Molecular structure of poly(L-lysine) (PLL) grafted with poly(ethylene glycol) (PEG) and (b) model view of a titanium oxide surface covered by PLL-g-PEG for rendering surfaces specifically interactive with the biological environment. Biological molecules (e.g, RGD-peptide or growth factors) can be coupled to a fraction of the PEG-chains, allowing an optimum interaction with cells and tissues.

Epithelium:
Formation of a firm seal to prevent bacterial penetration into underlying tissue. Elimination and/or reduction of epithelial downgrowth.

Connective tissue:
Preferably a biomimetic ligament-like attachment or alternatively a non-adherent but tightly adapting tissue-titanium interface.

Bone:
Tight contact to prevent relative motion between implant and adjacent tissue, rapid initial bone-formation to permit early loading, and permissive conditions for bone remodeling to obtain long-term stability.

Figure 1.3: Scheme of a dental implant illustrating the local interfacing to host tissues and the corresponding material-tissue interface requirement for successful performance and long-term stability (adapted from Scacchi *et al.* [16]).

1.2   Objectives

The main goals of my PhD thesis were:

1. Synthesis and characterization of PLL-g-PEG polymers that are modified with either integrin-binding peptide containing the arginine-glycine-aspartic acid (RGD) motive or heparin-binding peptides with the lysine-arginine-serine-lysine (KRSR) and phenylalanine-histidine-arginine-arginine-isoleucine-lysine-alanine (FHRRIKA) sequences, as well as scrambled (inactive) peptides as controls.

2. Testing and screening of bio-functionalized smooth and particle-blasted and acid-etched (SLA) titanium surfaces *in vitro* using cell types selected on the basis of tissues that contact dental implants: epithelium (epithelial cells), connective tissue (fibroblasts) and bone (osteoblasts).

3. Testing and screening non-fouling multi-peptide modified SLA titanium surfaces containing mixed KRSR/RGD and FHRRIKA/RGD peptides with quantitatively controlled peptide densities and their response towards osteoblast proliferation and differentiation.

4. Development of strategies for the immobilization of growth factors and/or drug delivery systems using PLL-g-PEG chemistry to design new types of implant surfaces (Figure 1.4).

The idea of combining surface topography/roughness (smooth vs. (SLA) surfaces) and surface (bio)chemistry was a basic aspect of this thesis. The hypothesis was that different local requirements of a dental implant exist and, therefore, different interface functionalities are needed for an optimum interfacial tissue development and clinical performance (Figure 1.3).
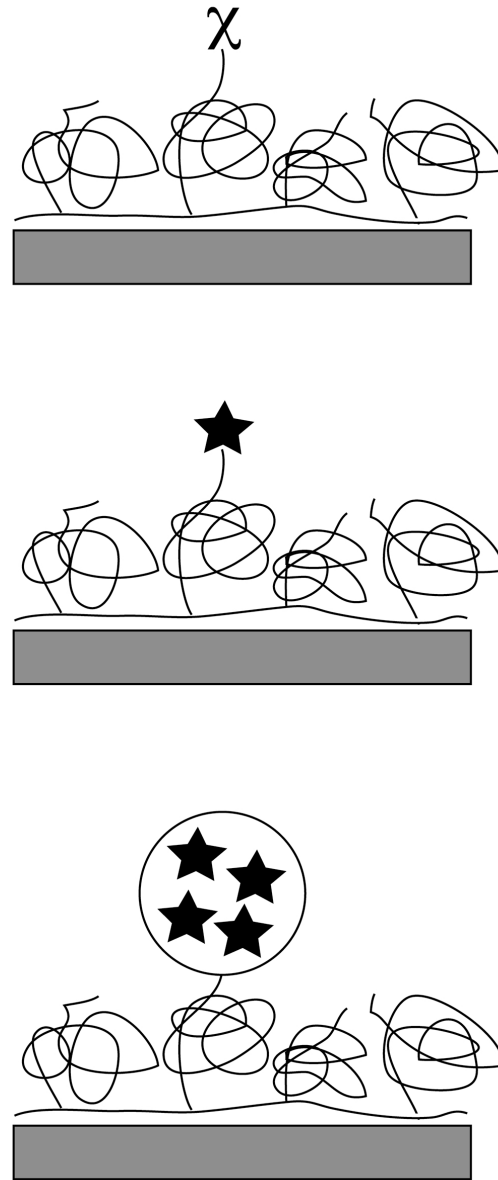
Figure 1.4: Cartoon of (bio)chemical titanium surface modification strategies developed within this thesis, top-down: Direct binding of small peptide sequences (χ) to PLL-g-PEG; linking of growth factors ("star") to PLL-g-PEG; drug delivery systems loaded with biological factors ("stars") and linked to the surface via standard PLL-g-PEG chemistry.

1.3   Overview of my Thesis

Chapter 2 provides a general review about surface modification of titanium implants and cell carriers. This review focuses on recent selected techniques and strategies to modify the (bio)chemistry of titanium surfaces through ultra-thin organic adlayers and/or biological molecules; the discussion is structured into four sections: (i) surfaces with controlled physicochemical properties, (ii) surfaces with immobilized biological molecules, (iii) surfaces with non-fouling character, and (iv) surfaces with drug-eluting abilities. Furthermore, some *in vivo* and stability considerations are also presented.

Chapter 3 provides information about PLL-*g*-PEG including synthesis, assembly and stability aspects. A brief summary about cell cultures and protocols and a general overview about the principle of all methods used in this thesis are also given in this chapter. Additionally, more detailed information about instrumentations used in each chapter can be found in the corresponding "Materials and Methods" sections.

Fabrication of substrates with identical surface topographies and chemistries using an epoxy replica technique is described in **Chapter 4**. Reproducibility of the technique, the production of samples with two different topographies (smooth and SLA) on the same specimen and their use in rat calvarial osteoblasts assays are also discussed.

Chapter 5 describes the response of rat calvarial osteoblasts, 3T3 fibroblasts and porcine epithelial cells to RGD-peptide modified smooth and SLA titanium surfaces using the PLL-*g*-PEG system. Cell number, cell footprint area and cell shape factor are extensively discussed as a function of surface topography and/or surface (bio)chemistry.

In **Chapter 6** a comparison between the response of cultured rat calvarial osteoblasts and osteoblasts outgrown from rat calvarial bone chips to KRSR- and FHRRIKA-peptide modified SLA titanium surfaces using PLL-*g*-PEG is presented. Human gingival fibroblasts served as controls cell type for the cultured osteoblasts.

Chapter 7 provides preliminary data of MG63 osteoblast-like cell differentiation assays on KRSR- and RGD-peptide modified SLA titanium surfaces using PLL-*g*-PEG chemistry.

A summary of my thesis and an outlook as well as future perspectives can be found in **Chapter 8**.

Bibliography

[1] Albrektsson, T., Branemark, P. I., Hansson, H. A. and Lindstrom, J. Osseointegrated Titanium Implants - Requirements for Ensuring a Long-Lasting, Direct Bone-to-Implant Anchorage in Man. *Acta Orthopaedica Scandinavica*, **52**(2), 155–170, 1981.

[2] Steinemann, S. G. and Claes, L. Metallic implant anchorable to bone tissue for replacing a broken diseased bone, 1992.

[3] Buser, D., Schenk, R. K., Steinemann, S., Fiorellini, J. P., Fox, C. H. and Stich, H. Influence of Surface Characteristics on Bone Integration of Titanium Implants - a Histomorphometric Study in Miniature Pigs. *Journal of Biomedical Materials Research*, **25**(7), 889–902, 1991.

[4] Buser, D., Nydegger, T., Oxland, T., Cochran, D. L., Schenk, R. K., Hirt, H. P., Snetivy, D. and Nolte, L. P. Interface shear strength of titanium implants with a sandblasted and acid-etched surface: A biomechanical study in the maxilla of miniature pigs. *Journal of Biomedical Materials Research*, **45**(2), 75–83, 1999.

[5] Ratner, B. D. A Perspective on Titanium Biocompatibility. In Brunette, D. M., Tengvall, P., Textor, M. and Thomsen, P., editors, *Titanium in Medicine*, pages 1–12. Springer-Verlag, Berlin Heidelberg, 2001.

[6] Morra, M. On the molecular basis of fouling resistance. *Journal of Biomaterials Science-Polymer Edition*, **11**(6), 547–569, 2000.

[7] Kenausis, G. L., Voros, J., Elbert, D. L., Huang, N. P., Hofer, R., Ruiz-Taylor, L., Textor, M., Hubbell, J. A. and Spencer, N. D. Poly(L-lysine)-g-poly(ethylene glycol) layers on metal oxide surfaces: Attachment mechanism and effects of polymer architecture on resistance to protein adsorption. *Journal of Physical Chemistry B*, **104**(14), 3298–3309, 2000.

[8] Huang, N. P., Michel, R., Voros, J., Textor, M., Hofer, R., Rossi, A., Elbert, D. L., Hubbell, J. A. and Spencer, N. D. Poly(L-lysine)-g-poly(ethylene glycol) layers on metal oxide surfaces: Surface-analytical characterization and resistance to serum and fibrinogen adsorption. *Langmuir*, **17**(2), 489–498, 2001.

[9] Tosatti, S., De Paul, S. M., Askendal, A., VandeVondele, S., Hubbell, J. A., Tengvall, P. and Textor, M. Peptide functionalized poly(L-lysine)-g-poly(ethylene glycol) on titanium: resistance to protein adsorption in full heparinized human blood plasma. *Biomaterials*, **24**(27), 4949–4958, 2003.

[10] Pasche, S., De Paul, S. M., Voros, J., Spencer, N. D. and Textor, M. Poly(L-lysine)-graft-poly(ethylene glycol) assembled monolayers on niobium oxide surfaces: A quantitative study of the influence of polymer interfacial architecture on resistance to protein adsorption by ToF-SIMS and in situ OWLS. *Langmuir*, **19**(22), 9216–9225, 2003.

[11] VandeVondele, S., Voros, J. and Hubbell, J. A. RGD-Grafted poly-l-lysine-graft-(polyethylene glycol) copolymers block non-specific protein adsorption while promoting cell adhesion. *Biotechnology and Bioengineering*, **82**(7), 784–790, 2003.

[12] Pierschbacher, M. D. and Ruoslahti, E. Cell Attachment Activity of Fibronectin Can Be Duplicated by Small Synthetic Fragments of the Molecule. *Nature*, **309**(5963), 30–33, 1984.

[13] Ruoslahti, E. RGD and other recognition sequences for integrins. *Annual Review of Cell and Developmental Biology*, **12**, 697–715, 1996.

[14] Dee, K. C., Andersen, T. T. and Bizios, R. Design and function of novel osteoblast-adhesive peptides for chemical modification of biomaterials. *Journal of Biomedical Materials Research*, **40**(3), 371–377, 1998.

[15] Rezania, A. and Healy, K. E. Biomimetic peptide surfaces that regulate adhesion, spreading, cytoskeletal organization, and mineralization of the matrix deposited by osteoblast-like cells. *Biotechnology Progress*, **15**(1), 19–32, 1999.

[16] Scacchi, M. The development of the ITI (R) DENTAL IMPLANT SYSTEM - Part 1: A review of the literature. *Clinical Oral Implants Research*, **11**, 8–21, 2000.

2

Biomedical Interfaces: Titanium Surface Technology for Implants and Cell Carriers

Martin Schuler, Diana Trentin, Marcus Textor, Samuele G.P. Tosatti

Titanium and its alloys have become key materials for biomedical applications mainly owing to their compatibility with human tissues and their mechanical strength. Effects of surface topography on cell and tissue response have been investigated extensively in the past, while (bio)chemical surface modification and its combination with designed topographies have remained largely unexplored. The following report describes some of the strategies used or intended to modify titanium surfaces, based on biological principles, with a focus on ultra-thin biomimetic adlayers. One of the visions behind such approaches is to achieve improved healing and integration responses after implantation for patients, especially for those suffering from deficiencies, for example, diabetes or osteoporosis, two diseases that have increased drastically in our society during the last century.

Keywords: bioligand, biomimetic, drug delivery, implant, non-fouling, peptide, polyethylene glycol, surface (bio)chemistry, surface modification, surface topography, titanium.

2.1   Introduction

Titanium and its alloys are key materials for biomedical applications [1, 2]. Commercially pure titanium, for example, is used widely in dental implants and titanium alloys, such as Ti-6Al-4V and Ti-6Al-7Nb, have been used in various orthopedic and osteosynthesis systems, as parts of hip and knee implants, bone screws or plates. Titanium is also one of the preferred materials within cardiovascular devices, such as pacemaker cases, peripheral stents and heart valves.

But what makes titanium so unique? Titanium has favorable mechanical strength, low specific weight, excellent corrosion resistance and biocompatibility [3], does not cause allergic reactions [4] and also develops good interfacial strength with bone [5]. Furthermore, titanium oxide has a high refractive index that is useful in biosensor applications that are based on optical detection methods [6].

Important efforts have been made in the past to optimize the surface topography of titanium implants in bone-contact applications [7] focusing mainly on designed surface structuring to reduce healing times and accelerate integration into the host tissue. The most prominent fabrication methods used previously to produce defined macro, micro- and nanotopographies [8, 9] included micromachining, plasma spraying, particle blasting and acid etching [10–15]. More recent techniques include electrochemical micromachining of titanium through a laser patterned oxide film [16, 17] and processing of titanium foams through powder-metallurgy [18]. Meanwhile, microfabrication [8] and replica techniques [14, 19–21] have led to the development of designed model surfaces and cell carrier systems for laboratory use. As discussed by Ratner in 2001, the next evolution in titanium implants is likely to be through biologically inspired specific surface modifications [22]. This trend to modify surfaces with (bio)chemical moieties is also supported through increased research in other related areas, such as biosensors and diagnostics. The various approaches in this field aim to obtain a more controlled interaction between implant and tissue and can be further motivated by a number of specific objectives:

(i) Triggering cell-selective response, for example, supporting osteogenic cell adhesion and rapid differentiation towards osteoblast phenotype;

(ii) Resistance to bacterial attachment with the aim of reducing infection rate and the need of antibiotics prescription;

(iii) Reduction of the risk of inflammation;

(iv) Improvement of reliability and long-term performance of the device.

These aspects, among others, are particularly (but not only) relevant for patients with deficiencies such as diabetes or osteoporosis, which can influence the biological response upon implantation [23]. Therefore, new surfaces may be the only successful strategy for implantation in these cases. The number of people suffering from diabetes, for example, is expected to increase more than 2.5-times, from 84 million in 1995 to 228 million in 2025, whereas 1.66 million hip fractures owing to osteoporosis occur each year worldwide, with an expected fourfold increase by 2050, as reported by the World Health Organization (WHO) [24]. Modification of surface (bio)chemistry of implants (e.g., in bone-contact applications) can be achieved through, for example:

(i) Biological species (e.g., proteins or peptides);

(ii) Organic, ultra-thin (nanometer-range), monomolecular adlayers onto which drugs or other biomolecules are linked;

(iii) Hydroxyapatite/calcium phosphate coating (micrometer-range), where drugs or other biomolecules are entrapped;

(iv) Hydrogels (nanometer-/millimeter-range) with incorporated drugs or biomolecules.

The scope of this review does not allow us to cover all aspects of this field, therefore, we will focus only on some selected techniques and strategies that can be used to modify the surface (bio)chemistry of titanium surfaces through ultra-thin organic adlayers and/or biological molecules [25]. The advantage of an ultra-thin coating is the capability of tailoring surface (bio)chemistry independently from surface topography since the coating thickness is typically three to four orders of magnitude smaller than the topographical features of an implant surface (Figure 2.1).

For detailed information regarding calcium phosphate and hydroxyapatite coatings [26–28], hydrogels [29, 30] and also the aforementioned modification of surface topography [31–34], the reader is referred to relevant reviews.
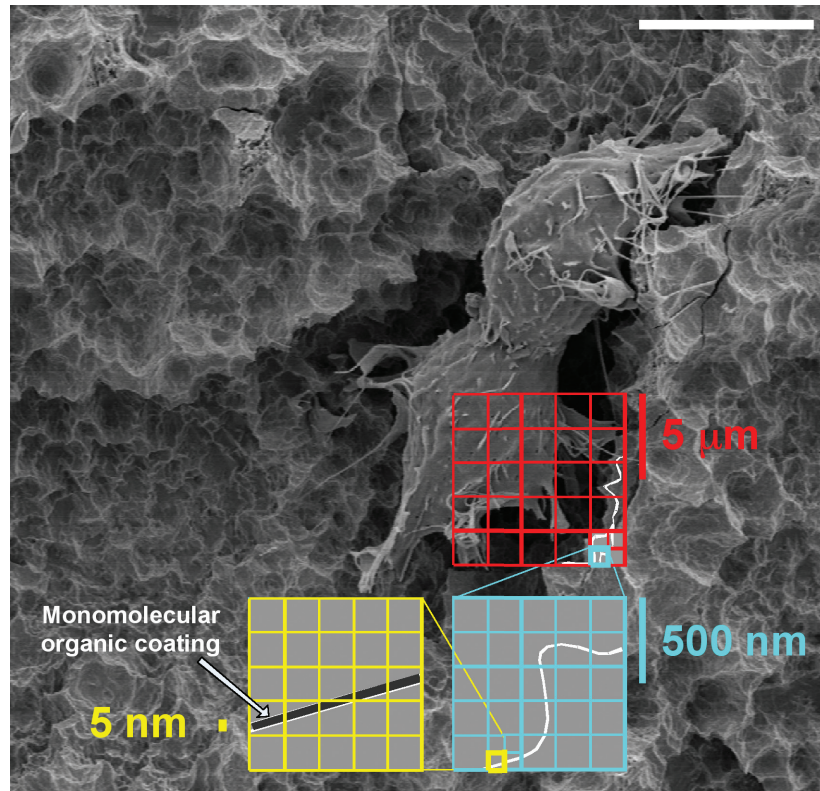
Figure 2.1: Scanning electron micrograph showing rat 3T3 fibroblasts attached on a rough (SLA) titanium surface coated with arginine-glycine-aspartic acid (RGD)-peptide modified poly(L-lysine)-*graft*-poly(ethylene glycol) (PLL-*g*-PEG/PEG-RGD). The peptide density was 3.0 pmol/cm^2. The thickness of the ultra-thin PLL-*g*-PEG/PEG-RGD coating (as shown schematically in three length scales) is three or four orders of magnitude smaller than the topographical features of the surface, allowing a modification of the surface (bio)chemistry without influencing the surface topography. White scale bar corresponds to 10 μm.

2.2 Modification of Surface (Bio)chemistry

The amount and type of biological species, proteins in particular, adsorbed on titanium implant surfaces upon exposure to blood and other body fluids [35] (Figure 2.2a) is considered to be a non-specific response of the body to the artificial implant material [22]. To abolish or reduce non-specific reactions towards the implant material and simultaneously improve the bio-responsiveness of the implant surface, a

number of approaches based on depositing ultra-thin adlayers onto titanium can be found in the literature. This review focuses rather on surfaces that have:

(i) Controlled physicochemical properties (Figure 2.2b)

(ii) Immobilized biological molecules (Figure 2.2d, e)

(iii) Non-fouling character (Figure 2.2c, e)

(iv) Drug-eluting abilities (Figure 2.2f)

2.2.1 Surfaces with Controlled Physicochemical Properties

The aim of using thin film technologies [36–38], which allows the tailoring of physicochemical properties, such as wettability or surface charge, is to generate a material with a well defined and controlled surface chemistry, capable of influencing passively the interaction between surface and biological species, such as proteins. Different studies have shown that protein adsorption onto a surface might be influenced by physicochemical surface properties [39] and the need for such a controlled surface is evident (besides the already aforementioned non-specific response of non-modified implanted devices) since many techniques used in producing surface topographies for implants have the tendency to alter surface chemistry, surface charge or surface energy. Massaro *et al.*, compared surface compositions of different commercially available ready-to-use titanium implants, and observed large variations from the expected TiO_2 surface composition, depending on manufacturing technology and packaging history [40]. In this respect, the introduction of an ultra-thin adlayer could be considered as a "deliberate but controlled contamination" that improves the reproducibility and safety of an implant. One way of controlling physicochemical properties is through self-assembled monolayers (SAMs) (Figure 2.2b), that is, spontaneous adsorption and arrangement of single layers of molecules on a substrate (e.g., alkane thiols adsorbed on gold surfaces) [41]. A number of groups have developed alkane phosph(on)ate SAMs that are compatible with metal oxide surfaces (e.g., Al_2O_3, TiO_2, Nb_2O_5) [42–47]. Textor's lab, for example, have coated smooth and particle-blasted, large grit, acid-etched (SLA) titanium surfaces with methyl-terminated (hydrophobic) or hydroxy-terminated (hydrophilic) alkane phosphates
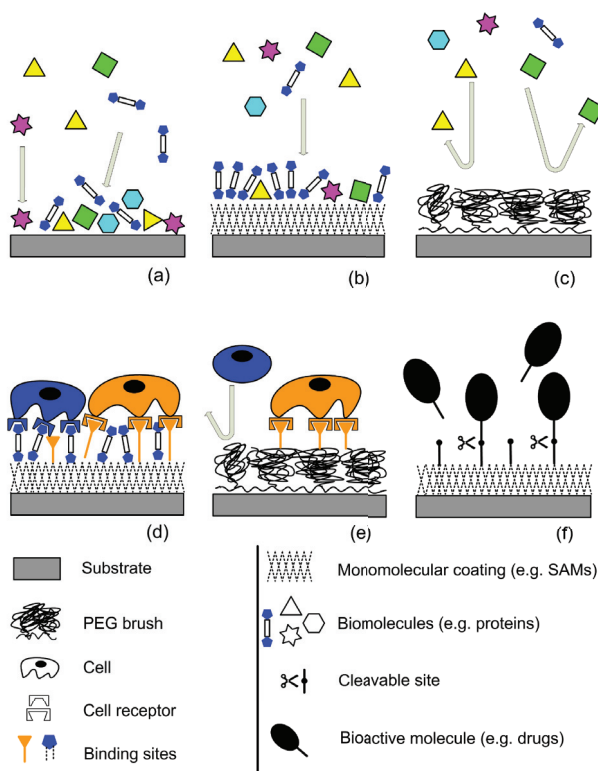
Figure 2.2: Schematic drawing representing the processes taking place at the interface between a titanium implant (with different surface (bio)chemistries) and its biological environment. (a) Bare titanium surface upon implantation encountering non-specific adsorption of proteins. (b) Titanium surface with controlled physicochemical properties (e.g., SAM). A control of the protein adsorption mechanism (over a short time) through hydrophilicity/hydrophobicity is generally observed. (c) Titanium surface with non-fouling character, reducing non-specific protein adsorption drastically. (d) Titanium surface with immobilized biological molecules, with the goal of influencing selectively the cell-surface interaction. However, non-specific protein adsorption interferes with the selective response of the immobilized molecules. (e) Titanium surface with immobilized biological molecules using a non-fouling strategy. The cell-surface interaction can be studied without the influence of any non-specific protein answer from the surface. (f) Titanium surface showing a drug-eluting strategy. Drugs are linked covalently to the surface and can be released owing to enzymatically cleavable binding sites. PEG: Polyethylene glycol; SAM: Self-assembled monolayer.

[38] and exposed them to human gingival fibroblasts for 24 h [48]. Surface wetta-
bility was much less important than surface roughness (i.e., more fibroblasts were
found on smooth compared with rough surfaces and fibroblasts on rough surfaces
were also less spread) and only partly influenced cell behavior. Furthermore, serum
content of culture media influenced cell attachment, spreading and shape, which
led to the conclusion that cell attachment and spreading in the presence of serum
proteins was not induced directly by the SAM surface but rather through the interac-
tion between cells and adsorbed proteins, which interact strongly with hydrophobic
and also many hydrophilic surfaces (e.g., clean metal oxides or hydroxy-terminated
SAMs) [49]. Additionally, when alkane phosphate SAMs were exposed to cell cul-
ture media, they showed time-dependent changes in contact angle, indicating a loss
of stability and subsequent changes in the protein adsorption properties.
These facts led to the hypothesis that much larger effects of surface chemistry on the
cell-surface interaction can be expected with (bio)chemial surface systems that allow
a direct influence on the protein adsorption process. Such approaches are discussed
in detail in the following sections.

2.2.2   Surfaces with Immobilized Biological Molecules

The easiest way of immobilizing (macro)molecules of biological nature on an implant
surface is by simply dipping the implant into a solution that contains biological
molecules, with the rationale of presenting active groups and structures to the bio-
logical environment present on the adsorbed species. For example, Ku *et al.*, have
adsorbed fragments of fibronectin and vitronectin passively on titanium surfaces.
MC3T3-E1 cells cultured on fibronectin showed increased cell attachment, prolifer-
ation and differentiation (e.g., alkaline phosphatase activity(ALP)) compared with
bare titanium surfaces and those coated with vitronectin [50]. Another study used
adsorbed collagen (Type I and III) and fibronectin onto Ti-6Al-4V substrates, which
influenced the behavior of rat calvarial osteoblasts such that differences in ALP activ-
ity and collagen synthesis were found between different composed collagen coatings.
An increase in collagen Type III resulted in an increase in collagen synthesis and
a concomitant decrease in ALP activity and calcium deposition [51, 52]. Becker
et al. used Type I collagen adsorbed onto Ti-6Al-4V surfaces and reported that a
collagen coating alone was not sufficient to accelerate differentiation of rat calvarial
osteoblasts [53]. Similar observations were described in a study that used adsorbed

fibronectin and collagen I coatings on titanium fiber mesh [54], and proliferation and differentiation of rat bone marrow cells were not stimulated by the presence of fibronectin and collagen.

These 4 cases have already revealed the complex situation when working with passively adsorbed proteins on surfaces. The adsorption process is very often reversible owing to the phase equilibrium between adsorbed molecules and protein solution. This means that such adsorbed species could be washed off when working with buffer solutions or easily replaced by other biomolecules (e.g., Vroman effect [55]). To avoid this problem, biomolecules could be linked covalently to the surface. Morra *et al.*, for example, have used a technique for deposition of a thin film from hydrocarbon plasma, followed by acrylic acid grafting to link collagen covalently to titanium surfaces [56]. *In vitro* studies revealed that growth rates of osteoblast-like SaOS-2 cells on collagen-modified surfaces were lower than on bare titanium and no significant difference in ALP existed. However, *in vivo* experiments using a rabbit femur model showed enhanced bone healing of collagen surfaces (see below). Another approach was described by Scharnweber *et al.*, who immobilized collagen Type I by partial incorporation into the anodic oxide layer on commercially pure titanium using the anodic oxidation technique [57]. It was found that after 24 h of exposure in simulated body fluid, a higher density of spherical calcium phosphate particles were detected on adsorbed collagen in comparison with collagen that was partially incorporated into the anodic oxide layer. After 30 days of exposure, no differences were found between both surface states.

Other general aspects associated with the coupling or adsorption of whole proteins or protein fragments to a surface include the risks of changing the 3D structure of the biomolecules, leading to protein denaturation, protein conjugation, protein-induced immunogenicity and limited shelf life [25, 58]. An alternative approach, which would reduce many of the problems elucidated above, would be the use of peptides derived from native proteins [59, 60]. A frequently used peptide sequence is arginine-glycine-aspartic acid (RGD) [61], located on a loop on the tenth domain of fibronectin (FN III-10) [62]. Nearly half of the over 20 known α/β integrins recognize this sequence in their adhesion protein ligands [63]. Another group of cell-interacting moieties are heparin-binding peptides such as KRSR and FHRRIKA. Both sequences are present in the extracellular matrix (ECM) of osteoblasts and, therefore, are of potential interest for bone-related applications. KRSR can be located in fibronectin, vitronectin, bone sialoprotein, thrombospondin and osteopontin

[64], whereas FHRRIKA is derived from bone sialoprotein alone [65]. These poly-cationic heparin-binding peptides bind to negatively charged glycosaminoglycans associated with proteoglycans found in the cell membrane. Other investigated peptide sequences are GFOGER, derived from collagen [66] and IKVAV and YIGSR from laminin [67]. Such peptide sequences are usually used in linear conformation; however, cyclic RGD-peptides, for example, have much higher affinity [68, 69] and are also more resistant to proteolysis [70]. Combining two different peptide sequences, as for example RGD and FHRRIKA could result in synergistic effects [65]. It has also been demonstrated that a more "complete" cell response (as indicated through cell attachment and spreading, as well as formation of discrete focal contacts and organized cytoskeletal assembly) was obtained by providing the cell with both the cell-binding (RGD-containing) and heparin-binding (FHRRIKA-containing) domains of fibronectin [71, 72]. Peptide sequences mentioned above are most frequently used in combination with (non-fouling) immobilization systems. We discuss some of these systems in detail in the following section.

There are also some examples of using peptides adsorbed "directly" onto titanium surfaces via, for example, silanization or polypyrrole (PPy) chemistry. Zreiqat *et al.* bound the peptide sequences RGD and RGE (negative control) to Ti-6Al-4V surfaces using 3-aminopropyltriethoxysilane chemistry [73]. Human bone-derived cells were studied on peptide-modified and non-modified titanium surfaces, on which protein levels of osteocalcin, pro-collagen I and alkaline phosphatase were upregulated on the RGD-modified compared with native titanium surfaces. Another study compared linear RGD and cyclo-DfKRG immobilized via silanization to Ti-6Al-4V surfaces [74]. More human osteoprogenitor cells were found on both RGD-containing substrates in comparison with the bare Ti-6Al-4V surface. On cyclo-DfKRG, cell attachment was improved compared to the linear RGD-peptide surfaces, a finding mentioned already. Senyah *et al.* studied cell behavior with respect to specific RGD-peptide titanium surfaces with different hydrophobicity [75]. They observed that the number of adhering cells increased following changes in the peptide hydrophobicity, demonstrating that not only the RGD sequence but also physicochemical properties were responsible for enhanced adhesion of cells to non-biological surfaces. However, the influence of the latter can be advantageous in terms of synergy, but can also be detrimental in masking the effect elucidated by the specific bio-functional species (e.g., RGD-peptide). Pallu *et al.* investigated the differentiation of human osteoprogenitor cells on simply physisorbed cyclo-DfKRG compared to cyclo-DfKRG linked

covalently (using a thiol or phosphonate anchor) to Ti-6Al-4V surfaces, as mentioned above [76]. Peptides with a phosphonate anchor contributed to higher cell adhesion and a stronger alkaline phosphatase and core binding factor 1 mRNA expression than the other two surfaces (thiol-anchored and bare titanium). By contrast, the same peptide coated with a thiol anchor stimulated differentiation of human osteo-progenitor cells better than the other two surface types within 3 days of culture. Whether this difference was the result of the different anchoring system or a different peptide density remains unclear. Another strategy is the use of polypyrrole for coupling CDRGDSPK to titanium surfaces [77]. Neonatal rat calvarial osteoblasts were studied on these peptide-PPy modified surfaces and higher amounts of cells attached in comparison to unmodified PPy titanium.

In our view, an immobilization of peptide sequences needs a carrier system that "shields" the implant surface from the biological environment, resulting in significantly reduced non-specific processes, such as protein adsorption. Thus, it is possible to study peptide-cell interaction directly without any interference from blood plasma or serum proteins. Such an approach, based on a "silent" background, might be less common in implant applications, although it is already strongly recognized as a prerequisite in the development of bioaffinity sensor chips [48]. Some of these approaches are discussed in more detail in the next section.

2.2.3 Surfaces with Non-fouling Character

Different approaches have been reported to render surfaces resistant to protein adsorption, the so called "non-fouling" or "anti-fouling" surfaces [78]. Polyethylene glycol (PEG) (or polyethylene oxide (PEO)), which was discovered almost 40 years ago [79], is still the most frequently used material to produce non-fouling surfaces. Excluded volume, osmotic and entropic repulsion effects, as well as screening of interfacial charges [80], have been discussed in the context of the mechanisms involved in rendering PEGylated surfaces anti-fouling. Other chemical systems are similarly effective, including poly(2-methyl-2-oxazoline) (PMOXA) [81], N-vinyl pyrrolidone (NVP) [82] and polysaccharides [83], as well as other neutral polymers such as poly(hydroxyethyl) methacrylate (PHEMA) [84], polyacrylamide (PAAm) [85] and phosphorylcholine [86]. Many approaches can be used to immobilize PEG onto surfaces and some are compatible with titanium surface chemistry. Covalent attachment of reactive PEGs, preferentially under cloud-point conditions [87], molecular

assembly approaches [20, 88] and formation of Interpenetrating Networks (IPNs) [89–92] are a few examples of successfully used approaches. IPNs can be considered as hydrogels and are therefore not further discussed within this review. However, at present, the most interesting strategy involves the combination of gaining control over non-specific protein adsorption and introducing specific bioligands, such as cell-interactive peptides linked covalently to the non-fouling adlayer. Such biomimetic surface modifications [65, 93], provided that the coatings are thin enough, can then be applied to topographically structured, rough surfaces (as often used for metal implants in bone applications), without altering the overall surface topography. This gives the bioengineer a tool to steer attachment, shape and motility of cells by controlled presentation of both topographical cues and specific peptides at controlled surface density [94]. Some selected examples of biomimetic surface modifications are described hereafter.

An effective and simple way to minimize protein adsorption onto a surface is the use of a poly(L-lysine)-*graft*-poly(ethylene glycol) (PLL-*g*-PEG) molecular assembly system [95–97]. These PEGylated surfaces reduce adsorbed protein mass to less than <5 ng/cm^2 [98]. Furthermore, peptide sequences can be attached covalently via vinyl sulfone-cysteine coupling reaction to a fraction of the PEG side chains [99]. RGD-peptide modified PLL-*g*-PEG coated onto smooth and SLA titanium surfaces influenced the attachment and spreading of rat calvarial osteoblasts (Figure 2.3) [20]. Osteoblast spreading increased with increasing RGD-peptide surface density. However, MG63 osteoblast-like cells were found to behave in a less "osteoblastic" way (as assessed, for example, by decreased transforming growth factor (TGF)-β1 and prostaglandin E$_2$ (PGE$_2$) expression) on high-density RGD-PEG surfaces on titanium in comparison with non-adhesive PEGylated surfaces (e.g., R<u>DG</u>-PEG control) or low-density RGD-PEG surfaces (<0.05 pmol/cm^2) [98]. It appears, therefore, that surfaces that maximize osteoblast adhesion and spreading (e.g., high RGD-PEG surface densities) might not be the optimum if one aims to maximize osteoblast differentiation *in vitro*. Furthermore, it appears, that a surface that "forces" osteoblasts into a more spherical and therefore less stretched shape (as observed on low-concentrated RGD surfaces) may be more favorable in terms of early bone differentiation [100]. An alternative approach to create a surface that might be more suitable for bone-contacting implants could be the use of other, osteoblast-specific sequences such as KRSR or FHRRIKA. The PLL-*g*-PEG/PEG-peptide immobilization system demonstrated that primary osteoblasts outgrown from bone

chips of rat calvariae covered a significantly larger area in contact with KRSR- or FHRRIKA-peptide modified rough titanium surfaces, compared with an unmodified PLL-*g*-PEG surface [101]. Bacteria adhesion (*Staphylococcus aureus*, *Staphylococcus epidermidis*, *Streptococcus mutans* and *Pseudomonas aeruginosa*) on both non-functionalized PLL-*g*-PEG and RGD-functionalized PLL-*g*-PEG surfaces was also significantly reduced after 24 h (Figure 2.3) [102, 103]. Thus, a coating with RGD-functionalized PLL-*g*-PEG has the potential to modify medical implants, as it inhibits bacterial growth, while still having the ability to interact with cells, such as osteoblasts, via the presented bioligands (peptides).

Groll *et al.* described another approach using star-shaped poly(ethylene glycol) prepolymers (star-PEG) that were modified with linear RGD peptides (gRGDsc) [104]. Cell adhesion, spreading and survival for up to 30 days were observed on RGD-peptide coatings, whereas no cell adhesion could be detected on unmodified star-PEG layers. In addition, cell attachment was controlled by variation of the RGD concentration. Expression of osteogenic marker genes after 14 days using differentiation conditions and RGD-star-PEG modified surfaces showed comparable data with tissue culture polystyrene (TCPS) substrates, indicating that this new type of polymer does not influence the differentiation process in a negative way.

To open new windows into therapeutics and preventive approaches, a surface modification using peptides might not be the final solution. Surfaces with additional functionalities may be required to rapidly stimulate formation of desired tissue at the interface; for example, growth factor-containing coatings.
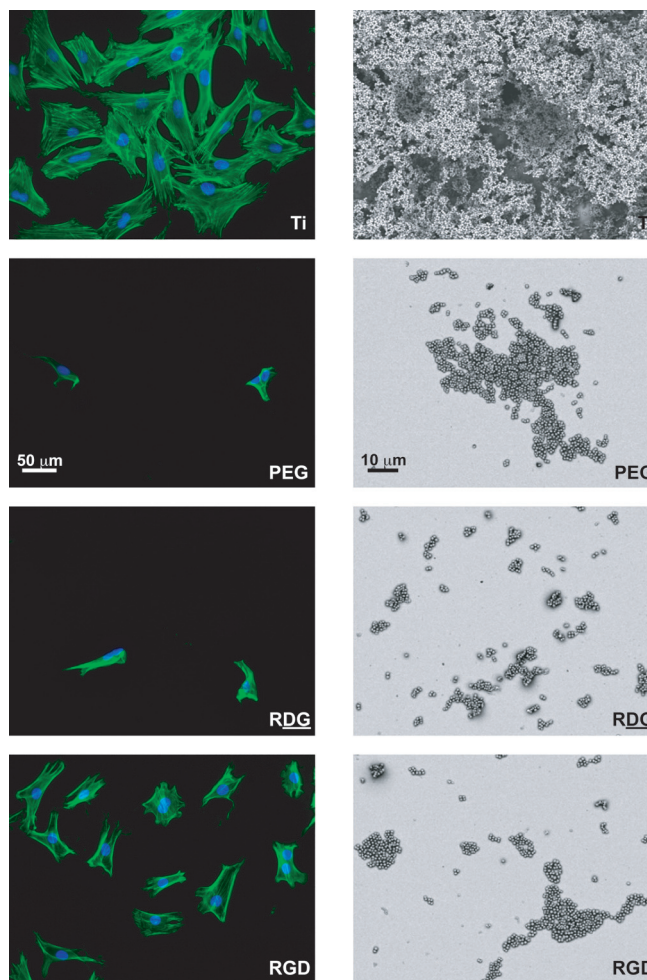
Figure 2.3: Fluorescent images of rat calvarial osteoblasts (left column) stained for actin (green) and nuclei (blue) and scanning electron micrographs of *Staphylococcus aureus* (right column) on different poly(L-lysine)-*graft*-poly(ethylene glycol)(PLL-*g*-PEG) modified surfaces in comparison with bare titanium (Ti) after 24 h in culture. A coating with the non-fouling polymer PLL-*g*-PEG (PEG) and PLL-*g*-PEG/PEG-RDG (scrambled peptide, bio-inactive; RDG) reduced osteoblast and bacteria adhesion significantly compared with bare titanium. The linking of the RGD-peptide to the PLL-*g*-PEG system resulted in a restoration of osteoblast attachment similar to that found on titanium, *S. aureus*, however, was not recognized by the RGD-peptide and its adhesion was in the range of unfunctionalized PLL-*g*-PEG. The used RGD-peptide density was 3.0 pmol/cm^2. The SEM images are a courtesy of Dr. Llinos Harris, AO Resarch Institute Davos, Switzerland.

2.2.4 Surfaces with Drug-eluting Abilities

Biomaterials represent an essential component of modern medical therapy and helped to significantly improve quality of life of thousands of patients, especially in orthopedic surgery, such as joint replacement, dental implants, osteosynthesis and cardiovascular stents. Up until now, the biomaterials story had been an impressive success. However, complications owing, for example, to patients with impaired healing, loosening of implant and infection, still limit their unrestricted application. To create a new implant surface with improved performance after surgical intervention, especially for patients defined as critical from the perspective of bone formation or wound healing, the approach to deliver drugs locally, through drug-eluting surfaces, is finding increased interest among researchers. Instead of systemic application, the use of a locally applied drug delivery system has not only the advantage that the pharmacological properties of conventional drugs can be improved by altering their biodistribution (BD) and pharmacokinetics [105, 106], but can also reduce undesired side effects in the patient's body.

Improved BD and pharmacokinetics are able to provide continuous drug levels in a therapeutically relevant range, reduced side effects owing to targeted delivery, decreased amount of drug required, better patient compliance and better administration of drugs with short half lives (e.g., peptides).

In the new millennium, drug-eluting stents (DES) have emerged, especially to solve in-stent restenosis. Being one of the hot research topics currently, many products can be expected from that specific area in the near future [107, 108], stimulating other fields of biomedical devices, for example, dental implants. Since stents are only one of the many possible implant surfaces, investigated for drug delivery, a few other approaches will now be discussed.

A relatively new technique is a dipping the implant in platelet-rich plasma (PRP), a modification of fibrin glue made from autologous blood [109]. However, there is a lack of scientific evidence to support this novel and potentially promising technique and more well-designed and controlled studies are required. By contrast, autologous materials preclude the manufacture of implants outside the operation room and thus remain relatively complicated to handle. Another approach is the covalent linking of proteins to surfaces as reported, for example, by Puleo *et al.*. They have used plasma polymerization of allyl amine on Ti–6Al–4V surfaces to immobilize bone morphogenetic protein (BMP)-4 [110]. Pluripotent C3H10T1/2 cells cultured

on these surfaces showed higher alkaline phosphatase activity than cells on simply adsorbed BMP-4 surfaces or control substrates. Smith *et al.* have shown that the incorporation of diazeniumdiolates as nitric oxide (NO) donors used in polymers [111] to coat medical devices, thus mimicking the non-thrombogenic endothelial cells, reduced platelet aggregation on implants significantly [112]. A number of attempts to incorporate and release growth factors from biodegradable polymers have also been reported, for example, for musculoskeletal tissue engineering purposes, nerve regeneration [113] or wound healing [114, 115]. However, only few examples are known of growth factor delivery from titanium implant surfaces. One is the approach of linking BMP-2 covalently to titanium surfaces through a chemical conjugation process [116], promoting osteogenic attachment to implants. Not only enhanced implant integration, but also prevention of infections at site of implant, is of great interest. Local delivery of antimicrobial therapy can reduce significantly the side effects of the systemic use of antibiotics. Ambrosio's lab used the sol-gel method to incorporate ampicillin into $TiO_2/poly(\epsilon$-caprolactone) (PCL) hybrid material for local delivery to implant sites [117].

2.2.5 Some *in vivo* and Stability Considerations

Many studies have demonstrated that a (bio)chemically modified titanium surface can influence cell responses *in vitro*. However, *in vivo* data is still rare and sometimes very difficult to interpret or compare, owing to non-standardized experimental setups. Additionally, a careful, quantitative characterization of the surfaces implanted is sometimes missing (e.g., contamination, "available" peptide density), making it difficult to judge the "real" influence of biological factors on the performance of the (bio)chemically modified implant.

Buser *et al.* have investigated titanium implants with a modified SLA surface (modSLA; commercial name is SLActive^{TM} [118]), that were stored in physiological NaCl solution following acid-etching to avoid contamination with molecules from the atmosphere prior to implantation in miniature pigs. A greater mean percentage of bone implant contact at 2 weeks and 4 weeks of healing compared with the standard implant surface (SLA) was found [119] (Figure 2.4). After 8 weeks, the results were similar, indicating enhanced bone apposition only during early stages of bone regeneration. Analogically, removal torque experiments from the same group revealed that modSLA implants showed 8–21% higher values than those of SLA implants for

week 2 and 4 [120].
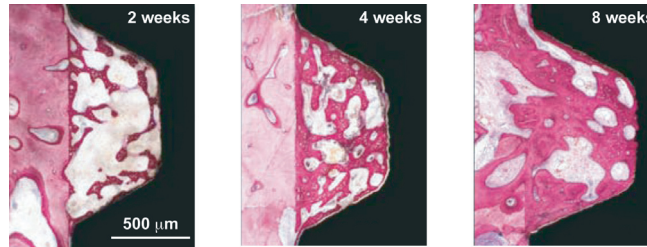
Figure 2.4: Histological sections showing bone apposition (undecalcified ground section, surface-stained with toluidine blue and basic fuchsin) to a titanium implant with modified SLA surface (modSLA; commercial name SLActive^{TM} [118]) using a miniature pig model. At 2 weeks, bone was deposited on the bony wall of the tissue chamber and on the implant surface. At 4 weeks, the volume density of this scaffold had increased both by the formation of new trabeculae and by deposition of more mature, parallel-fibered bone onto the primary scaffold. At 8 weeks, growth and reinforcement resulted in a further increase in bone density and an almost perfect coating of the implant surface with bone. Remodeling had started, replacing the primary bone by secondary osteons. Reprinted with permission from [119].

As previously mentioned, Morra *et al.* studied collagen-coated titanium implant model surfaces using a rabbit tibia model and observed improved bone maturation and mineralization at the interface in comparison with titanium [121, 122]. Kroese-Deutman *et al.* showed that cyclic RGD-modified titanium fiber mesh had a positive effect on bone formation compared to titanium fiber mesh alone *in vivo* [123]. Similar surfaces were used in another study that investigated Ti-6Al-4V coated with cyclic RGD implanted in canine [124]. Pushout and histomorphometry experiments revealed a significant increase in bone and a decrease in fibrous tissue anchorage. Titanium implants coated with collagen Type I/III or RGD and inserted into the femur of goats were investigated by Bernhardt *et al.* [125]. All three coatings showed a significant increase in bone volume in comparison with the uncoated reference, with the highest results for the collagen coatings. In another study, titanium substrates were coated with bone sialoprotein (BSP) and implanted into rat femurs. Histological sectioning revealed that the BSP-coating was in fact osteoinductive although the pullout strengths were a function of implant surface topography and not affected by the coating [126]. This finding reveals a problem often encountered when per-

forming *in vivo* studies with (bio)chemically modified substrates and highlights the importance of such studies, always including biomechanical tests to prove whether the newly formed bone is firmly linked to the implant and whether the implant is mechanically loadable or not.

Germanier *et al.* coated SLA titanium implant surfaces with RGD-modified PLL-*g*-PEG and studied bone apposition *in vivo* using a miniature pig model [127]. Enhanced bone apposition was only shown during the early stages of bone regeneration, whereas there was no difference in bone apposition at later stages of bone regeneration compared with control surfaces. This could be an indication that the PLL-*g*-PEG polymeric coating had a limited life-time. Long-term stability of PLL-*g*-PEG polymer surfaces was investigated by VandeVondele *et al.* [99]. Adlayers adsorbed onto TCPS were incubated with phosphate buffered saline (PBS) or serum-containing media over 10 days and then seeded with cells. Cell proliferation was assessed with WST-1 and shown to be comparable with data obtained on freshly prepared corresponding PLL-*g*-PEG coatings.

There is little known about the fate of such polymeric coatings *in vivo* and predictability is correspondingly difficult under *in vivo* conditions; the benefit of monolayer coatings might be strongly dependent on a particular application or a dramatic effect elucidated on the very short term. Indeed, the question about the time during which a (bio)chemical coating has to be stable and functional *in vivo* is far from being answered definitely. Would it be enough to be stable over a short time period of a couple of days to "attract" certain cell types (or stop others from attachment) and to avoid inflammatory processes (or bacterial adhesion) or must the coating place and active for weeks or even months to ensure cell differentiation and finally bone formation?

Other disadvantages associated with the use of adsorbed coatings on surfaces might be the limited wear resistance and possible alteration and degradation over longer time periods owing to biological activity. Damage or removal of such a coating when exposed to wear (as can happen during implantation) can be reduced to some extent through topographical features of the implant surface, such as the rough SLA dental implant surface [128]. Another approach would be the covalent bond of the biological species with the substrate. However, it must be kept in mind that, although such a bound biomolecule is in general much more stable under physiological conditions and also more resistant to disruption, its conformation or orientation can be altered during the chemical immobilization, resulting in disturbance of the bioactive center

and hence reduction or even loss of its biological activity.

Before successful industrial application of ultra-thin organic surface coatings, more tests, including sterilization and stability experiments as well as aging assays to investigate shelf-life behavior, are required. A problematic point might be X-ray treatment, a technique typically used for sterilizing implants. It was found recently that sterilization of PEG by X-ray radiation led to a degradation of the polymer and, thus, a loss of protein resistance [129]. However, other sterilization techniques such as filtration of the polymer solution prior surface coating, used successfully in the laboratory [20] can also be applied on an industrial scale. In terms of scalability, large batch sizes and compatibility with modern industrial and environmentally acceptable production techniques, surface coatings using monomolecular assembly techniques have clear advantages and, even from an economic point of view, are potentially very cost-effective (e.g., material costs are in the order of 1 cent/cm^2) [48].

2.3   Conclusion

Although titanium is already an excellent implant material and used widely in bone-contact applications, surface modification has significantly improved its performance. Modification of titanium surfaces can be more or less divided chronologically into these three areas: (i) Modification of topography, (ii) Modification of (bio)chemistry using biologically inspired surfaces, (iii) Modification of (bio)chemistry using drug-eluting surfaces.

Modification of surface topography has led to defined macro, micro- and nano-topographies to reduce healing times and accelerate integration into the host tissue. Most of the development of newly structured surfaces, however, was made in the past and only a few new techniques have been developed in recent years.

However, modification of surface (bio)chemistry based on biological principles has become very promising nowadays, in terms of triggering cell-selective response, resistance to bacteria attachment, reduction of the risk of inflammation, improvement in reliability and long-term performance of the device. Such new strategies might also be the only solution for osteoporosis and diabetes patients defined as critical from the perspective of bone-forming capacity or wound healing. Although many approaches have been described in the literature, the focus of this review is on biologically in-

spired, specific surface modifications by means of ultra-thin organic adlayers and/or biological molecules: surfaces with controlled physicochemical properties, surfaces containing biological molecules, non-fouling surfaces and surfaces with drug-eluting character. Each of these approaches has clear advantages and disadvantages and both *in vitro* and *in vivo* studies have been discussed extensively.

Many studies using different immobilization strategies, such as passive adsorption, covalent linking of biomolecules or immobilization thereof using (non-fouling) polymeric surfaces, are presented in this review. However, we strongly believe that the future of modifying titanium surfaces for biomedical applications will make use of even more sophisticated surfaces with, for example, drug delivery abilities, which, in turn, have the potential to bring a significant new boost to therapeutics and preventive approaches.

2.4   Future Perspectives

Cellular biologists and material scientists are really coaxing bone-healing cells to improve the way titanium bonds with bone. Titanium is already an excellent implant material, being inert and rarely causing adverse reactions. But still the bond formed when bone meets bone cannot be entirely mimicked by titanium meeting bone. This process can be very slow and sometimes not successful at all. To improve osseointegration, one could think of different approaches. A rather straightforward method would be the direct covalent immobilization of growth factors or drugs that stimulate osteoblast proliferation and/or differentiation to the implant titanium surface. Thinking of more refined approaches, a biodegradable linker, releasing growth factors or drugs upon cellular contact, could be combined with titanium surfaces (Figure 2.4f). As a drug delivery approach, poly(lactic-*co*-glycolic) acid (PLGA) biodegradable microbeads or lipid vesicles that contain drugs could be either linked covalently to the titanium surface or incorporated into polymer multilayers or hydrogels, serving at the same time as a scaffold.

Bibliography

[1] Brunette, D. M., Tengvall, P., Textor, M. and Thomsen, P. *Titanium in Medicine.* Springer-Verlag, Berlin Heidelberg, 2001.

[2] Leyens, C. and Peters, M. *Titanium and Titanium Alloys: Fundamentals and Applications.* Wiley-VCH, Weinheim, 2003.

[3] Textor, M., Sittig, C., Frauchiger, V. M., Tosatti, S. G. P. and Brunette, D. M. Properties and biological significance of natural oxide films on titanium and its alloys. In Brunette, D. M., Tengvall, P., Textor, M. and Thomsen, P., editors, *Titanium in Medicine*, pages 171–230. Springer-Verlag, Berlin Heidelberg, 2001.

[4] Jansen, J. A., Vonrecum, A. F., Vanderwaerden, J. and Degroot, K. Soft-Tissue Response to Different Types of Sintered Metal Fiber-Web Materials. *Biomaterials*, **13**(13), 959–968, 1992.

[5] Albrektsson, T. and al., e. The Interface Zone of Inorganic Implants in vivo - Titanium Implants in Bone. *Annals of Biomedical Engineering*, **11**, 1–27, 1983.

[6] Rossetti, F. F., Bally, M., Michel, R., Textor, M. and Reviakine, I. Interactions between titanium dioxide and phosphatidyl serine-containing liposomes: Formation and patterning of supported phospholipid bilayers on the surface of a medically relevant material. *Langmuir*, **21**(14), 6443–6450, 2005.

[7] Davies, J. *Bone Engineering.* Em Squared Inc., Toronto, 1999.

[8] Jaeger, N. and Brunette, D. M. Production of microfabricated surfaces and their effects on cell behavior. In Brunette, D. M., Tengvall, P., Textor, M. and Thomsen, P., editors, *Titanium in Medicine*, pages 343–374. Springer-Verlag, Berlin Heidelberg, 2001.

[9] Brunette, D. M., Kenner, G. S. and Gould, T. R. L. Grooved Titanium Surfaces Orient Growth and Migration of Cells from Human Gingival Explants. *Journal of Dental Research*, **62**(10), 1045–1048, 1983.

[10] Sykaras, N., Iacopino, A. M., Marker, V. A., Triplett, R. G. and Woody, R. D. Implant materials, designs, and surface topographies: Their effect on osseointegration. A literature review. *International Journal of Oral Maxillofacial Implants*, **15**(5), 675–690, 2000.

[11] Wennerberg, A., Albrektsson, T. and Andersson, B. Design and surface characteristics of 13 commercially available oral implant systems. *Int J Oral Maxillofac Implants*, **8**, 622–633, 1993.

[12] Wieland, M. *Experimental determination and quantitative evaluation of the surface composition and topography of medical implant surfaces and their influence on osteoblastic cell-surface interactions*. Ph.D. Thesis No. 13247, Swiss Federal Institute of Technology Zurich, 1999.

[13] Wieland, M., Textor, M., Spencer, N. D. and Brunette, D. M. Measurement and Evaluation of the Chemical Composition and Topography of Titanium Implant Surface. In Davies, J. E., editor, *Bone Engineering*. Em Squared Inc., 2000.

[14] Wieland, M., Chehroudi, B., Textor, M. and Brunette, D. M. Use of Ti-coated replicas to investigate the effects on fibroblast shape of surfaces with varying roughness and constant chemical composition. *Journal of Biomedical Materials Research*, **60**(3), 434–444, 2002.

[15] Wieland, M., Textor, M., Spencer, N. D. and Brunette, D. M. Wavelength-dependent roughness: A quantitative approach to characterizing the topography of rough titanium surfaces. *International Journal of Oral Maxillofacial Implants*, **16**(2), 163–181, 2001.

[16] Chauvy, P. F., Hoffmann, P. and Landolt, D. Electrochemical micromachining of titanium through a laser patterned oxide film. *Electrochemical and Solid State Letters*, **4**(5), C31–C34, 2001.

[17] Chauvy, P. F., Hoffmann, P. and Landolt, D. Electrochemical micromachining of titanium using laser oxide film lithography: excimer laser irradiation of anodic oxide. *Applied Surface Science*, **211**(1-4), 113–127, 2003.

[18] Dunand, D. C. Processing of titanium foams. *Advanced Engineering Materials*, **6**(6), 369–376, 2004.

[19] Schuler, M., Kunzler, T. P., Sprecher, C. M., de Wild, M., Tosatti, S. and Textor, M. Innovative Method for the Production of Similar TiO2-coated Epoxy Replicas Used in Cell Culture Assays. In Hofmann, H., Hubbell, J., Textor, M., Spencer, N., Richards, R., Hofmann, M., Hanawa, T., Grainger, D. and Petimermet, M., editors, *Biosurf VI, Tissue-Surface-Interaction*,, page BSI 20, Lausanne, Switzerland, 2005.

[20] Schuler, M., Owen, G., Hamilton, D. W., de Wild, M., Textor, M., Brunette, D. M. and Tosatti, S. Biomimetic modification of titanium dental implant model surfaces using the RGDSP-peptide sequence: A cell morphology study. *Biomaterials*, **27**(21), 4003–4015, 2006.

[21] Kunzler, T., Sprecher, C. M., Schuler, M., Drobek, T. and Spencer, N. D. Fabrication of material-independent morphology gradients for high-throughput applications. *Applied Surface Science*, **253**(4), 2148–2153, 2006.

[22] Ratner, B. D. A Perspective on Titanium Biocompatibility. In Brunette, D. M., Tengvall, P., Textor, M. and Thomsen, P., editors, *Titanium in Medicine*, pages 1–12. Springer-Verlag, Berlin Heidelberg, 2001.

[23] Porter, J. and von Fraunhofer, J. Success or failure of dental implants? A literature review with treatment considerations. *General Dentistry*, **53**(6), 423–32, 2005.

[24] WHO. Diet, nutrition and the prevention of chronic diseases: report of a joint WHO/FAO expert consultation. Technical report, WHO, 2002.

[25] Morra, M. Biochemical modification of titanium surfaces: peptides and ECM proteins. *European Cells and Materials*, **24**(12), 1–15, 2006.

[26] Liu, Y., Li, J. P., Hunziker, E. B. and De Groot, K. Incorporation of growth factors into medical devices via biomimetic coatings. *Philosophical Transactions of the Royal Society a-Mathematical Physical and Engineering Sciences*, **364**(1838), 233–248, 2006.

[27] Yang, Y. Z., Kim, K. H. and Ong, J. L. Review on calcium phosphate coatings produced using a sputtering process - an alternative to plasma spraying. *Biomaterials*, **26**(3), 327–337, 2005.

[28] Sun, L. M., Berndt, C. C., Gross, K. A. and Kucuk, A. Material fundamentals and clinical performance of plasma-sprayed hydroxyapatite coatings: A review. *Journal of Biomedical Materials Research*, **58**(5), 570–592, 2001.

[29] Hoffman, A. S. Hydrogels for biomedical applications. In *Bioartificial Organs Iii: Tissue Sourcing, Immunoisolation, and Clinical Trials*, volume 944 of *Annals of the New York Academy of Sciences*, pages 62–73. New York Acad Sciences, New York, 2001.

[30] Hoffman, A. S. Hydrogels for biomedical applications. *Advanced Drug Delivery Reviews*, **54**(1), 3–12, 2002.

[31] Lausmaa, J. Mechanical, Thermal, Chemical and Electrochemical Surface Treatment of Titanium. In Brunette, D. M., Tengvall, P., Textor, M. and Thomsen, P., editors, *Titanium in Medicine*, pages 231–266. Springer-Verlag, Berlin Heidelberg, 2001.

[32] Piveteau, L.-D. Sol-Gel Coatings on Titanium. In Brunette, D. M., Tengvall, P., Textor, M. and Thomsen, P., editors, *Titanium in Medicine*, pages 267–282. Springer-Verlag, Berlin Heidelberg, 2001.

[33] Thull, R. and Grant, D. Physical and Chemical Vapor Deposition and Plasma-assisted Techniques for Coating Titanium. In Brunette, D. M., Tengvall, P., Textor, M. and Thomsen, P., editors, *Titanium in Medicine*, pages 283–341. Springer-Verlag, Berlin Heidelberg, 2001.

[34] Gruner, H. Thermal Spray Coatings on Titanium. In Brunette, D. M., Tengvall, P., Textor, M. and Thomsen, P., editors, *Titanium in Medicine*, pages 375–416. Springer-Verlag, Berlin Heidelberg, 2001.

[35] Tengvall, P. Proteins at titanium interfaces. In Brunette, D. M., Tengvall, P., Textor, M. and Thomsen, P., editors, *Titanium in Medicine*, pages 457–484. Springer-Verlag, Berlin Heidelberg, 2001.

[36] Schwartz, J., Avaltroni, M. J., Danahy, M. P., Silverman, B. M., Hanson, E. L., Schwarzbauer, J. E., Midwood, K. S. and Gawalt, E. S. Cell attachment and spreading on metal implant materials. *Materials Science Engineering C-Biomimetic and Supramolecular Systems*, **23**(3), 395–400, 2003.

[37] Zwahlen, M., Tosatti, S., Textor, M. and Hahner, G. Orientation in methyl- and hydroxyl-terminated self-assembled alkanephosphate monolayers on titanium oxide surfaces investigated with soft X-ray absorption. *Langmuir*, **18**(10), 3957–3962, 2002.

[38] Tosatti, S., Michel, R., Textor, M. and Spencer, N. D. Self-assembled monolayers of dodecyl and hydroxy-dodecyl phosphates on both smooth and rough titanium and titanium oxide surfaces. *Langmuir*, **18**(9), 3537–3548, 2002.

[39] Michael, K. E., Vernekar, V. N., Keselowsky, B. G., Meredith, J. C., Latour, R. A. and Garcia, A. J. Adsorption-induced conformational changes in fibronectin due to interactions with well-defined surface chemistries. *Langmuir*, **19**(19), 8033–8040, 2003.

[40] Massaro, C., Rotolo, P., De Riccardis, F., Milella, E., Napoli, A., Wieland, M., Textor, M., Spencer, N. D. and Brunette, D. M. Comparative investigation of the surface properties of commercial titanium dental implants. Part I: chemical composition. *Journal of Materials Science-Materials in Medicine*, **13**(6), 535–548, 2002.

[41] Nuzzo, R. G. and Allara, D. L. Adsorption of Bifunctional Organic Disulfides On Gold Surfaces. *Journal of the American Chemical Society*, **105**(13), 4481–4483, 1983.

[42] Maege, I., Jaehne, E., Henke, A., Adler, H. J. P., Bram, C., Jung, C. and Stratmann, M. Self-assembling adhesion promoters for corrosion resistant metal polymer interfaces. *Progress in Organic Coatings*, **34**(1-4), 1–12, 1998.

[43] Maege, I., Jaehne, E., Henke, A., Adler, H. J. P., Bram, C., Jung, C. and Stratmann, M. Ultrathin organic layers for corrosion protection. *Macromolecular Symposia*, **126**, 7–24, 1998.

[44] Brovelli, D., Hahner, G., Ruiz, L., Hofer, R., Kraus, G., Waldner, A., Schlosser, J., Oroszlan, P., Ehrat, M. and Spencer, N. D. Highly oriented, self-assembled alkanephosphate monolayers on tantalum(V) oxide surfaces. *Langmuir*, **15**(13), 4324–4327, 1999.

[45] Hofer, R., Textor, M. and Spencer, N. D. Alkyl phosphate monolayers, self-assembled from aqueous solution onto metal oxide surfaces. *Langmuir*, **17**(13), 4014–4020, 2001.

[46] Gawalt, E. S., Avaltroni, M. J., Koch, N. and Schwartz, J. Self-assembly and bonding of alkanephosphonic acids on the native oxide surface of titanium. *Langmuir*, **17**(19), 5736–5738, 2001.

[47] Silverman, B. M., Wieghaus, K. A. and Schwartz, J. Comparative properties of siloxane vs phosphonate monolayers on a key titanium alloy. *Langmuir*, **21**(1), 225–228, 2005.

[48] Textor, M., Tosatti, S., Wieland, M. and Brunette, D. M. Use of Molecular Assembly Techniques For Tailoring the Chemical Properties On Smooth and Rough Titanium Surfaces. In Ellingsen, J. and Lyngstadaas, S., editors, *Bio-Implant Interface: Improving Biomaterials and Tissue Reaction*. CRC Press, 2003.

[49] Wilson, C. J., Clegg, R. E., Leavesley, D. I. and Pearcy, M. J. Mediation of biomaterial-cell interactions by adsorbed proteins: A review. *Tissue Engineering*, **11**(1-2), 1–18, 2005.

[50] Ku, Y., Chung, C. P. and Jang, J. H. The effect of the surface modification of titanium using a recombinant fragment of fibronectin and vitronectin on cell behavior. *Biomaterials*, **26**(25), 5153–5157, 2005.

[51] Bierbaum, S., Beutner, R., Hanke, T., Scharnweber, D., Hempel, U. and Worch, H. Modification of Ti6Al4V surfaces using collagen I, III, and fibronectin. I. Biochemical and morphological characteristics of the adsorbed matrix. *Journal of Biomedical Materials Research Part A*, **67A**(2), 421–430, 2003.

[52] Bierbaum, S., Hempel, U., Geissler, U., Hanke, T., Scharnweber, D., Wenzel, K. W. and Worch, H. Modification of Ti6Al4V surfaces using collagen I, III, and fibronectin. II. Influence on osteoblast responses. *Journal of Biomedical Materials Research Part A*, **67A**(2), 431–438, 2003.

[53] Becker, D., Geissler, U., Hempel, U., Bierbaum, S., Scharnweber, D., Worch, H. and Wenzel, K. W. Proliferation and differentiation of rat calvarial osteoblasts on type I collagen-coated titanium alloy. *Journal of Biomedical Materials Research*, **59**(3), 516–527, 2002.

[54] van den Dolder, J., Bancroft, G. N., Sikavitsas, V. I., Spauwen, P. H. M., Mikos, A. G. and Jansen, J. A. Effect of fibronectin- and collagen I-coated titanium fiber mesh on proliferation and differentiation of osteogenic cells. *Tissue Engineering*, **9**(3), 505–515, 2003.

[55] Slack, S. M. and Horbett, T. A. The Vroman effect - A critical review. In *Proteins at Interfaces Ii*, volume 602 of *Acs Symposium Series*, pages 112–128. Amer Chemical Soc, Washington, 1995.

[56] Morra, M., Cassinelli, C., Cascardo, G., Cahalan, P., Cahalan, L., Fini, M. and Giardino, R. Surface engineering of titanium by collagen immobilization. Surface characterization and in vitro and in vivo studies. *Biomaterials*, **24**(25), 4639–4654, 2003.

[57] Scharnweber, D., Born, R., Flade, K., Roessler, S., Stoelzel, M. and Worch, H. Mineralization behaviour of collagen type I immobilized on different substrates. *Biomaterials*, **25**(12), 2371–2380, 2004.

[58] Mrksich, M. and Whitesides, G. M. Using self-assembled monolayers to understand the interactions of man-made surfaces with proteins and cells. *Annual Review of Biophysics and Biomolecular Structure*, **25**, 55–78, 1996.

[59] Dettin, M., Conconi, M. T., Gambaretto, R., Bagno, A., Di Bello, C., Menti, A. M., Grandi, C. and Parnigotto, P. P. Effect of synthetic peptides on osteoblast adhesion. *Biomaterials*, **26**(22), 4507–4515, 2005.

[60] Xiao, S. J., Textor, M., Spencer, N. D. and Sigrist, H. Covalent attachment of cell-adhesive, (Arg-Gly-Asp)-containing peptides to titanium surfaces. *Langmuir*, **14**(19), 5507–5516, 1998.

[61] Pierschbacher, M. D. and Ruoslahti, E. Cell Attachment Activity of Fibronectin Can Be Duplicated by Small Synthetic Fragments of the Molecule. *Nature*, **309**(5963), 30–33, 1984.

[62] Main, A. L., Harvey, T. S., Baron, M., Boyd, J. and Campbell, I. D. The 3-Dimensional Structure of the 10th Type-Iii Module of Fibronectin - an Insight into Rgd-Mediated Interactions. *Cell*, **71**(4), 671–678, 1992.

[63] Ruoslahti, E. RGD and other recognition sequences for integrins. *Annual Review of Cell and Developmental Biology*, **12**, 697–715, 1996.

[64] Dee, K. C., Andersen, T. T. and Bizios, R. Design and function of novel osteoblast-adhesive peptides for chemical modification of biomaterials. *Journal of Biomedical Materials Research*, **40**(3), 371–377, 1998.

[65] Rezania, A. and Healy, K. E. Biomimetic peptide surfaces that regulate adhesion, spreading, cytoskeletal organization, and mineralization of the matrix deposited by osteoblast-like cells. *Biotechnology Progress*, **15**(1), 19–32, 1999.

[66] Kapyla, J., Jaalinoja, J., Tulla, M., Ylostalo, J., Nissinen, L., Viitasalo, T., Vehvilainen, P., Marjomaki, V., Nykvist, P., Saamanen, A. M., Farndale, R. W., Birk, D. E., Ala-Kokko, L. and Heino, J. The fibril-associated collagen IX provides a novel mechanism for cell adhesion to cartilaginous matrix. *Journal Of Biological Chemistry*, **279**(49), 51677–51687, 2004.

[67] Gunn, J. W., Turner, S. D. and Mann, B. K. Adhesive and mechanical properties of hydrogels influence neurite extension. *Journal of Biomedical Materials Research Part A*, **72A**(1), 91–97, 2005.

[68] Cheng, S., Craig, W. S., Mullen, D., Tschopp, J. F., Dixon, D. and Pierschbacher, M. D. Design and Synthesis of Novel Cyclic Rgd-Containing Peptides as Highly Potent and Selective Integrin Alpha(Iib)Beta(3) Antagonists. *Journal of Medicinal Chemistry*, **37**(1), 1–8, 1994.

[69] Samanen, J., Ali, F., Romoff, T., Calvo, R., Sorenson, E., Vasko, J., Storer, B., Berry, D., Bennett, D., Strohsacker, M., Powers, D., Stadel, J. and Nichols, A. Development of a Small Rgd Peptide Fibrinogen Receptor Antagonist with Potent Antiaggregatory Activity Invitro. *Journal of Medicinal Chemistry*, **34**(10), 3114–3125, 1991.

[70] Schaffner, P. and Dard, M. M. Structure and function of RGD peptides involved in bone biology. *Cellular and Molecular Life Sciences*, **60**(1), 119–132, 2003.

[71] Dalton, B. A., McFarland, C. D., Underwood, P. A. and Steele, J. G. Role of the Heparin-Binding Domain of Fibronectin in Attachment and Spreading of Human Bone-Derived Cells. *Journal of Cell Science*, **108**, 2083–2092, 1995.

[72] Woods, A., Couchman, J. R., Johansson, S. and Hook, M. Adhesion and Cytoskeletal Organization of Fibroblasts in Response to Fibronectin Fragments. *Embo Journal*, **5**(4), 665–670, 1986.

[73] Zreiqat, H., Akin, F. A., Howlett, C. R., Markovic, B., Haynes, D., Lateef, S. and Hanley, L. Differentiation of human bone-derived cells grown on GRGDSP-peptide bound titanium surfaces. *Journal of Biomedical Materials Research Part A*, **64A**(1), 105–113, 2003.

[74] Porte-Durrieu, M. C., Guillemot, F., Pallu, S., Labrugere, C., Brouillaud, B., Bareille, R., Amedee, J., Barthe, N., Dard, M. and Baquey, C. Cyclo-(DfKRG) peptide grafting onto Ti-6Al-4V: physical characterization and interest towards human osteoprogenitor cells adhesion. *Biomaterials*, **25**(19), 4837–4846, 2004.

[75] Senyah, N., Hildebrand, G. and Liefeith, K. Comparison between RGD-peptide-modified titanium and borosilicate surfaces. *Analytical and Bioanalytical Chemistry*, **383**(5), 758–762, 2005.

[76] Pallu, S., Bourget, C., Bareille, R., Labrugere, C., Dard, M., Sewing, A., Jonczyk, A., Vernizeau, M., Durrieu, M. C. and Amedee-Vilamitjana, J. The effect of cyclo-DfKRG peptide immobilization on titanium on the adhesion and differentiation of human osteoprogenitor cells. *Biomaterials*, **26**(34), 6932–6940, 2005.

[77] De Giglio, E., Sabbatini, L., Colucci, S. and Zambonin, G. Synthesis, analytical characterization, and osteoblast adhesion properties on RGD-grafted polypyrrole coatings on titanium substrates. *Journal of Biomaterials Science-Polymer Edition*, **11**(10), 1073–1083, 2000.

[78] Morra, M. On the molecular basis of fouling resistance. *Journal of Biomaterials Science-Polymer Edition*, **11**(6), 547–569, 2000.

[79] Davis, F. F. Commentary - The origin of pegnology. *Advanced Drug Delivery Reviews*, **54**(4), 457–458, 2002.

[80] Pasche, S., Textor, M., Meagher, L., Spencer, N. D. and Griesser, H. J. Relationship between interfacial forces measured by colloid-probe atomic force microscopy and protein resistance of poly(ethylene glycol)-grafted poly(L-lysine) adlayers on niobia surfaces. *Langmuir*, **21**(14), 6508–6520, 2005.

[81] Woodle, M. C., Engbers, C. M. and Zalipsky, S. New Amphipatic Polymer Lipid Conjugates Forming Long-Circulating Reticuloendothelial System-Evading Liposomes. *Bioconjugate Chemistry*, **5**(6), 493–496, 1994.

[82] Golander, C. G., Jonsson, S., Vladkova, T., Stenius, P. and Eriksson, J. C. Preparation and Protein Adsorption Properties of Photopolymerized Hydrophilic Films Containing N-Vinylpyrrolidone (Nvp), Acrylic-Acid (Aa) or Ethyleneoxide (Eo) Units as Studied by Esca. *Colloids and Surfaces*, **21**, 149–165, 1986.

[83] Morra, M. and Cassineli, C. Non-fouling properties of polysaccharide-coated surfaces. *Journal of Biomaterials Science-Polymer Edition*, **10**(10), 1107–1124, 1999.

[84] Yoshikawa, C., Goto, A., Tsujii, Y., Fukuda, T., Kimura, T., Yamamoto, K. and Kishida, A. Protein repellency of well-defined, concentrated poly(2-hydroxyethyl methacrylate) brushes by the size-exclusion effect. *Macromolecules*, **39**(6), 2284–2290, 2006.

[85] Yang, S. Y., Mendelsohn, J. D. and Rubner, M. F. New class of ultrathin, highly cell-adhesion-resistant polyelectrolyte multilayers with micropatterning capabilities. *Biomacromolecules*, **4**(4), 987–994, 2003.

[86] Chen, S. F., Liu, L. Y. and Hang, S. Y. Strong resistance of oligo(phosphorylcholine) self-assembled monolayers to protein adsorption. *Langmuir*, **22**(6), 2418–2421, 2006.

[87] Saeki, S., Kuwahara, N., Nakata, M. and Kaneko, M. Upper and Lower Critical Solution Temperatures in Poly (Ethyleneglycol) Solutions. *Polymer*, **17**(8), 685–689, 1976.

[88] Dalsin, J. L., Lin, L. J., Tosatti, S., Voros, J., Textor, M. and Messersmith, P. B. Protein resistance of titanium oxide surfaces modified by biologically inspired mPEG-DOPA. *Langmuir*, **21**(2), 640–646, 2005.

[89] Barber, T. A., Golledge, S. L., Castner, D. G. and Healy, K. E. Peptide-modified p(AAm-co-EG/AAc) IPNs grafted to bulk titanium modulate osteoblast behavior in vitro. *Journal of Biomedical Materials Research Part A*, **64A**(1), 38–47, 2003.

[90] Barber, T. A., Harbers, G. M., Park, S., Gilbert, M. and Healy, K. E. Ligand density characterization of peptide-modified biomaterials. *Biomaterials*, **26**(34), 6897–6905, 2005.

[91] Harbers, G. A., Gamble, L. J., Irwin, E. F., Castner, D. G. and Healy, K. E.
Development and characterization of a high-throughput system for assessing
cell-surface receptor-ligand engagement. *Langmuir*, **21**(18), 8374–8384, 2005.

[92] Harbers, G. M. and Healy, K. E. The effect of ligand type and density
on osteoblast adhesion, proliferation, and matrix mineralization. *Journal of
Biomedical Materials Research Part A*, **75A**(4), 855–869, 2005.

[93] Healy, K. E., Harbers, G. M., Barber, T. A. and Sumner, D. R. Osteoblast
Interactions with Engineered Surfaces. In Davies, J., editor, *Bone Engineering*,
pages 268–281. EMSSquared Inc., Toronto, 2000.

[94] Garcia, A. J., Collard, D. M., Keselowsky, B. G., Cutler, S. M., Gallant,
N. D., Byers, B. A. and Stephansson, S. N. Engineering of Integrin-Specific
Biomimetic Surfaces to Control Cell Adhesion and Function. In Dillow, A. K.
and Lowman, A. M., editors, *Biomimetic Materials and Design*, pages 29–53.
Dekker, New York, 2002.

[95] Huang, N. P., Michel, R., Voros, J., Textor, M., Hofer, R., Rossi, A., Elbert,
D. L., Hubbell, J. A. and Spencer, N. D. Poly(L-lysine)-g-poly(ethylene gly-
col) layers on metal oxide surfaces: Surface-analytical characterization and
resistance to serum and fibrinogen adsorption. *Langmuir*, **17**(2), 489–498,
2001.

[96] Kenausis, G. L., Voros, J., Elbert, D. L., Huang, N. P., Hofer, R., Ruiz-
Taylor, L., Textor, M., Hubbell, J. A. and Spencer, N. D. Poly(L-lysine)-g-
poly(ethylene glycol) layers on metal oxide surfaces: Attachment mechanism
and effects of polymer architecture on resistance to protein adsorption. *Journal
of Physical Chemistry B*, **104**(14), 3298–3309, 2000.

[97] Tosatti, S., De Paul, S. M., Askendal, A., VandeVondele, S., Hubbell,
J. A., Tengvall, P. and Textor, M. Peptide functionalized poly(L-lysine)-
g-poly(ethylene glycol) on titanium: resistance to protein adsorption in full
heparinized human blood plasma. *Biomaterials*, **24**(27), 4949–4958, 2003.

[98] Tosatti, S., Schwartz, Z., Campbell, C., Cochran, D. L., VandeVondele, S.,
Hubbell, J. A., Denzer, A., Simpson, J., Wieland, M., Lohmann, C. H.,
Textor, M. and Boyan, B. D. RGD-containing Peptide GCRGYGRGDSPG

Reduces Enhancement of Osteoblast Differentiation by Poly(L-lysine graft-poly(ethylene glycol) Coated Titanium Surfaces. *accepted in Journal of Biomedical Materials Research*, **68A**(3), 458–472, 2004.

[99] VandeVondele, S., Voros, J. and Hubbell, J. A. RGD-Grafted poly-l-lysine-graft-(polyethylene glycol) copolymers block non-specific protein adsorption while promoting cell adhesion. *Biotechnology and Bioengineering*, **82**(7), 784–790, 2003.

[100] Boyan, B. D., Lohmann, C. H., Dean, D. D., Sylvia, V. L., Cochran, D. L. and Schwartz, Z. Mechanisms involved in osteoblast response to implant surface morphology. *Annual Review of Materials Research*, **31**, 357–371, 2001.

[101] Schuler, M., Tosatti, S., Hamilton, D. W., Sprecher, C. M., de Wild, M., Brunette, D. M. and Textor, M. A Novel Experimental Setup for Testing Primary Osteoblasts on Non-fouling Peptide-modified Titanium Surfaces. In *19th European Conference on Biomaterials*, Sorrento, Naples, Italy, 2005.

[102] Harris, L. G., Tosatti, S., Wieland, M., Textor, M. and Richards, R. G. Staphylococcus aureus adhesion to titanium oxide surfaces coated with non-functionalized and peptide-functionalized poly(L-lysine)-grafted-poly(ethylene glycol) copolymers. *Biomaterials*, **25**(18), 4135–4148, 2004.

[103] Maddikeri, R., Tosatti, S., Schuler, M., Chessari, S., Textor, M., Richards, R. and Harrs, L. Effect of modifying titanium surfaces with PLL-g-PEG and RGD-functionalised PLL-g-PEG on bacterial adhesion. *Journal of Biomedical Materials Research, submitted*, , 2007.

[104] Groll, J., Fiedler, J., Engelhard, E., Ameringer, T., Tugulu, S., Klok, H. A., Brenner, R. E. and Moeller, M. A novel star PEG-derived surface coating for specific cell adhesion. *Journal of Biomedical Materials Research Part A*, **74A**(4), 607–617, 2005.

[105] Allen, T. M. and Cullis, P. R. Drug delivery systems: Entering the mainstream. *Science*, **303**(5665), 1818–1822, 2004.

[106] Langer, R. Drug delivery and targeting. *Nature*, **392**(6679), 5–10, 1998.

[107] Palmaz, J. C. Intravascular stents in the last and the next 10 years. *Journal of Endovascular Therapy*, **11**, 200–206, 2004.

[108] Serruys, P. and Rensing, B. *Handbook of Coronary Stents*. Verlag Martin Dunitz, 4th edition, 2002.

[109] Sanchez, A. R., Sheridan, P. J. and Kupp, L. I. Is platelet-rich plasma the perfect enhancement factor? A current review. *International Journal of Oral Maxillofacial Implants*, **18**(1), 93–103, 2003.

[110] Puleo, D. A., Kissling, R. A. and Sheu, M. S. A technique to immobilize bioactive proteins, including bone morphogenetic protein-4 (BMP-4), on titanium alloy. *Biomaterials*, **23**(9), 2079–2087, 2002.

[111] Smith, D. J., Chakravarthy, D., Pulfer, S., Simmons, M. L., Hrabie, J. A., Citro, M. L., Saavedra, J. E., Davies, K. M., Hutsell, T. C., Mooradian, D. L., Hanson, S. R. and Keefer, L. K. Nitric oxide-releasing polymers containing the [N(O)NO](-) group. *Journal of Medicinal Chemistry*, **39**(5), 1148–1156, 1996.

[112] Frost, M. C., Reynolds, M. M. and Meyerhoff, M. E. Polymers incorporating nitric oxide releasing/generating substances for improved biocompatibility of blood-contactincy medical devices. *Biomaterials*, **26**(14), 1685–1693, 2005.

[113] Piotrowicz, A. and Shoichet, M. S. Nerve guidance channels as drug delivery vehicles. *Biomaterials*, **27**(9), 2018–2027, 2006.

[114] Ehrbar, M., Djonov, V. G., Schnell, C., Tschanz, S. A., Martiny-Baron, G., Schenk, U., Wood, J., Burri, P. H., Hubbell, J. A. and Zisch, A. H. Cell-demanded liberation of VEGF(121) from fibrin implants induces local and controlled blood vessel growth. *Circulation Research*, **94**(8), 1124–1132, 2004.

[115] Holland, T. A., Tessmar, J. K. V., Tabata, Y. and Mikos, A. G. Transforming growth factor-beta 1 release from oligo(poly(ethylene glycol) fumarate) hydrogels in conditions that model the cartilage wound healing environment. *Journal of Controlled Release*, **94**(1), 101–114, 2004.

[116] Seol, Y., Park, Y., Lee, S., Kim, K., Lee, J., Kim, T., Lee, Y., Ku, Y., Rhyu, I., Han, S. and Chung, C. Enhanced osteogenic promotion around dental implants with synthetic binding motif mimicking bone morphogenetic protein (BMP)-2. *J Biomed Mater Res A*, , 2006.

[117] Catauro, M., Raucci, M., de Marco, D. and Ambrosio, L. Release kinetics of ampicillin, characterization and bioactivity of TiO2/PCL hybrid materials synthesized by sol-gel processing. *J Biomed Mat Res Part A*, , 2006.

[118] Rupp, F., Scheideler, L., Olshanska, N., de Wild, M., Wieland, M. and Geis-Gerstorfer, J. Enhancing surface free energy and hydrophilicity through chemical modification of microstructured titanium implant surfaces. *Journal of Biomedical Materials Research Part A*, **76A**(2), 323–334, 2006.

[119] Buser, D., Broggini, N., Wieland, M., Schenk, R. K., Denzer, A. J., Cochran, D. L., Hoffmann, B., Lussi, A. and Steinemann, S. G. Enhanced bone apposition to a chemically modified SLA titanium surface. *Journal of Dental Research*, **83**(7), 529–533, 2004.

[120] Ferguson, S. J., Broggini, N., Wieland, M., de Wild, M., Rupp, F., Geis-Gerstorfer, J., Cochran, D. L. and Buser, D. Biomechanical evaluation of the interfacial strength of a chemically modified sandblasted and acid-etched titanium surface. *Journal of Biomedical Materials Research Part A*, **78A**(2), 291–297, 2006.

[121] Morra, M., Cassinelli, C., Meda, L., Fini, M., Giavaresi, G. and Giardino, R. Surface analysis and effects on interfacial bone microhardness of collagen-coated titanium implants: A rabbit model. *International Journal of Oral Maxillofacial Implants*, **20**(1), 23–30, 2005.

[122] Morra, M., Cassinelli, C., Bruzzone, G., Carpi, A., Di Santi, G., Giardino, R. and Fini, M. Surface chemistry effects of topographic modification of titanium dental implant surfaces: 1. Surface analysis. *International Journal of Oral Maxillofacial Implants*, **18**(1), 40–45, 2003.

[123] Kroese-Deutman, H. C., Van Den Dolder, J., Spauwen, P. H. M. and Jansen, J. A. Influence of RGD-loaded titanium implants on bone formation in vivo. *Tissue Engineering*, **11**(11-12), 1867–1875, 2005.

[124] Elmengaard, B., Bechtold, J. E. and Soballe, K. In vivo effects of RGD-coated titanium implants inserted in two bone-gap models. *Journal of Biomedical Materials Research Part A*, **75A**(2), 249–255, 2005.

[125] Bernhardt, R., van den Dolder, J., Bierbaum, S., Beutner, R., Scharnweber, D., Jansen, J., Beckmann, F. and Worch, H. Osteoconductive modifications of Ti-implants in a goat defect model: characterization of bone growth with SR mu CT and histology. *Biomaterials*, **26**(16), 3009–3019, 2005.

[126] O'Toole, G. C., Salih, E., Gallagher, C., FitzPatrick, D., O'Higgins, N. and O'Rourke, S. K. Bone sialoprotein-coated femoral implants are osteoinductive but mechanically compromised. *Journal of Orthopaedic Research*, **22**(3), 641–646, 2004.

[127] Germanier, Y., Tosatti, S., Broggini, N., Textor, M. and Buser, D. Enhanced bone apposition around biofunctionalized sandblasted and acid-etched titanium implant surfaces - A histomorphometric study in miniature pigs. *Clinical Oral Implants Research*, **17**(3), 251–257, 2006.

[128] Scacchi, M. The development of the ITI (R) DENTAL IMPLANT SYSTEM - Part 1: A review of the literature. *Clinical Oral Implants Research*, **11**, 8–21, 2000.

[129] Zainuddin, Albinska, J., Ulanski, P. and Rosiak, J. M. Radiation-induced degradation and crosslinking of poly(ethylene oxide) in solid state. *Journal of Radioanalytical and Nuclear Chemistry*, **253**(3), 339–344, 2002.

3

Materials and Methods and Complementary Information

3.1 Poly(**L**-lysine)-*graft*-poly(ethylene glycol)

3.1.1 Synthesis and Characterization

Unfunctionalized PLL-*g*-PEG

Unfunctionalized PLL-*g*-PEG was synthesized according to protocols by [1, 2]. In brief, poly(**L**-lysine) hydrobromide (PLL-HBr) was dissolved in sodium borate buffer and sterilized with a 0.22 μm filter. Succinimide propoinate methoxy-PEG (mPEG-SPA) at a molecular ratio corresponding to a grafting ratio g=3.5 was added and the reaction was allowed to proceed for 6 hours at room temperature. Dialyzation was done first against phosphate buffered saline (PBS, pH 7.4) and then deionized water each for 24 hours before the product was freeze-dried and stored at -20 °C.

Table 3.1: Components used for the synthesis of poly(**L**-lysine)-*graft*-poly(ethylene glycol)

Name	Molecular weight [kDa]	Supplier
PLL-HBr	15.9	Sigma[1]
mPEG-SPA	3.4	Nektar[2]

[1]purchased from Sigma-Aldrich, Buchs, CH.

[2]purchased from Nektar Therapeutics, Bradford, UK.

Peptide-functionalized PLL-*g*-PEG

Table 3.2: Components used for the synthesis of functionalized poly(L-lysine)-*graft*-poly(ethylene glycol)polymers including abbreviations, molecular weights and supplier. Data for PLL and mPEG-SPA can be found in Table 3.1.

Name	Abbreviation	Molecular weight [kDa]	Supplier
NHS-PEG-VS	-	3.4	Nektar[1]
N-acetyl-GCRGYG**RGD**SPG- NH$_2$	RGD	1.222	Schoenmaker[2], JPT[3]
N-acetyl-GCRGYG**RDG**SPG- NH$_2$	RDG	1.222	Schoenmaker[2], JPT[3]
N-acetyl-GCRGYG**KRSR**SPG- NH$_2$	KRSR	1.197	JPT[3], Jerini[4]
N-acetyl-GCRGYG**KSSR**SPG- NH$_2$	KSSR	1.128	JPT[3], Jerini[4]
N-acetyl-GCRGYG**FHRRIKA**SPG- NH$_2$	FHRRIKA	1.578	Jerini[4]
N-acetyl-GCRGYG**RFHARIK**SPG- NH$_2$	RFHARIK	1.578	Jerini[4]
N-actyl-FKGGGPQGIWGQERCG- NH$_2$	Lyspep	1.781	neosystem[5]
NQEQVSPLERCG- NH$_2$	TG	1.358	neosystem[5]

[1]purchased from Nektar Therapeutics, Bradford, UK.

[2]synthesized by Dr. Ronald Schoenmaker, ETH Zurich.

[3]purchased from JPT Peptide Technologies GmbH, Berlin, GER.

[4]purchased from Jerini AG, Berlin, GER.

[5]purchased from neosystem, neoMPS SA, Strasbourg, FRA.

Peptide-functionalized PLL-*g*-PEG was synthesized starting off from the protocol of VandeVondele *et al.* [3]. However, in the course of this thesis some changes

and improvements were introduced. Thus, the protocol presented is the results of a continuous improvement process especially in terms of yield and degree of functionalization. PLL-*g*-PEG/PEG-Lyspep and PLL-*g*-PEG/PEG-TG used for linking growth factors or drug delivery carrier, respectively, were synthesized the same way (for abbreviations: see Table 3.2). All amounts used in this protocol have been optimized for a synthesis of 50-100 mg total weight.

Peptides and NHS-PEG-VS were reacted for 5 min in a salt buffer solution containing 10 mM HEPES (N-(2-hydroxyethyl)-piperazine-N'-2-ethanesulfonic acid; Sigma-Aldrich, Buchs, CH) at pH 8.4. PLL hydrobromide was dissolved in HEPES and added to the reaction. After one hour mPEG-SPA was dissolved in HEPES and added to the final mixture that was stirred for 24 hours at room temperature. 50 μl of β-mercaptoethanol (Fluka, Buchs, CH) was used for quenching and prior to freeze-drying, the mixture was dialyzed against deionized water for 48 hours. Deionized water was changed twice a day. Polymers resulted in a white powder and were kept frozen at -20 °C before use.

Polymer architecture defined through grafting ratio g and amount of functionalization were investigated by nuclear magnetic resonance spectroscopy (NMR; kindly performed by Doris Sutter, NMR service at ETH Zurich) whereas adsorbed mass of polymers and their resistance against non-specific protein adsorption were examined with optical waveguide light mode spectroscopy (see 3.3.1).

3.1.2 Formation of the PLL-*g*-PEG Adlayer (Coating)

Frozen samples of dehydrated PLL-*g*-PEG polymer powders were warmed up to room temperature, dissolved in a salt buffer solution (denoted hereafter as HEPES 2) containing 10 mM HEPES and 150 mM NaCl at pH 7.4 (to reach a final concentration of 0.5 mg/ml) and filter sterilized (0.22 μm filter, Milian, Basel, CH). Functionalized PLL-*g*-PEG polymers were diluted with unfunctionalized PLL-*g*-PEG to prepare the designated peptide surface densities. Substrates were sterilized in an oxygen plasma cleaner for 2 minutes, transferred to a 24 well plate and covered immediately with PLL-*g*-PEG solution (300 μl for smooth samples, 500 μl for SLA discs). Control surfaces (e.g., bare TiO$_2$) were exposed to HEPES2 in order to minimize adventitious contamination on the surface. Substrates were incubated for at least 30 min at room temperature followed by a wash with HEPES2 to re-

move loosely bound PLL-*g*-PEG polymer. HEPES2 was removed not until cells were seeded.

3.1.3   Formation of Growth Factor Modified PLL-*g*-PEG

Frozen samples of PLL-*g*-PEG/PEG-Lyspep powders were warmed to room temperature, dissolved in a salt buffer solution (denoted hereafter as TBS) containing 10 mM Tris and 150 mM NaCl at pH 7.4 (to reach a final concentration of 0.5 mg/ml), filter sterilized (0.22 μm filter, Milian, Basel, CH) and used to coat the surfaces. Substrates were sterilized for 2 min using oxygen plasma and subsequently coated with PLL-*g*-PEG/PEG-Lyspep polymer solutions (300 μl for smooth substrates and 500 μl for SLA discs). Substrates were washed twice with TBS after 30 min, and following reaction mixture, containing 4 μl of the growth factor TG-VEGF (1.3 μg/μl, kindly provided by Dr. Martin Ehrbar, University Hospital of Zurich), 10 μl of 1M CaCl$_2$ (Sigma), 12 μl Thrombin (human Thrombin, Sigma) activated FactorXIII (kindly provided by Dr. Martin Ehrbar, University Hospital of Zurich) and 174 μl TBS, was added to covalently link TG-VEGF to the polymer. The substrates were incubated at 37 °C for 45 min and subsequently washed twice with TBS.

3.1.4   Shelf-life and Stability Investigations

Stability of dehydrated PLL-*g*-PEG coatings after 3 weeks of storage was investigated. SLA CP Ti discs were coated with PLL-*g*-PEG polymer using standard coating protocol. Surfaces were washed twice with HEPES2 and twice with Millipore water prior to dehydration in a vacuum oven for 24 hours (room temperature, 0.01 mbar) and subsequent storage for 3 weeks at ambient lab conditions (room temperature, 40-50% relative humidity, no light). After 3 weeks, half of the samples were rehydrated with HEPES2 for 30 min prior cell seeding with MG63 osteoblast-like cells whereas the other half of the samples were seeded directly. For comparison, freshly prepared PLL-*g*-PEG coated substrates were used. After 7 days, approximately 5 times more MG63 cells were attached on "dry" PLL-*g*-PEG surfaces than on freshly prepared ones, indicating a loss of protein-resistance (Kruskal-Wallis: χ_2^2=34.69, p<0.001, Figure 3.1, 3.2). In addition, cells started to agglomerate preferential on the edges or in the center of "dry" PLL-*g*-PEG surfaces (Figure 3.2). However, a rehydration of the "dry" PLL-*g*-PEG surfaces prior cell seeding resulted in slightly
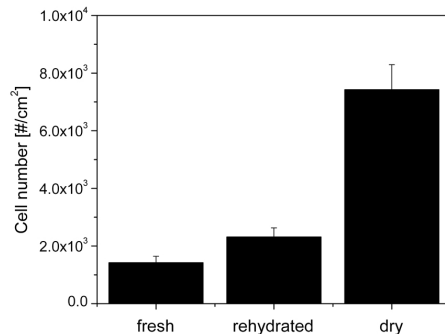
Figure 3.1: MG63 osteoblast-like cell proliferation assay on PLL-*g*-PEG modified SLA CP Ti discs after 7 days. "Fresh" refers to a newly prepared PLL-*g*-PEG coating prior cell seeding; "reyhdrated" and "dry" are PLL-*g*-PEG surfaces that were stored at room temperature for 3 weeks; "rehydrated" samples were incubated with HEPES2 buffer solution prior to cell seeding, while the "dry" samples were not rehydrated before use in cell culture.

higher MG63 cell number in comparison with cells found on freshly prepared coatings but differences were not statistically significant (Tamhane test: p=0.262; Figure 3.1, 3.3).

 In parallel, a stability test was performed using rat calvarial osteoblasts on SLA CP Ti discs and TiO_2/OWLS waveguides that were coated with PLL-*g*-PEG polymer and then subsequently incubated for 1, 7, 14 and 28 days in HEPES2 buffer solution prior use.

OWLS measurement revealed that there were no differences in terms of human serum albumin adsorption on PEGylated TiO_2/waveguides that were incubated for up to 28 days in HEPES2 prior measurement (Kruskal-Wallis:χ_4^2=2.92, p=0.57, Figure 3.4). No differences were also found for rat calvarial osteoblast cell numbers after 24 hours in culture between the 5 precoated and differently stored surfaces (Kruskal-Wallis: χ_4^2=7.31, p=0.12, Figure 3.4).

3.1.5   Wettability

Contact angle measurements were performed on all novel PLL-*g*-PEG polymers to investigate whether functionalization with different peptide sequences had an
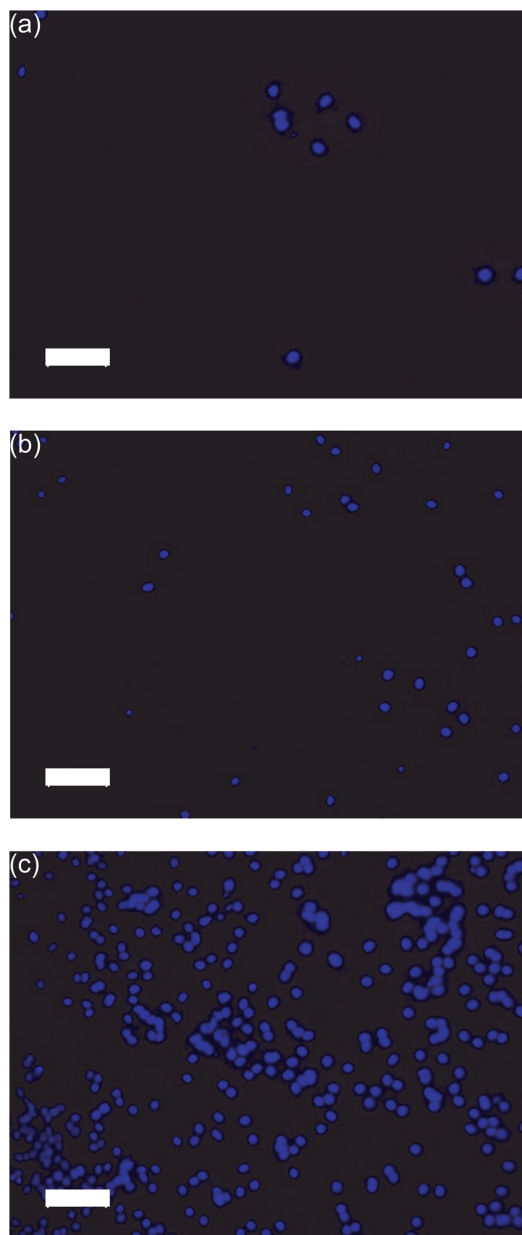
Figure 3.2: MG63 osteoblast-like cells stained for nuclei with DAPI on "fresh" (a), "rehydrated" (b) and "dry" (c) PLL-g-PEG SLA CP Ti surfaces after 7 days in culture. Scale bars correspond to 100 μm.

influence on the surface wettability [4]. TiO$_2$-coated Si wafer were coated with peptide-functionalized PLL-g-PEG polymers using standard protocols. Contact an-
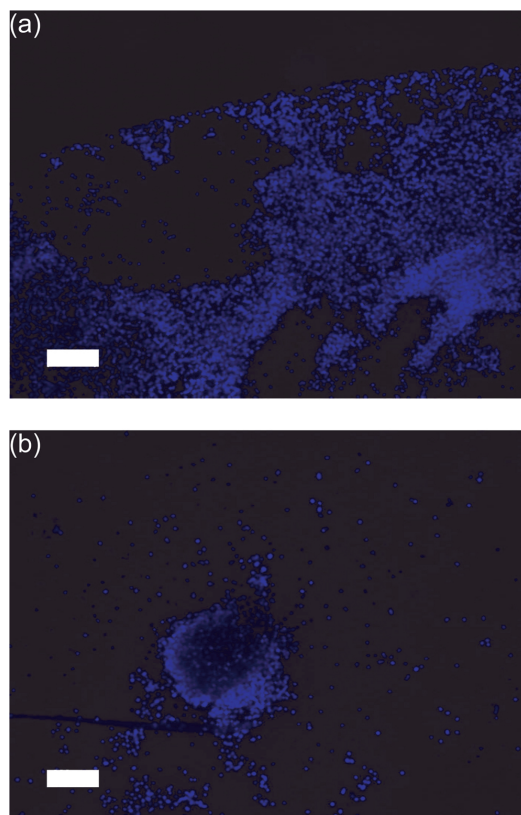
Figure 3.3: MG63 osteoblast-like cells stained for nuclei with DAPI on "dry" PLL-g-PEG SLA CP Ti surfaces after 7 days in culture. Cell agglomerations were visible on the edge of the samples (a) or in the center (b). Scale bars correspond to 200 μm.

gle measurements were performed immediately after drying the coated substrates. No differences were found for advancing and for receding contact angles between the different types of polymers (Figure 3.5).

3.2   Cells

3.2.1   Cell Cultures

In this thesis several, cell culture systems were used (see Table 3.3). They are all extensively described in the "Materials and Method" parts of the corresponding chap-
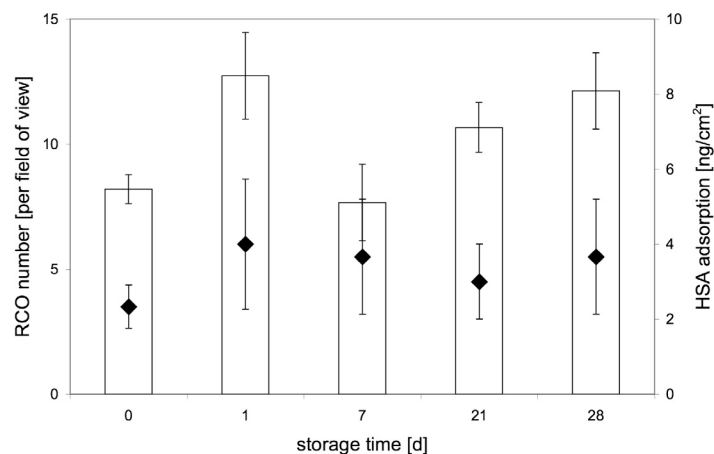
Figure 3.4: (a) Rat calvarial osteoblast (RCO) cell numbers (white bars with left y-axis) after 24 hours in culture found on PLL-g-PEG coated CP SLA Ti substrates that were incubated in HEPES2 buffer solution for 0 (freshly coated), 1, 7, 14 and 28 days at 4 °C. (b) Human serum albumin (HAS) adsorption (black squares with right y-axis) measured with OWLS on PLL-g-PEG coated TiO$_2$/waveguides that were incubated in HEPES2 buffer solution for 0 (freshly coated), 1, 7, 14 and 28 days at 4 °C.
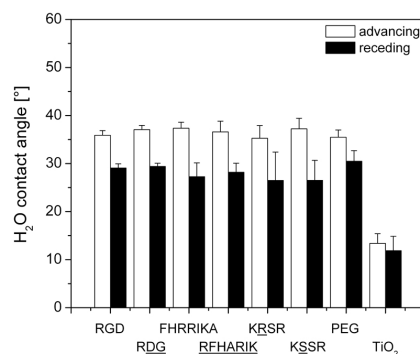
Figure 3.5: Advancing and receding contact angles of a drop of deionized water found on different peptide-functionalized PLL-g-PEG polymer modified smooth titanium substrates in comparison with bare titanium. The total peptide surface density was standardized for 3.0 pmol/cm^2.

ters. Cell types were selected on the basis of tissues that contact dental implants: epithelium (epithelial cells), connective tissue (fibroblasts) and bone (osteoblasts).

Table 3.3: Cell types used within this thesis, their abbreviations, origins, descriptions.

Cell Culture	Abbreviation	Origin	Description and Use
Rat calvarial osteoblasts	RCO	UBC, Brunette lab	Chapters 3, 4, 5, 6
MG63 osteoblast-like cells	MG63	Purchased from ATCC[1]	Chapters 3, 7
Porcine epithelial cells	PEC	UBC, Brunette lab	Chapter 5
Swiss Balb/c 3T3 fibroblasts	3T3	AO Davos	Chapter 5
Human gingival fibroblasts	HGF	UBC, Brunette lab	Chapter 6

[1]American Type Culture Collection (LGC Promochem Sarl, Molsheim Cedex, FRA).

3.2.2 Cell Staining

Protocols for fluorescent staining of focal adhesions (e.g., vinculin) or components of the cytoskeleton (e.g., actin or microtubules) are usually described very vaguely in publications. Thus, the following two protocols, developed in collaboration with Dr. Hamilton (UBC, Vancouver, CAN) [5, 6] are providing all necessary details for obtaining successful labeling of vinculin, F-actin and microtubules of rat calvarial osteoblasts, human gingival fibroblasts or porcine epithelial cells. Note: the reader is strongly recommended to carefully read the data sheet of the chemicals used and to take precautions into account since some of these chemicals are highly toxic or even carcinogenic.

Labeling of Vinculin and F-actin

Vinculin is a cytoskeletal protein (117 kDa) associated with cell-cell and cell-matrix junctions, where it is thought to function as one of several interacting proteins involved in anchoring F-actin (filamentous actin) to the membrane. It is localized to focal adhesions and may carry out its function by stabilizing the interaction between talin and actin and/or the interaction between talin and cell membrane [7]. The actin cytoskeleton is essential for the integrity and movement of all animal cells. Actin polymerization, organization of actin networks, and actin-dependent motor proteins are responsible for cell movements. In addition, vesicles and organelles can move along the actin filaments and actin filaments also form a scaffold for many signalling proteins in the cells [7].

Antibodies and Phalloidin
1° AB Ms x Human Vinculin (Chemicon International, MAB1624)
2° AB Texas Red Goat anti-mouse IgG (H+L) (Molecular Probes, T-862)
Phalloidin FITC labeled (Sigma, P5282), very toxic!

Protocol
How to use the following protocol:

a) Set up appropriate experiments ensuring that a primary delete surface is included (negative secondary antibody control).

b) All the solutions have to be warmed up to room temperature and the incubation also takes place at room temperature unless otherwise stated.

c) for **vinculin** staining only, start with step 1 and skip step 12 and 13

d) for **actin** staining only, do step 1-5 and 13-15

e) for **combined vinculin and actin** use the whole protocol

1. Rinse samples with warm (37 °C) PBS.

2. Fix cells with 3.7% formaldehyde/PBS Note: Freshly prepared 3.7% formaldehyde/PBS solution using paraformaldehyde powder provides even better image quality. Cells can be fixed in advance and stored for a few days in PBS @ at low temperatures.

3. Wash samples 3x with PBS for 5 minutes.

4. Permeabilize cells using 0.5% Triton X-100/PBS for 20 minutes.

5. Wash samples 3x with PBS for 5 minutes.

6. Block unspecific antibody binding using 1% BSA/PBS for 20 minutes.

7. Wash samples with 0.1% BSA/PBS 3 times for 5 minutes.

8. Incubate samples with a 1:200 dilution (in 0.1% BSA/PBS) of the primary antibody (1° AB) for 90 minutes. Note: Place a drop of 30-40 μl on each sample and cover it directly with a piece of parafilm to avoid evaporation or invert sample on a drop of antibody solution.

9. Wash samples 3x with 0.1% BSA/PBS for 5 minutes. Note: Fill enough solution into the well to either remove the parafilm from the sample or remove the sample itself from the tissue culture surface.

10. Incubate samples with a 1:200 dilution (in 0.1% BSA/PBS) of the appropriate secondary antibody (2° AB) for 60 minutes. Note: Start using aluminum foil for all the following steps since the 2° AB is fluorescent (light-sensitive).

11. Fix samples in 3.7% formaldehyde/PBS for 5 minutes to stabilize the antibodies.

12. Go directly to step 14 or continue with F-actin staining. Wash samples 3 x in PBS

13. Incubate with 1:100 dilution (in PBS) of Phalloidin FITC for 60 minutes. Note: No fixation is necessary since Phalloidin reaction is irreversible.

14. Wash samples 10x in PBS.

15. Samples are ready for light microscopy, but can be mounted using mounting media if desired.

Labeling of β-tubulin

Microtubules form the part of the cytoskeleton that gives structure and shape to a cell, serve as conveyor belts moving other organelles through the cytoplasm, are the major components of cilia and flagella, and participate in the formation of spindle fibers during cell division (mitosis). Microtubules can function individually or join with other proteins to create larger structures. These (proto)filaments are composed of linear polymers of tubulin, which are globular proteins, and can increase or decrease in length by adding or removing tubulin proteins [7].

Antibodies
1° AB Mouse x Tubulin Beta (Chemicon International, MAB3408)
2° AB Alexa Fluor 594 Goat anti-mouse IgG2b (γ2b) (Molecular Probes A 21145)

Protocol
How to use the following protocol:

a) Set up appropriate experiments ensuring that a primary delete surface is included (negative secondary antibody control).

b) All the solutions have to be warmed up to room temperature and the incubation also takes place at room temperature unless otherwise stated.

1. Rinse samples with warm (37 °C) PBS.

2. Fix cells in ice-cooled aceton for 20 minutes in a freezer @ -20 °C. Use cold aceton (stored in freezer) and cover well plate with parafilm for incubation. Note: Cells can be fixed in advance and stored for a few days in PBS @ at low temperatures.

3. Wash samples 3x with PBS for 5 minutes.

4. Permeabilize cells using 0.5% Triton X-100/PBS for 20 minutes.

5. Wash samples 3x with PBS for 5 minutes.

6. Block unspecific antibody binding using 1% BSA/PBS for 20 minutes.

7. Wash samples with 0.1% BSA/PBS 3 times for 5 minutes.

8. Incubate samples with a 1:500 dilution (in 0.1% BSA/PBS) of the primary antibody (1° AB) for 90 minutes. Note: Place a drop of 30-40 μl on each sample and cover it directly with a piece of parafilm to avoid evaporation or invert sample on a drop of antibody solution.

9. Wash samples 3x with 0.1% BSA/PBS for 5 minutes. Note: Fill enough solution into the well to either remove the parafilm from the sample or remove the sample itself from the tissue culture surface.

10. Incubate samples with a 1:200 dilution (in 0.1% BSA/PBS) of the appropriate secondary antibody (2° AB) for 60 minutes. Note: Start using aluminum foil for all the following steps since the 2° AB is fluorescent (light-sensitive).

11. Fix samples in 3.7% formaldehyde/PBS for 5 minutes to stabilize the antibodies.

12. Wash samples 10x in PBS.

13. Samples are ready for light microscopy, but can be mounted using mounting media if desired.

3.3 Methods

This section provides information about the principle of the techniques used. Further information can be found in textbooks (since techniques are widely known) and more details about instrumentation and settings are given in the corresponding chapters.

3.3.1 Optical Waveguide Lightmode Spectroscopy

Optical waveguide lightmode spectroscopy (OWLS) is a powerful in situ technique for measuring the adsorption of (macro)molecules onto a surface [8, 9] (Figure 3.6). The functional principle is based on the evanescent electromagnetic field (approximately 200 nm in height) of guided light, generated by coupling laser light into a grated waveguide system. The adsorbed mass is calculated from the change of refractive index in the vicinity of the surface upon adsorption of molecules from solution. By varying the angle of the incident light beam, the polarization modes
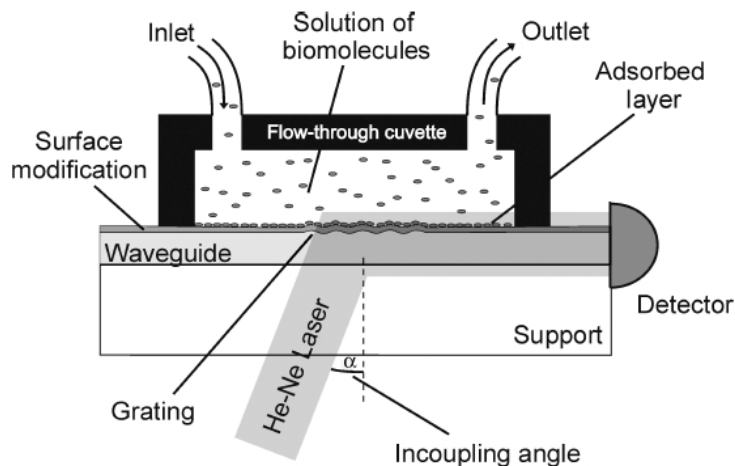
Figure 3.6: Schematic drawing of the OWLS sensor device (see text for details): the incoupling angle α is sensitive to changes in the refractive index of the interfacial layer. Adsorption processes and reactions close to the surface can be monitored in situ and in real time. The substrate (optical chip) has to be transparent. Surface modifications can be applied to the chip according to the particular requirements of the study, e.g., by depositing a thin, transparent oxide film such as titanium oxide, or by the controlled assembly of functional molecules at the oxide surface. Source Titanium in Medicine [10].

transverse electric (TE) and transverse magnetic (TM) can be excited. From the changes of angles of incidence for TE and TM upon molecular adsorption, both the refractive index and the thickness of the adsorbed layer can be calculated. OWLS is a fast and convenient technique for the study of polymer and protein adsorption and its sensitivity is typically 1-2 ng/cm^2. Adsorbed masses m_a were calculated according to deFeijter's approximation:

$$m_a = \frac{n_a - n_c}{d_n/d_c} d_a \qquad (3.1)$$

where n_a and n_c are respectively, the refractive indices of the adsorbed layer and the covering medium. d_n/d_c is the refractive index increment with concentration and d_a the thickness of the adlayer. For this study the d_n/d_c value was set to 0.158 cm^3/g for all PLL-g-PEG based polymers and 0.182 cm^3/g for the serum was used.

3.3.2 Contact Angle

Contact angle (CA) is a very sensitive technique for obtaining information about a surface at the solid/liquid/vapor or solid/liquid/liquid interface. The principle is based on the equilibrium at the three-phase boundary (Figure 3.7).
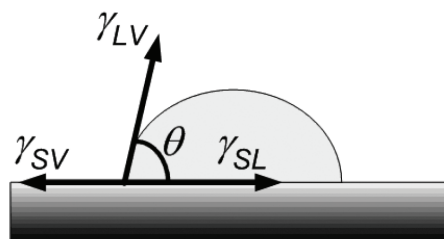
Figure 3.7: Drop of liquid on a solid surface. The interfacial tensions γ_{ij} are related to Young's equation due to the equilibrium at the three-phase boundary (see text).

A drop of liquid on a solid surface will adjust its shape due to the different interfacial tensions until a equilibrium is reached as described by Young's equation:

$$\gamma_{sv} - \gamma_{sl} = \gamma_{lv} cos\theta \tag{3.2}$$

In this study, dynamic contact angle measurements were performed. In brief, a drop of water was placed onto the sample through capillary feeding increasing the static contact angle until a stable contact angle was reached and therefore named as advancing contact angle. Receding contact angles were obtained vice versa through decreasing of the volume. Advancing and receding contact angles as well as their hysteresis are important for the characterization of surface wettability.

3.3.3 X-Ray Photoelectron Spectroscopy

X-Ray Photoelectron Spectroscopy (XPS) also known as ESCA (Electron Spectroscopy for Chemical Analysis) is a very useful method for surface analysis and it has become a standard surface-analytical technique. In brief, a sample is irradiated with monoenergetic soft X-ray (usually from a Mg or Al anode) and the kinetic

energy of the emitted electrons is measured. The photoelectric effect can be written as:

$$E_{kin} = \hbar\nu - \phi - E_{bin} \tag{3.3}$$

where E_{kin} denotes the kinetic energy of the emitted electron, $\hbar\nu$ the energy of the photon and E_{bin} the binding energy of the atomic orbital from which the electron originates. The parameter ϕ corresponds to a combined work function, which is dependent on the work function of the sample and the instrument detection system. Each element has a unique set of binding energies and therefore XPS can be used to identify the type and concentration of the elements at the surface. Even though X-rays penetrate deeply into the material, the emitted photoelectrons escape from the outermost 5-10 nm of the surface only, making XPS a surface sensitive technique (Figure 3.8).

3.3.4   Scanning Electron Microscopy

In a scanning electron microscope (SEM) a focussed electron beam (5-35 kV) of primary electrons is rastered over a sample. Secondary electrons (SE), backscattered electrons (BSE) and X-rays are emitted from its surface and detected for evaluation. Thus a SEM can provide information about surface topography (SE mode), material contrast (BSE mode) or chemical composition (characteristic X-rays). The information depth of this technique is depending on the energy of the electron and varies typically between 8 nm for the SE and 100-1000 nm for the BSE mode. Main advantages of this technique include the large depth of focus (especially in comparison with a light microscope), the high lateral resolution (nm range), the feasibility to study structures with high aspect ratio and the direct production of images of the surface.

3.3.5   Atomic Force Microscopy

Atomic force microscopy (AFM) uses a sharp microfabricated tip to probe the interaction forces between tip and surface. A laser beam impinges on the back of the
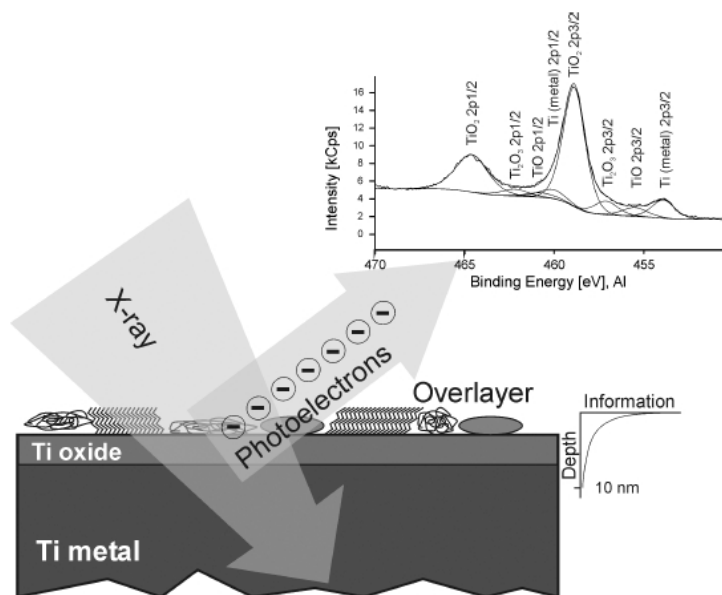
Figure 3.8: Schematic drawing of the X-ray photoelectronic spetroscopy measuring principle (see text for details). A detail spectrum (Ti 2p photoelectrons) of a titanium metal surface covered by a natural titanium oxide film is inserted as an example of the type of analytical/chemical information XPS can provide. The sampling depth is typically around 5–10 nm, slightly larger than the (natural) oxide film thickness of the sample (3–4 nm). The spectrum contains information on the type (titanium valence or oxidation state) and thickness of the oxide film. Source Titanium in Medicine [10].

cantilever (holding the tip) and the reflection is detected with a photodiode (Figure 3.9). Scanning in x and y direction of either sample or tip is performed through high precision piezo-electric devices. Scanning in z direction (also achieved by piezos) is controlled with a closed feedback system, which keeps either distance or the interaction strength between cantilever and sample constant. In general, AFM is used to measure topography or roughness of a surface, but force-distance curves can also provide information on the chemical composition of the surface. One of the main advantages is that AFM can be used in vacuum, under ambient conditions or even in liquids.
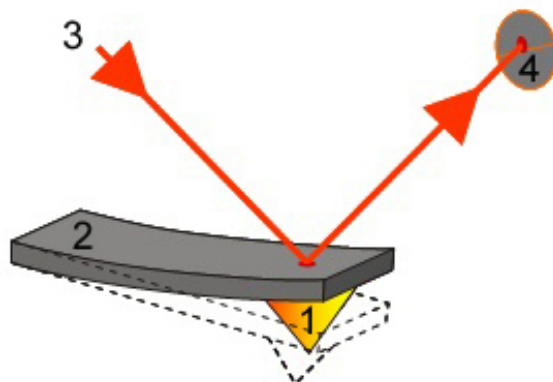
Figure 3.9: Atomic force microscopy principle (see text): (1) microfabricated tip, (2) cantilever. (3) laser beam and (4) photodiode. Source www.physics.leidenuniv.nl

3.3.6   Confocal 3D White Light Microscopy

In contrast to a conventional microscope, a confocal microscope initially creates just a single point (Figure 3.10a), which is taken exactly from the focal plane. To get an optical gauge of the entire surface, the specimen has to be scanned step by step and put together by special software. In this study, the optical illustration of the full surface was done by a rotating disk (Nipkow disk), where pinholes are arranged in spiral form (Figure 3.10b). The light travels through the pinholes and onto the specimen and the returning light passes through the same pinholes. As the disc spins, a defined area of the specimen is illuminated several times in a single rotation. The Nipkow-disk works as illumination and detector hole diaphragm for depth-discrimination. The illumination pinhole is depicted with a microscope objective on the specimen. A beam splitter decouples the reflected light and deflects it towards the detector pinhole located on the focus level of the microscope objective. Therefore, a maximum light level is measured at the detector when the specimen is with the focus of the objective. The 3D height information is obtained by displacing of the movement of the microscope objective with the aid of a piezo. For each height an intensity picture is stored. Therefore, each pixel channel contains the height information of the respective spot on the specimen. This means each single height is a function of its intensity [11, 12].
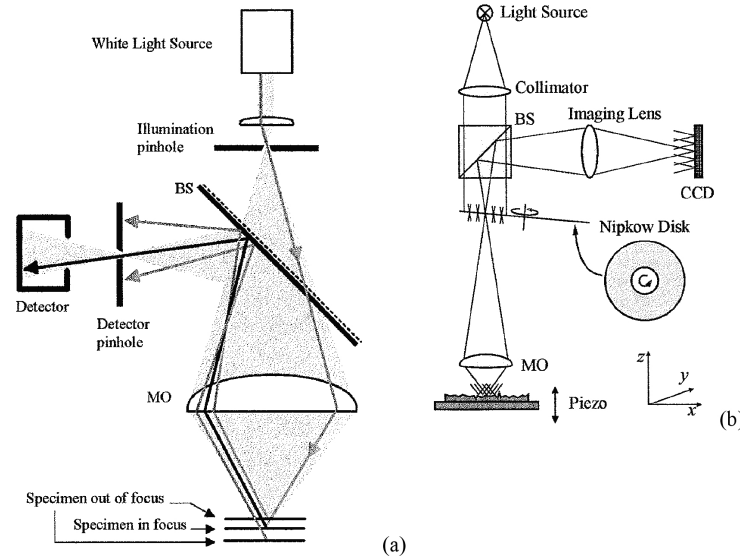
Figure 3.10: (a) Schematic principle of a confocal point distance measurement and (b) setup for obtaining 3D information about surface topographies through the use of a rotating Nipkow disk.

3.3.7   Fluorescence Microscopy

Fluorescence microscopy (FM) is an excellent method for analyzing materials that can be made fluorescent, either by auto fluorescence (natural form) or by labeling with fluorophores (secondary fluorescence). The latter technique is frequently used in biology where labeled antibodies serve as specific reagents for the localization of tissue constituents (immunocytochemistry). The light travels from a powerful light source (e.g., Xe lamp) through a filter set (exciter filter, heat-protection filter, red-attenuation filter and luminous-field diaphragm). The dichroic beam splitter reflects the short-wave exciting light into the sample via the objective. The resulting emission is gathered by the objective and transmitted by the dichroic beam splitter because it exhibits longer wavelengths than the excitation light. The rays then also pass through the emission filter, where the remaining excitation light is filtered out. As usual, the tube lens and the eyepiece form the microscope image, which now only consists of fluorescence light.
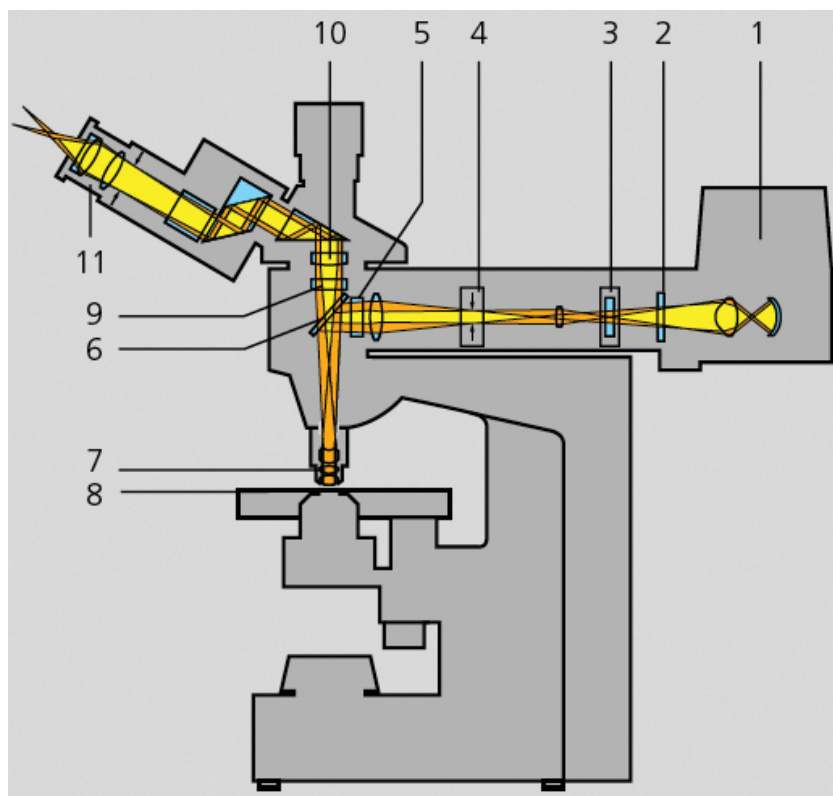
Figure 3.11: Illustration showing the beam path in a fluorescence microscope. The principle is explained in the text. Legend: (1) light source, (2) heat-protection filter, (3) red-attenuation filter/barrier slider, (4) luminous-field diaphragm, (5) exciter filter, (6) beam splitter, (7) objective, (8) specimen (8) sample, (9) emission filter, (10) tube lens and (11) the eyepiece. Source "Microscopy from the very beginning", Zeiss, GER.

Bibliography

[1] Huang, N. P., Michel, R., Voros, J., Textor, M., Hofer, R., Rossi, A., Elbert, D. L., Hubbell, J. A. and Spencer, N. D. Poly(L-lysine)-g-poly(ethylene glycol) layers on metal oxide surfaces: Surface-analytical characterization and resistance to serum and fibrinogen adsorption. *Langmuir*, **17**(2), 489–498, 2001.

[2] Pasche, S., De Paul, S. M., Voros, J., Spencer, N. D. and Textor, M. Poly(L-lysine)-graft-poly(ethylene glycol) assembled monolayers on niobium oxide surfaces: A quantitative study of the influence of polymer interfacial architecture on resistance to protein adsorption by ToF-SIMS and in situ OWLS. *Langmuir*, **19**(22), 9216–9225, 2003.

[3] VandeVondele, S., Voros, J. and Hubbell, J. A. RGD-Grafted poly-l-lysine-graft-(polyethylene glycol) copolymers block non-specific protein adsorption while promoting cell adhesion. *Biotechnology and Bioengineering*, **82**(7), 784–790, 2003.

[4] Senyah, N., Hildebrand, G. and Liefeith, K. Comparison between RGD-peptide-modified titanium and borosilicate surfaces. *Analytical and Bioanalytical Chemistry*, **383**(5), 758–762, 2005.

[5] Hamilton, D. W. and Brunette, D. M. "Gap guidance" of fibroblasts and epithelial cells by discontinuous edged surfaces. *Experimental Cell Research*, **309**(2), 429–437, 2005.

[6] Schuler, M., Owen, G., Hamilton, D. W., de Wild, M., Textor, M., Brunette, D. M. and Tosatti, S. Biomimetic modification of titanium dental implant model surfaces using the RGDSP-peptide sequence: A cell morphology study. *Biomaterials*, **27**(21), 4003–4015, 2006.

[7] Alberts, B., Johnson, A., Lewis, J., Raff, M., Roberts, K. and Walter, P. *Molecular Biology of the Cell*. Garland Science, Taylor Francis Group, New York, 4th edition, 2002.

[8] Voros, J., Ramsden, J. J., Csucs, G., Szendro, I., De Paul, S. M., Textor, M. and Spencer, N. D. Optical grating coupler biosensors. *Biomaterials*, **23**(17), 3699–3710, 2002.

[9] Hook, F., Voros, J., Rodahl, M., Kurrat, R., Boni, P., Ramsden, J. J., Textor, M., Spencer, N. D., Tengvall, P., Gold, J. and Kasemo, B. A comparative study of protein adsorption on titanium oxide surfaces using in situ ellipsometry, optical waveguide lightmode spectroscopy, and quartz crystal microbalance/dissipation. *Colloids and Surfaces B-Biointerfaces*, **24**(2), 155–170, 2002.

[10] Textor, M., Sittig, C., Frauchiger, V. M., Tosatti, S. G. P. and Brunette, D. M. Properties and biological significance of natural oxide films on titanium and its alloys. In Brunette, D. M., Tengvall, P., Textor, M. and Thomsen, P., editors, *Titanium in Medicine*, pages 171–230. Springer-Verlag, Berlin Heidelberg, 2001.

[11] Semwogerere, D. and Weeks, E. Confocal Microscopy. In *Encyclopedia of Biomaterials and Biomedical Engineering*, pages 1–10. 2005.

[12] Kagerer, B., Brodmann, R., Valentin, J., Filzek, J. and Popp, U. 3D-confocal microscopy for surface analysis of microstructured materials. In *Proc. SPIE*, volume 4773, pages 52–62. 2002.

4

Fabrication of TiO$_2$-coated Epoxy Replicas with Identical Dual-type Surface Topographies for Use in Cell Culture Assays

Martin Schuler, Tobias P. Kunzler, Michael de Wild, Christoph M. Sprecher, Diana Trentin, Donald M. Brunette, Marcus Textor, Samuele G. P. Tosatti

The goal of this study was to reproducibly generate samples with complex surface topographies and chemistries identical to a "master surface" and to test their response in cell culture using rat calvarial cells. Negative replicas of dual-type topography were fabricated using dental impression material with half of the surface exhibiting smooth and rough topography, respectively. Positive epoxy resin replicas were cast from the same negative replica eight times consecutively and coated with a 60 nm thin film of titanium dioxide using a vapor deposition technique. Atomic force microscopy, scanning electron microscopy, confocal white light microscopy and X-ray photoelectron spectroscopy, all indicated that TiO$_2$-coated epoxy replicas had surface topographical features and surface compositions nearly indistinguishable from the original titanium master surfaces. The described technique showed high reproducibility over at least eight generations of replication using the same negative replica. Rat calvarial osteoblasts proliferated just as well on dual topography surfaces as on single topography

surfaces. The advantage of the dual-type substrates is that they facilitate comparison within a single culture dish thus eliminating dish-to-dish variation as well as saving material, time and costs compared to the usual method of evaluating surfaces in separate dishes.

Keywords: Titanium, surface roughness, replica, physical vapor deposition, cell morphology.

4.1 Introduction

Surface topography has been shown to be an important characteristic that directly affects cell responses [1] including attachment and adhesion [2, 3], morphology [4], proliferation [5], differentiation [6] and orientation [7, 8]. Thus, for systematic understanding of cell responses, surfaces with well-defined physicochemical properties are a crucial prerequisite in the design of new implant materials. Diverse fabrication methods have been used, such as micromachining, particle blasting, plasma spraying and particle blasting combined with acid etching [9–14] to produce rough metallic surfaces with stochastic micro- and nanoroughness [8, 15]. Another approach for surface modification is microfabrication that creates geometrically defined microstructures typically used for the study of single cells in the laboratory [15–17]. However, some of the techniques above can alter surface charge, surface energy or surface chemistry [11]. Massaro *et al.*, for example, have found in the case of commercially manufactured titanium dental implants a variety of elements and chemical compounds not related to the metal composition [18]. Besides the usually time-consuming and cost-intensive fabrication methods, another important drawback is that the surface topographies obtained differ from sample to sample due to the random character of the techniques applied, or, as in the case of microfabrication, typically only a limited number of substrates is available.

One way to overcome the variability between sample topographies and to produce a large number of samples with surface properties as identical as possible, is the use of an epoxy resin-based replica technique as described, for example, by Wieland *et al.* [13]. This replica process consists of three steps: (1) cast of a negative replica from a master substrate (Figure 4.1a), (2) cast of a (positive) epoxy replica from the negative (Figure 4.1b), and (3) coating of the epoxy replica with a relevant thin metal or metal oxide film.

The advantage of this system is that only one master sample is needed and, therefore, all the produced replicas will have identical surface topography. As a result, the reproducibility of standard cell culture assays on structured surfaces can be increased. Furthermore, the replica technique allows the combination of different surface topographies (from different master samples) on one substrate (Figure 4.2a). This opens new windows in designing cell culture assays since, up to now, most studies on cell behavior have used samples with only one type of topography on the same surface. A third aspect is that this approach allows the production of surfaces with identical surface topographies but different chemical composition as there is a wide range of materials that can be deposited in a controlled manner on smooth and rough substrates.

Although the use of the epoxy replica technique is not entirely new, (see for example [13, 19–27]) in this study, we describe for the very first time the production and use of samples with two different topographies (dual-type) on the same specimen (Figure 4.2a). Moreover, as the fidelity of the replica technique for multiple uses of the same negative impression is unknown, we tested the reproducibility of eight consecutive generations of TiO_2-coated dual-type epoxy substrates using scanning electron microscopy (SEM), confocal white light microscopy (CWLM) and X-ray photoelectron spectroscopy (XPS). The micro- and nano-scale roughness of negative samples and epoxy replicas were determined with atomic force microscopy (AFM). In order to test cell response to the TiO_2-coated dual-type vs. single-type topography substrates we investigated the proliferation and morphology of rat calvarial osteoblasts (RCO) after 24 hours of incubation time.

4.2 Materials and Methods

4.2.1 Production of TiO_2-coated Epoxy Replicas

Impression of Negatives

Commercially pure (CP) titanium discs exhibiting the so-called SLA surface (particle-blasted and acid-etched; manufactured by Straumann, Basel, Switzerland) were chosen as model surfaces for a rough topography. The SLA surface is a type of topography widely used in titanium dental implants for improved osseointegration.
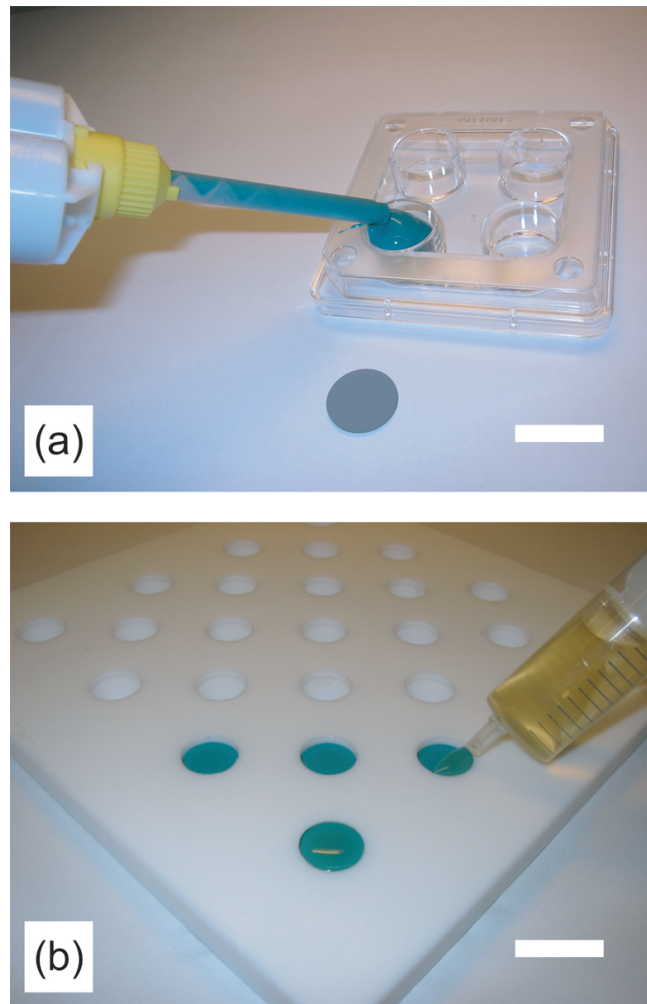
Figure 4.1: Overview of the two casting steps of the epoxy replica process. (a) Cast of vinyl polysiloxane negative replica from a master SLA CP Ti substrate (hidden). For comparison, another SLA CP Ti disc lies besides the 4-well plate. (b) Cast of (positive) epoxy replica from vinyl polysiloxane negative. Negative replicas were inserted in a PTFE form to reproduce the macroscopic shape with plane-parallel surfaces, constant thickness and diameter. Scale bars correspond to 20 mm for both images.
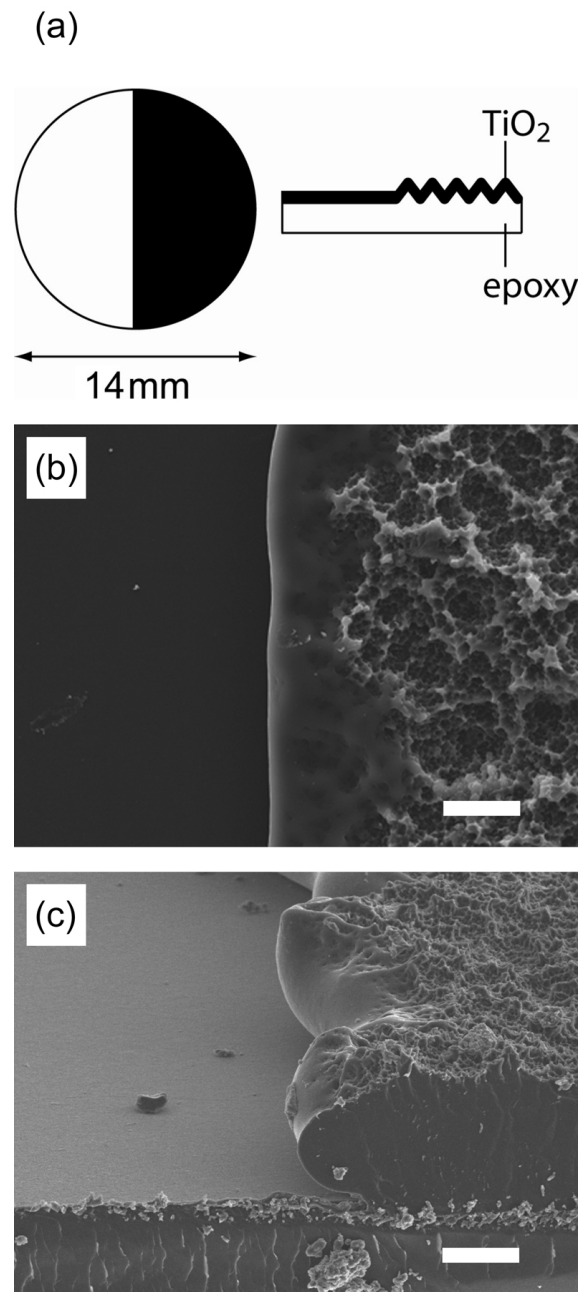
Figure 4.2: (a) Idealized view of a smooth/SLA replica sample with half smooth, half SLA surface topography, coated with a thin layer of TiO_2. Top (b) and side (c) view of a scanning electron micrograph of a TiO_2-coated epoxy replica at the interface smooth/SLA. The epoxy replica in (c) was fractioned using cryo-fracture technique to allow a cross-sectional view. Scale bars for images (b) and (c) correspond to 20 μm.

Its duplex surface structure is obtained through a blasting process with fractured corundum particles (particle size 250-500 μm) in a first step and a subsequent acid-etching treatment using a mixture of hot $HCl/H_2SO_4/H_2O$ (1:8:1) [28].

Negative replicas of a SLA CP Ti disc were taken (Figure 4.1a) using vinyl polysiloxane (PROVIL novo Light, Heraeus-Kulzer, Switzerland). The siloxane dental impression material was forced into the small cavities with the use of pressurized N_2 (5.0 quality, PanGas, Switzerland; 0.22 μm filtered) and dried at room temperature for 10 min. The obtained negative replicas were cut in half and placed face down in a 24 well plate (NUNC, Milian, Basel, Switzerland). The uncovered half of the well plate surface (tissue culture polystyrene (TCPS)) served as master for the smooth topography and was backfilled with additional impression material. These vinyl polysiloxane samples were used as negative replicas to cast epoxy-resin (see next section). Several negative replicas from the same master SLA sample were produced to fabricate a larger number of samples in parallel. All negative replicas were degassed at room temperature for 24 hours to remove trapped gas that may interfere with the epoxy-resin cast resulting in undesirable bubble formation. Quality of negative replicas and potential contamination of the master sample with dental impression material was surveyed using light microscopy.

Cast of Epoxy Replica

Negatives replicas were inserted (from the bottom) in a polytetrafluoroethylene (PTFE) template and cleaned with a flow of pressurized N_2. Epoxy resin (EPO-TEK 302-3M; Epoxy Technology, Polyscience AG, Switzerland) was poured into the designated holes with a diameter of 14 mm (Figure 4.1b) and the surplus wiped off with a PTFE ruler to ensure plane-parallel samples with a thickness of 2 mm. The whole set was dried overnight at room temperature and for subsequently three days in an oven at 60 °C. Baked epoxy samples were removed and dismantled from the negatives. Vinyl polysiloxane negatives were ultrasonically cleaned in Millipore water (18 MΩcm) for 10 minutes, dried under a nitrogen atmosphere and used for the production of further generations of epoxy replicas (up to a total of 8 casts).

Coating with TiO$_2$

Epoxy replicas were ultrasonicated with 2% Hellmanex (HELLMA GmbH Co. KG, Müllheim, Germany) in Millipore water for 15 min and extensively rinsed for 10 times with H$_2$O. Samples were dried with pressurized N$_2$ and sterile packed under laminar flow before coating. Clean epoxy substrates were coated with a thin film (60 nm) of titanium dioxide using physical vapor deposition technique (PVD, reactive magnetron sputtering, Paul Scherrer Institute, Villigen, Switzerland).

4.2.2 Characterization of TiO$_2$-coated Epoxy Replicas

Atomic Force Microscopy

Nano-scale roughness on smooth commonly used model surfaces (TCPS, polished CP Ti disc and TiO$_2$-coated Si wafer) and TiO$_2$-coated epoxy replicas was measured with a Nanoscope IIIa (Digital Instruments, Santa Barbara, CA, USA) in contact mode using a Si$_3$N$_4$ tip (60 mN/m). The scanned area was 10 μm x 10 μm.

Confocal White Light Microscopy

Surface roughness of a SLA CP Ti disc and its TiO$_2$-coated epoxy replicas was quantitatively measured using confocal 3D white light microscopy (μSurf, NanoFocus AG, Oberhausen, Germany) over an area of 770 μm x 770 μm. Data were evaluated with Matlab software (Version 7.0.4 R14 for Mac OS X). For analysis, a plane fit was applied to the whole data set and then individual profiles were fitted with a polynomial of degree four [25]. The roughness parameters were calculated for each profile according to DIN EN ISO 4288-98.

Scanning Electron Microscopy

Surface topography was qualitatively examined using scanning electron microscopy (Hitachi S-4100, Hitachi, Japan) in the secondary-electron mode. The samples were coated with a 10 nm thin layer of carbon to minimize negative charge accumulation on the surface. Images were taken at a voltage of 5 kV and an emission current of 45 μA. The samples were divided using cryo-fracture technique for the investigation

of the TiO$_2$-film and the interface between smooth and SLA topography of the dual-type epoxy replicas. Therefore, a small cut (approx. 0.5 mm deep; perpendicular to the orientation of the interface smooth/SLA) from the backside was made using a saw. After 2 min incubation in liquid nitrogen, the sample was broken along the cut by hitting the backside edge on a hard table. This allowed a clean cut through the replica without damaging the titanium dioxide film.

X-Ray Photoelectron Spectroscopy

Surface chemistry was analyzed using X-ray photoelectron spectroscopy. All substrates were cleaned prior the measurements using an oxygen plasma (Harrick Plasma Cleaner/Sterilizer PDC-32G, Ossining, NY, USA) for 2 min. Spectra were recorded with a SAGE 100 system (Specs, Berlin, Germany) using non-monochromatized Al Kα radiation at 320 W (13 kV). Electron-energy analyzer pass energy was 50 eV for low-resolution surveys and 14 eV for high-resolution detailed scans. The take-off angle was 90° and the analyzed area was 6 mm^2 (see [29] for further details). The quantification of the spectra was carried out by dividing the integral area through the appropriate sensitivity coefficient [30].

4.2.3   Cell Experiments

Cell Culture

Osteogenic cells, obtained from newborn rat calvariae, were isolated and subcultured as published by Hasegawa *et al.* [31] and Chehroudi *et al.* [27]. Cells were removed with trypsin solution, diluted with Dulbecco's modified eagles medium (DMEM) supplemented with 10% fetal calf serum and 1% antibiotic/antimycotic (all purchased from Invitrogen, Basel, Switzerland) to obtain the desired cell seeding concentration of 10^4 cells/cm^2. All substrates were cleaned and sterilized in an oxygen plasma for 2 min prior cell seeding. The whole set of surfaces with attached cells was incubated for 24 hours at 37 °C in a humidified atmosphere of 93% air and 7% CO$_2$.

Fluorescent Labeling

Cells were double-stained for actin and nuclei. Samples were rinsed with warm 10 mM PBS (Sigma-Aldrich, Buchs, Switzerland) and fixed in 3.7% paraformaldehyde/PBS (Sigma-Aldrich) for 15 minutes. Cells were permeabilized using 0.5% Triton-X/PBS (Sigma-Aldrich) for 3 minutes and incubated with Alexa 488 (1:400 dilution in PBS; Invitrogen) for 30 min and after a wash exposed to DAPI (1:1000 dilution in PBS; Invitrogen).

Observation Methods

Osteoblast cell number and morphology were investigated with an epi-fluorescence microscope (Axioskop Imager M1m, Zeiss, Germany). A 10x objective was used for cell number and a 40x for cell morphology investigations. An overview image was created with a motorized stage (xy-table, 75 mm x 50 mm, Zeiss) and Mosaix software (Version 4.5.3 for Windows XP, Zeiss). Five random images of each surface topography (smooth and SLA) were taken for each sample. For the cell morphology evaluation, at least 30 single cells were randomly chosen and mapped. All images were analyzed with ImageJ software (Version 1.32i for Mac OS X).

4.2.4 Analysis of Cell Morphology

The morphology of cells was described by measuring the footprint area after attachment on the surface using a shape factor Φ which is defined as [4]:

$$\Phi = \frac{4\pi A}{p^2} \tag{4.1}$$

A is the footprint area and p the perimeter of the cell. A shape factor of 1 represents a perfect circle, whereas a thin thread-like object would have the lowest shape factor near 0.

4.2.5 Statistics

Comparisons between measurement series of the roughness values were made using nonparametric tests due to small sample sizes. Cell data was analyzed using para-

metric tests (SPSS 11.4 for Mac OS X). All mean values are shown $\pm$ SE (standard error). We set our level of significance at 0.05.

4.3   Results

4.3.1   Epoxy Replicas

Nano-scale Roughness of Smooth Surfaces

Roughness values measured with AFM of a standard tissue culture polystyrene surface were compared with other commonly used cell culture surfaces (Table 4.1). The TCPS surface was found to be slightly "smoother" than a polished CP titanium disc, a model substrate used in a previous publication of Wieland *et al.* [13], whereas the TiO₂-coated epoxy replica of the TCPS surface showed roughness values comparable with the ones of polished titanium.

Table 4.1: Roughness parameters R_a and R_q of smooth surfaces, typically used in cell culture assays, measured with atomic force microscopy on a 10 x 10 μm^2 area.

Surface	R_a	R_q
Tissue culture polystyrene (TCPS)[a]	2.30 ± 0.20 nm	2.80 ± 0.20 nm
Epoxy replica coated with 60 nm TiO₂[b]	2.66 ± 0.31 nm	3.33 ± 0.42 nm
Si wafer coated with 60 nm TiO₂	0.44 ± 0.02 nm	0.60 ± 0.03 nm
Polished CP titanium disc	2.50 ± 0.57 nm	3.35 ± 0.96 nm

[a]Master surface for replicating the smooth topography; mean values of 3 samples.

[b]Mean values of eight consecutive casts using the same negative replica.

R_a: arithmetic average of absolute values of all points of the profile.

R_q: root mean square of values of all points of the profile.

Characterization of the Topographical Features of SLA

The surface of the SLA CP Ti disc (Figure 4.3a) and its eight consecutive replicas (produced with the same vinyl polysiloxane negative) were assessed with SEM

and showed identical topographies (Figure 4.3b-d). However, a comparison at higher magnification (15'000 x) between SLA CP Ti disc images (Figure 4.3e) and its replicas (Figure 4.3f-h) showed a slightly "smoother" structure at the submicron range for the replicas.

The roughness values R_a (Mann-Whitney: U=2.0, p=0.068), R_q (U=5.0, p=0.201), R_z (U=3.0, p=0.100) of TiO_2-coated epoxy replicas with SLA topographies were similar to values found on the original SLA CP Ti disc, except for S_m (U=0.0, p=0.028). Additionally, low coefficients of variability (CV<4%) demonstrated that the replicas did not change significantly between eight consecutive casts (Table 4.2).

Table 4.2: Roughness values R_a, R_q, R_z, and S_m of a SLA commercially pure titanium disc and its eight TiO_2-coated epoxy replica measured with confocal white light microscopy on a 770 x 770 μm^2 area.

Surface	R_a [µm]	R_q [µm]	R_z [µm]	S_m [µm]
SLA CP Ti disc [a]	3.90 ± 0.08	4.93 ± 0.06	18.33 ± 0.15	32.76 ± 0.63
Epoxy replica coated with 60 nm TiO_2 [b]	4.08 ± 0.04	5.10 ± 0.05	19.30 ± 0.18	28.65 ± 0.46

[a]Mean values of 3 samples.

[b]Mean value of eight consecutive casts using the same negative replica.

R_a, R_a: see Table 4.1 for explanations.

R_z: arithmetic average of maximum peak-to-valley height.

S_m: arithmetic average spacing between falling flanks of peaks on mean line.

Interface Smooth-SLA of Dual-type Replicas

The interface between the smooth and the SLA part of the dual-type replica was investigated by SEM. An approximately 50-60 μm wide border area was found to consist of a mixture of smooth and SLA topography (Figure 4.2b). Observing the sample at an angle in the SEM, the difference in height (step) between the smooth and the SLA part of the replica could be estimated to be 50 μm (Figure 4.2c).
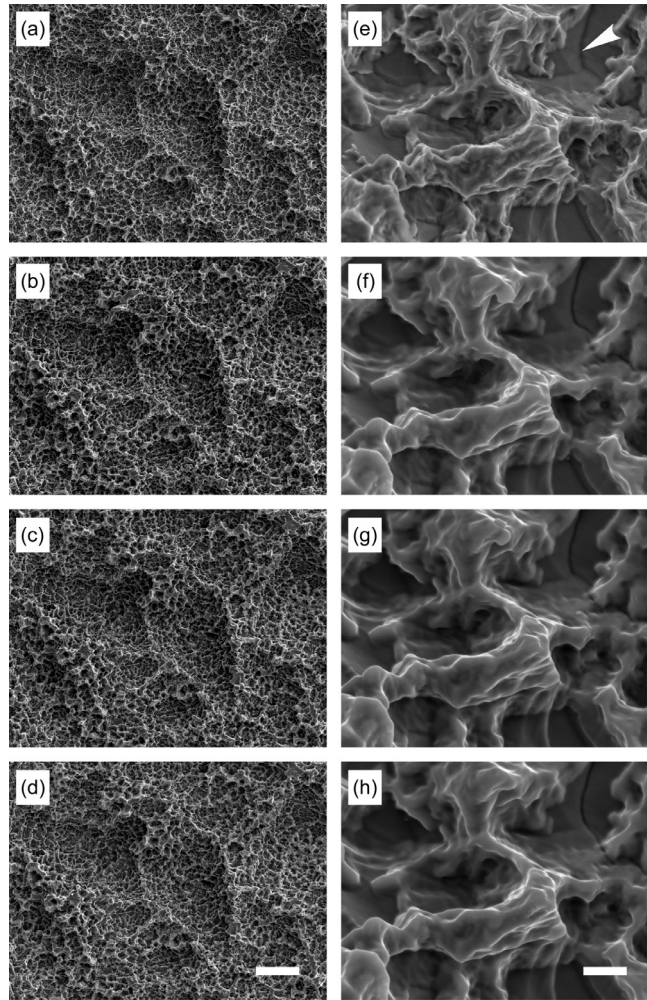
Figure 4.3: Scanning electron micrograph of a SLA commercially pure titanium disc (a, e) and its first (b, f), fourth (c, g) and eight (d, h) consecutive cast of epoxy resin. All epoxy replicas were manufactured using the same vinyl polysiloxane negative and were coated with a 60 nm thin film of titanium dioxide. A mechanical mark on the master substrate was used to find exactly the same area/position in the SEM. The arrow in (e) indicates a grain boundary. Scale bars correspond to 15 μm for (a-d) and 1 μm for (e-h).

Characterization of the TiO$_2$-film of Replicas

The physical-vapor-deposited TiO$_2$ film observed on the epoxy replicas was found to be homogenous for both surface topographies, smooth (Figure 4.4a) and SLA (Figure 4.4b). There were no visible surface defects in the TiO$_2$-layer. The thickness of the film was estimated to be approximately 60 nm by SEM.

Surface-chemical analysis by XPS of TiO$_2$-coated epoxy replicas showed pure titanium oxide (Table 4.3). The Ti/O ratio of TiO$_2$-coated replicas (0.34) was comparable with to ones found for TiO$_2$-coated Si wafers (0.36) but slightly lower than the ones measured for SLA CP Ti discs (0.41).

Table 4.3: XPS elemental concentrations of TiO$_2$-coated epoxy replica, TiO$_2$-coated Si wafer and commercially pure titanium SLA disc measured on a 6 mm^2 area.

| Element [a] | Smooth surfaces | | SLA surfaces | |
	TiO$_2$-coated epoxy replica	TiO$_2$-coated Si Wafer	TiO$_2$-coated epoxy replica	CP Ti disc
Ti [at%]	23.0 ± 0.1	25.5 ± 1.3	22.7 ± 1.1	26.8 ± 1.3
O [at%]	68.2 ± 0.9	70.8 ± 0.9	66.9 ± 0.9	65.8 ± 0.9
C [at%]	8.8 ± 0.2	3.7 ± 0.1	10.4 ± 0.2	7.3 ± 0.1

[a]Mean values of 3 samples.

4.3.2   Osteoblast Experiments

The numbers of osteoblasts attached after 24 hours ($t_{(36)}$=0.167, p=0.868; Figure 4.5a), their footprint areas ($t_{(159)}$=0.201, p=0.841; Figure 4.5b) and shape factors ($t_{(159)}$=0.307, p=0.759; Figure 4.5c) on smooth TiO$_2$-coated replicas with single topography were similar to the ones found on the smooth part of the TiO$_2$-coated dual-type substrates. The same correspondence was found for the SLA surfaces (numbers of osteoblasts: $t_{(43)}$=-0.134, p=0.868; footprint areas: $t_{(124)}$=-0.212, p=0.833; shape factors: $t_{(124)}$=-0.307, p=0.759).

 Significantly more osteoblasts were attached to SLA than smooth surfaces through-
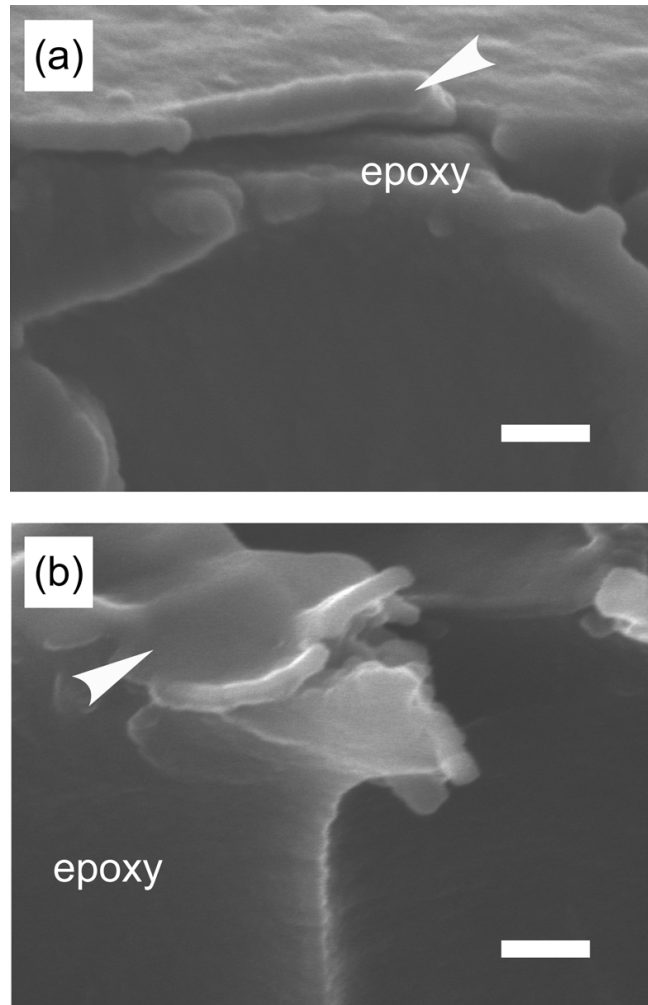
Figure 4.4: Scanning electron micrograph of the physical vapor deposited titanium oxide layer (marked by arrow) of an epoxy replica found on (a) the smooth and (b) on the SLA topography surface. The epoxy replica was fractioned using cryo-fracture technique to expose the titanium layer. Scale bars correspond to 300 nm for both images.
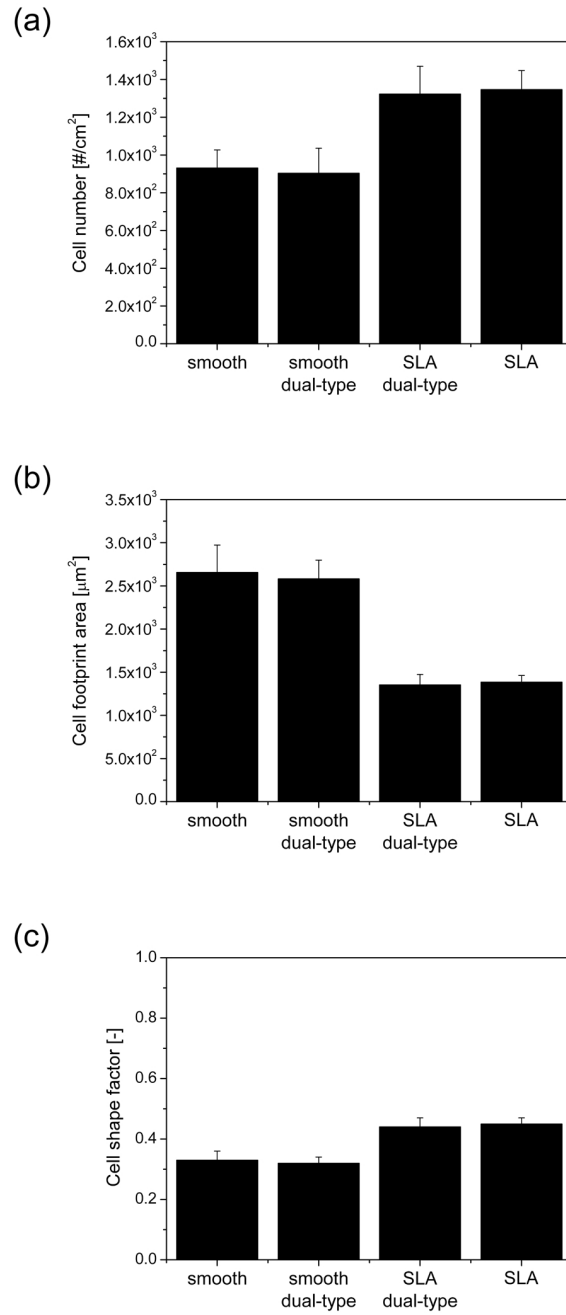
Figure 4.5: Cell number (a), cell footprint area (b) and cell shape factor (c) of rat calvarial osteoblasts on dual-type vs. single smooth and single SLA substrates. All substrates were manufactured via the epoxy replica technique and coated with a 60 nm thin film of titanium dioxide.

out the test set ($F_{(3,79)}$=4.387, p=0.007; Figure 4.5a). Mean osteoblast footprint areas were larger on smooth compared to SLA topographies ($F_{(3,283)}$=6.129, p<0.001; Figure 4.5b). Osteoblasts on SLA surfaces were more circular, i.e., they had higher mean cell shape factor compared to smooth substrates ($F_{(3,283)}$=9.738, p<0.001; Figure 4.5c).

4.4 Discussion

4.4.1 Master Substrates, Negatives and Their Replicas

Roughness values for the smooth TCPS surface were lower than those from polished CP Ti (Table 4.1) indicating that the chosen TCPS surface can be used as a reasonably "smooth" master surface for the replication process. Moreover, the TiO₂-coated epoxy replica had similar roughness values as the polished titanium surface, a "smooth" substrate commonly used in cell culture assays [13]. Curtis *et al.* [32] have reported that cells can react to objects as small as 5 nm, a value that is slightly larger than the mean roughness values of all the substrates as summarized in Table 4.1, suggesting that the cells should consider these surfaces as "smooth".

The described technique of "backfilling" half a SLA negative sample (that is lying upside down in a 24 well plate) with additional impression material had the consequence that some impression material flow slightly underneath the negative due to the (from the side) open SLA structure. Indeed, when considering the interface between smooth and SLA of a TiO₂-coated epoxy replica, a zone of approximately 50-60 μm in width with a mix of smooth and SLA topography was visible (Figure 4.2b). Additionally, a difference in height between these two topographies of approximately 50 μm was also observed (Figure 4.2c). One way to (partially) overcome this problem would be the design of a master substrate with both topographies on the same surface, for example through exact alignment of two substrates by means of tools used in photolithography. Such a sample might be quite difficult and also highly expensive to fabricate; also, combining a rough surface such as SLA with a smooth one always results in a small step (at most in the range of R_z≈20 μm; see Table 4.2) at the interface. This mixed zone, however, was small (50-60 μm) compared to the dimensions of the entire sample (14 mm in diameter) and, therefore, should be of only minor influence in standard cell culture assays. Additionally, the
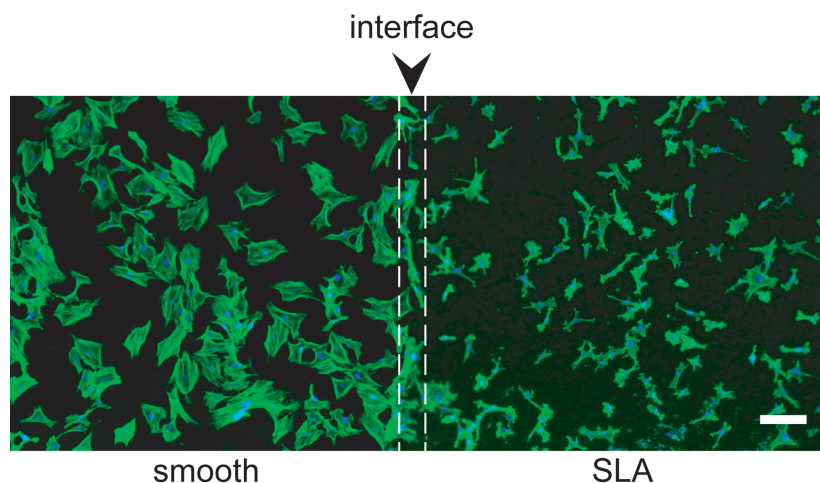
Figure 4.6: Fluorescence microscope image of rat calvarial osteoblasts stained for actin (green) and nuclei (blue) on a TiO$_2$-coated epoxy replica with half smooth (left) and half SLA (right) topography (arrow and white lines indicate the interface). Scale bar corresponds to 100 μm.

step between the smooth and the SLA topography was negligible when using light microscopy techniques, since the magnifications used to map both surface topographies at the same time in one image were usually low (4-10 x) and, therefore, always in the same depth of focus. Furthermore, when working with a position-controlled stage to image a large area of the sample (including the interface) each single picture can be taken with appropriate focus prior to stitching them together. (Figure 4.6). The technique used, precisely replicated the highly complex SLA topography at the micrometer level (Figure 4.3 and Figure 4.7). In some cases, depending on the absolute position of the feature in respect to the surface structure (e.g., top or bottom of cavities), it was possible to replicate very small details such as grain boundaries (Figure 4.3e-h, see arrow) over the entire replicating life of a negative. However, at the submicron scale, the TiO$_2$-coated epoxy replica showed a somewhat "smoother" topography than its SLA CP Ti disc, which was most likely the result of the PVD titanium coating (60 nm in thickness). This vapor-deposited titanium film smoothed the (nano)roughness of the replica in a similar way as for example a snowfall on a rocky landscape does (Figure 4.4). Reactive magnetron sputtering is a technique known to have a decent both macro- and micro-scale throwing power in comparison to essentially line-of-sight deposition such as for example evaporation.

TiO$_2$-coated replica surfaces showed similar Ti/O ratios as TiO$_2$-coated Si wafers, model substrates usually used for protein adsorption studies [29] (Table 4.3). These ratios (0.34-0.36), however, were slightly lower than the one found for SLA CP Ti discs (0.41) and also lower than the theoretical value (0.5) of stoichiometric TiO$_2$. This abundance for O on all surfaces can be explained through carbon contaminations (-C-O-H and -C-OOH; see [33] for details), whereas the higher Ti value of CP Ti in comparison with sputter coated TiO$_2$ surfaces is caused most likely by an additional peak detected for metallic Ti (see, for example, [13]).

The ability to cryo-fracture a sample made from epoxy resin, opened new approaches to examine in cross section the duplex nature of the SLA topography: namely the microstructured topography (20-50 μm) obtained through the blasting process and the sub-micrometer topography from the subsequent acid etching treatment (Figure 4.7). Furthermore, it has already been demonstrated that epoxy-made samples can be easily cut for histological sections [19] unlike titanium or other metal samples.

4.4.2 Reproducibility of the Epoxy Replica Technique

The quality of the rough SLA surface using the replica technique did not change significantly in terms of roughness values after a cast over eight series using the same vinyl polysiloxane master and were all similar to their SLA CP Ti master sample (Table 4.2). Although the SLA topography had undercuts produced by acid-etching, the impression material (vinyl polysiloxane) was not damaged to an appreciable extent during the dismantling as assessed by SEM (Figure 4.4b-d; f-h).

4.4.3 The Dual-type Surface Topography for Cell Experiments

The proliferation tests with rat calvarial osteoblasts have demonstrated that the samples with both a smooth and a SLA component on the same surface can be successfully used instead of single surface substrates in cell culture assays, saving material, time and costs. Osteoblast cell numbers, footprint areas and shape factors (Figure 4.5) were found to be statistically non-different for each surface topography (smooth or SLA) and also independent from type of substrate (dual-type or single type). In general, more osteoblasts were found on SLA in comparison with smooth
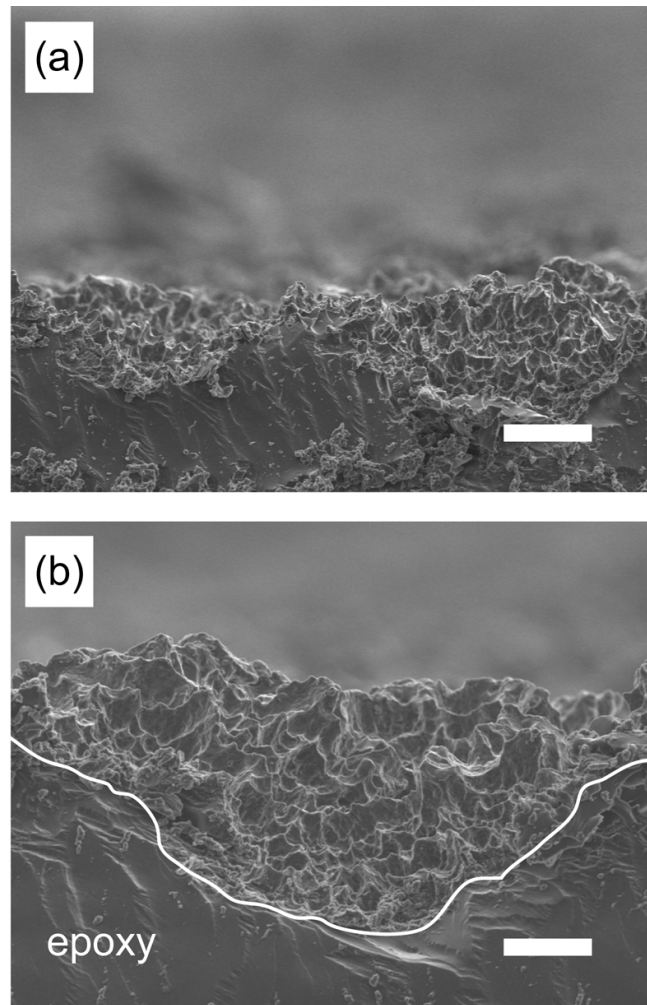
Figure 4.7: Scanning electron micrograph of the SLA part of a TiO_2-coated epoxy replica after cryo-fracture. The SLA shows clearly its duplex surface character: microstructured topography in the range of 20-50 μm originating from the blasting process and submicro-/nanostructured topography from the subsequent acid-etching treatment. The white line in (b) visualizes the effect of the particle-blasting. The scale bars correspond to 15 μm in (a) and 8 μm in (b).

surfaces. They were also found to have a smaller footprint area and being more spherical on SLA than on the smooth topography. This finding is in agreement with a previously published study [4].

Still, it should be noted that the current study was carried out over a time period of only 24 hours; over longer time periods there is the possibility of "cytokine crosstalk" between cells on different surface topographies that might influence each other in an unanticipated way. On the other hand, the dual-type surfaces might find application in studies where the intention is to examine cell responses to different topographies exposed to a common medium.

4.5 Conclusions

Our findings have demonstrated that the manufactured TiO₂-coated epoxy replicas had similar surface roughness and surface chemistry as comparable metallic samples. Furthermore, the replica technique showed high feasibility to precisely replicate highly complex 3-D structures in the millimeter, micrometer and (partially) sub-micrometer range and to produce identical surface topographies with constant surface chemistry over at least eight generations. Such replicas provide the possibility to observe exactly the same structure in different experiments, e.g., by applying a mechanical mark to the master. This advantage could open new windows in the observation of cell behavior on a randomly structured surface. Additionally, the feasibility of coating epoxy replica samples with practically any metal using PVD technique provides the possibility to investigate the effect of surface chemistry independently from surface topography on morphologically complex surfaces. Moreover, we have shown that the replica technique allows the fabrication of substrates with more than one type of topography on the same surface, which not only is difficult but also extremely expensive to obtain with other surface engineering techniques.

Bibliography

[1] Boyan, B. D., Dean, D. D., Lohmann, C. H., Cochran, D. L., Sylvia, V. L. and Schwartz, Z. The titanium-bone cell interface in vitro: the role of the surface in promoting osteointegration. In Brunette, D. M., Tengvall, P., Textor, M. and Thomsen, P., editors, *Titanium in Medicine*, pages 561–586. Springer-Verlag, Berlin Heidelberg, 2001.

[2] Martin, J. Y., Schwartz, Z., Hummert, T. W., Schraub, D. M., Simpson, J., Lankford, J., Dean, D. D., Cochran, D. L. and Boyan, B. D. Effect of Titanium Surface-Roughness on Proliferation, Differentiation, and Protein-Synthesis of Human Osteoblast-Like Cells (Mg63). *Journal of Biomedical Materials Research*, **29**(3), 389–401, 1995.

[3] Bowers, K. T., Keller, J. C., Wick, D. G. and Randolph, B. A. Optimization of Surface-Morphology for Osteoblast Attachment. *Journal of Dental Research*, **69**, 370–370, 1990.

[4] Schuler, M., Owen, G., Hamilton, D. W., de Wild, M., Textor, M., Brunette, D. M. and Tosatti, S. Biomimetic modification of titanium dental implant model surfaces using the RGDSP-peptide sequence: A cell morphology study. *Biomaterials*, **27**(21), 4003–4015, 2006.

[5] Davies, J. E., Lowenberg, B. and Shiga, A. The Bone Titanium Interface Invitro. *Journal of Biomedical Materials Research*, **24**(10), 1289–1306, 1990.

[6] Boyan, B. D., Lohmann, C. H., Dean, D. D., Sylvia, V. L., Cochran, D. L. and Schwartz, Z. Mechanisms involved in osteoblast response to implant surface morphology. *Annual Review of Materials Research*, **31**, 357–371, 2001.

[7] Brunette, D. M. Fibroblasts on Micromachined Substrata Orient Hierarchically to Grooves of Different Dimensions. *Experimental Cell Research*, **164**(1), 11–26, 1986.

[8] Brunette, D. M., Kenner, G. S. and Gould, T. R. L. Grooved Titanium Surfaces Orient Growth and Migration of Cells from Human Gingival Explants. *Journal of Dental Research*, **62**(10), 1045–1048, 1983.

[9] Sykaras, N., Iacopino, A. M., Marker, V. A., Triplett, R. G. and Woody, R. D. Implant materials, designs, and surface topographies: Their effect on osseointegration. A literature review. *International Journal of Oral Maxillofacial Implants*, **15**(5), 675–690, 2000.

[10] Wennerberg, A., Albrektsson, T. and Andersson, B. Design and surface characteristics of 13 commercially available oral implant systems. *Int J Oral Maxillofac Implants*, **8**, 622–633, 1993.

[11] Wieland, M. *Experimental determination and quantitative evaluation of the surface composition and topography of medical implant surfaces and their influence on osteoblastic cell-surface interactions.* Ph.D. Thesis No. 13247, Swiss Federal Institute of Technology Zurich, 1999.

[12] Wieland, M., Textor, M., Spencer, N. D. and Brunette, D. M. Measurement and Evaluation of the Chemical Composition and Topography of Titanium Implant Surface. In Davies, J. E., editor, *Bone Engineering*. Em Squared Inc., 2000.

[13] Wieland, M., Chehroudi, B., Textor, M. and Brunette, D. M. Use of Ti-coated replicas to investigate the effects on fibroblast shape of surfaces with varying roughness and constant chemical composition. *Journal of Biomedical Materials Research*, **60**(3), 434–444, 2002.

[14] Wieland, M., Textor, M., Spencer, N. D. and Brunette, D. M. Wavelength-dependent roughness: A quantitative approach to characterizing the topography of rough titanium surfaces. *International Journal of Oral Maxillofacial Implants*, **16**(2), 163–181, 2001.

[15] Jaeger, N. and Brunette, D. M. Production of microfabricated surfaces and their effects on cell behavior. In Brunette, D. M., Tengvall, P., Textor, M. and Thomsen, P., editors, *Titanium in Medicine*, pages 343–374. Springer-Verlag, Berlin Heidelberg, 2001.

[16] Hamilton, D. W., Wong, K. S. and Brunette, D. M. Microfabricated discontinuous-edge surface topographies influence osteoblast adhesion, migration, cytoskeletal organization, and proliferation and enhance matrix and mineral deposition in vitro. *Calcified Tissue International*, **78**(5), 314–325, 2006.

[17] Hamilton, D. W. and Brunette, D. M. "Gap guidance" of fibroblasts and epithelial cells by discontinuous edged surfaces. *Experimental Cell Research*, **309**(2), 429–437, 2005.

[18] Massaro, C., Rotolo, P., De Riccardis, F., Milella, E., Napoli, A., Wieland, M., Textor, M., Spencer, N. D. and Brunette, D. M. Comparative investigation of the surface properties of commercial titanium dental implants. Part I: chemical composition. *Journal of Materials Science-Materials in Medicine*, **13**(6), 535–548, 2002.

[19] Chehroudi, B., Gould, T. R. L. and Brunette, D. M. A Light and Electron-Microscopic Study of the Effects of Surface-Topography on the Behavior of Cells Attached to Titanium-Coated Percutaneous Implants. *Journal of Biomedical Materials Research*, **25**(3), 387–405, 1991.

[20] Listgarten, M. A., Buser, D., Steinemann, S. G., Donath, K., Lang, N. P. and Weber, H. P. Light and Transmission Electron-Microscopy of the Intact Interfaces between Non-Submerged Titanium-Coated Epoxy-Resin Implants and Bone or Gingiva. *Journal of Dental Research*, **71**(2), 364–371, 1992.

[21] Chehroudi, B., Soorany, E., Black, N., Weston, L. and Brunette, D. M. Computer-Assisted 3-Dimensional Reconstruction Of Epithelial-Cells Attached To Percutaneous Implants. *Journal Of Biomedical Materials Research*, **29**(3), 371–379, 1995.

[22] Chehroudi, B., McDonnell, D. and Brunette, D. M. The effects of micromachined surfaces on formation of bonelike tissue on subcutaneous implants as assessed by radiography and computer image processing. *Journal of Biomedical Materials Research*, **34**(3), 279–290, 1997.

[23] Chehroudi, B. and Brunette, D. M. Subcutaneous microfabricated surfaces inhibit epithelial recession and promote long-term survival of percutaneous implants. *Biomaterials*, **23**(1), 229–237, 2002.

[24] Wieland, M., Textor, M., Chehroudi, B. and Brunette, D. M. Synergistic interaction of topographic features in the production of bone-like nodules on Ti surfaces by rat osteoblasts. *Biomaterials*, **26**(10), 1119–1130, 2005.

[25] Kunzler, T., Sprecher, C. M., Schuler, M., Drobek, T. and Spencer, N. D. Fabrication of material-independent morphology gradients for high-throughput applications. *Applied Surface Science*, **253**(4), 2148–2153, 2006.

[26] Chehroudi, B., Gould, T. R. L. and Brunette, D. M. The Role of Connective-Tissue in Inhibiting Epithelial Downgrowth on Titanium-Coated Percutaneous Implants. *Journal of Biomedical Materials Research*, **26**(4), 493–515, 1992.

[27] Chehroudi, B., Ratkay, J. and Brunette, D. M. The Role of Implant Surface Geometry on Mineralization Invivo and Invitro - a Transmission and Scanning Electron-Microscopic Study. *Cells and Materials*, **2**(2), 89–104, 1992.

[28] Steinemann, S. G. and Claes, L. Metallic implant anchorable to bone tissue for replacing a broken diseased bone, 1992.

[29] Tosatti, S. *Functionalized Titanium Surfaces for Biomedical Applications: Physico-chemical Characterization and Biological in vitro Evaluation.* Ph.D. Thesis No. 15095, Swiss Federal Institute of Technology Zurich, 2003.

[30] Scofield, J. H. Hartree-Slater Subshell Photoionization Cross-Sections at 1254 and 1487ev. *Journal of Electron Spectroscopy and Related Phenomena*, **8**(2), 129–137, 1976.

[31] Hasegawa, S., Sato, S., Saito, S., Suzuki, Y. and Brunette, D. M. Mechanical Stretching Increases the Number of Cultured Bone- Cells Synthesizing DNA and Alters Their Pattern of Protein- Synthesis. *Calcified Tissue International*, **37**(4), 431–436, 1985.

[32] Curtis, A. and Wilkinson, C. Nantotechniques and approaches in biotechnology. *Trends in Biotechnology*, **19**(3), 97–101, 2001.

[33] Tosatti, S., Michel, R., Textor, M. and Spencer, N. D. Self-assembled mono-layers of dodecyl and hydroxy-dodecyl phosphates on both smooth and rough titanium and titanium oxide surfaces. *Langmuir*, **18**(9), 3537–3548, 2002.

5

Biomimetic Modification of Titanium Dental Implant Model Surfaces Using the RGDSP-Peptide Sequence: A Cell Morphology Study

Martin Schuler, Gethin Rh. Owen, Douglas W. Hamilton, Michael de Wild, Marcus Textor, Donald M. Brunette, Samuele G.P. Tosatti

Biomaterials , **27**(21), 4003–15, 2006.

Surface topography and (bio)chemistry are key factors in determining cell response to an implant. We investigated cell adhesion and spreading patterns of epithelial cells, fibroblasts and osteoblasts on biomimetically modified, smooth and rough titanium surfaces. The RGD bioactive peptide sequence was immobilized via a non-fouling poly(L-lysine)-graft-poly(ethylene glycol) (PLL-g-PEG) molecular assembly system, which allowed exploitation of specific cell–peptide interactions even in the presence of serum. As control surfaces, bare titanium and bio-inactive surfaces (scrambled R<u>DG</u> and unfunctionalized PLL-g-PEG) were used. Our findings demonstrated that surface topography and chemistry directly influenced the attachment and morphology of all cell types tested. In general, an increase in cell number and more spread cells were

observed on bioactive substrates (containing RGD) compared to bio-inactive surfaces. More fibroblasts were present on smooth than on rough topographies, whereas for osteoblasts the opposite tendency was observed. Epithelial cell attachment did not follow any regular pattern. Footprint areas for all cell types were significantly reduced on rough compared to smooth surfaces. Osteoblast attachment and footprint areas increased with increasing RGD-peptide surface density. However, no synergy (interaction) between RGD-peptide surface density and surface topography was observed for osteoblasts neither in terms of attachment nor footprint area.

Keywords: Titanium oxide, surface topography, surface modification, biomimetic material, peptide, cell morphology.

5.1   Introduction

The success of an implant in dental applications depends on its strong anchorage to the surrounding bone [1] in order to withstand the continuous cyclic loading that occurs during mastication. Several factors, such as surgical technique, implant design, surface topography and surface (bio)chemistry are known to influence the bone ingrowth to an implant [2] . The optimization of the surface properties based on topographical and (bio)chemical surface modification [3, 4] has become a key issue in the development of improved devices.

Topographical modification of titanium surfaces using either geometrically defined features [5, 6] or random structures [7–15] has been shown to affect cell behavior *in vitro* [16] and *in vivo* [17–20]. For example, osteoblasts exhibit a more mature osteoblastic phenotype on rougher titanium surfaces approximately one week after cell seeding [21], while fibroblasts [5], and in some cases epithelial cells [22–24] show a preference for smoother surfaces.

One approach for (bio)chemical (biomimetic) surface modification [25, 26] is the immobilization of small peptides found in extracellular matrix (ECM) proteins to promote cell adhesion. By using peptides present in the tissue of interest as a bridging unit between cell receptors and surface, different cellular pathways can in theory be activated [27]. Perhaps the most investigated peptide sequence is RGD (arginine–glycine–aspartic acid) [28], derived from fibronectin and recognized by almost all α/β integrins [29].

A number of systems using polymers have been developed to immobilize peptides

onto a biomaterial surface [30]. However, many such surfaces lack protein resistance so that proteins present in the medium adsorb to the surface and interfere with the direct study of peptide–cell interactions. An effective way to minimize protein adsorption onto a surface is the use of a poly(L-lysine)-*graft*-poly(ethylene glycol) (PLL-*g*-PEG) molecular assembly system (Figure 5.1) [31–33]. These PEGylated (nonfouling [34]) surfaces reduce adsorbed protein mass to as low as <5 ng/cm^2 [35, 36]. Osmotic and entropic repulsion effects as well as screening of interfacial charges [37] appear to be involved in producing the anti-fouling effects. Furthermore, peptide sequences can be covalently attached via vinyl sulfone–cysteine coupling reaction to the poly(-ethylene glycol) side chains [38]. The thickness of the adsorbed polymeric layer (1–1.5 nm in dry state and 5–10 nm in wet state [39]) is small in comparison to the dimensions of topographic features of rough surfaces such as the commercially used dental implant surface SLA from Institut Straumann that exhibits topographical features in the range of 0.5–50 μm [12]. Moreover, the topography of SLA surface is thought to protect the polymeric coating from damage caused by mechanical handling during surgical preparation and implantation. The main goal of this study was to determine cell response as a function of the topographical and chemical surface modification. Cells were selected on the basis of tissues that contact dental implants: Epithelium (Porcine Epithelial Cells), connective tissue (Swiss Balb/c 3T3 Mouse Murine Mesenchymal Embryo Fibroblasts) and bone (Rat Calvarial Osteoblasts). Cell attachment, cell morphology and distribution of cytoskeletal elements (microtubules and vinculin) were investigated using fluorescent microscopy techniques.

5.2   Materials and Methods

5.2.1   Substrates

Preparation

Samples were produced using the epoxy replica technique as described by Wieland *et al.* [11]. In brief, replicas of a rough SLA CP Ti disc (Institut Straumann, Basel, Switzerland) and a smooth Tissue Culture Polystyrene (TCPS; Multidish 24 well, Nunc, Milian, Basel, Switzerland) surface were taken using vinyl polysiloxane as the impression material (PROVIL novo Light; Unor, Dietikon, Switzerland), followed

Peptide sequence (e.g. RGD)

PEG side chains

PLL backbone

Biomaterial surface
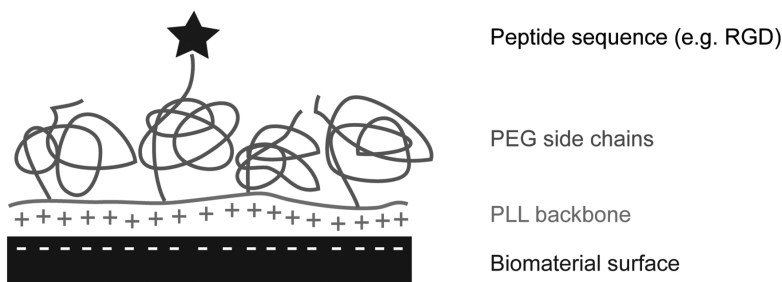
Figure 5.1: Schematic view of peptide-functionalized PLL-*g*-PEG polymer adsorbed as a monolayer on a negatively charged metal oxide surface (e.g., titanium oxide). The PLL backbone is positively charged at pH 7.4 due to its amine groups and the PEG-chains are exposed to the fluid as a brush. The peptide sequence arginine–glycine–aspartic acid (RGD) is covalently attached to a fraction of the PEG-chains.

by replicating these negative structures by casting into postive structures using epoxy-resin (EPO-TEK 302-3M; Epoxy Technology, Polyscience, Cham, Switzerland). These replicas were cleaned and coated with a thin film (60 nm) of titanium dioxide using reactive magnetron sputtering (Physical vapor deposition (PVD), Paul Scherrer Institute, Villigen, Switzerland) as model surfaces of titanium implants with defined surface topography and chemistry.

Characterization

Surface roughness values of all surfaces were determined by the use of atomic force microscopy (AFM, smooth topographies only) and scanning electron microscopy (SEM, see Wieland *et al.* [11, 12]). Stoichiometry and homogeneity of the deposited titanium oxide layer was controlled by X-ray photoelectron spectroscopy (XPS, see [40] for details).

5.2.2   Polymers

Synthesis

Peptide-functionalized and non-functionalized PLL-*g*-PEG polymers were synthesized according to earlier publications [31, 36, 38]. The general architecture of these polymers (as shown in Figure 5.1) was based on a PLL backbone of approximately

120 L-lysine units (average value in view of the polydispersity of 1.4 of the polymer; Sigma-Aldrich, Buchs, Switzerland), a PEG side chain of approximately 47 ethylene glycol units (PEG MW 2 kDa, polydispersity: 1.02; Nektar, Bradford, UK) and a grafting ratio g between 3.3 and 4.6, expressed as the number of lysine monomers per PEG side chain (see Table 5.1 for details). A vinyl sulfone-modified PEG chain of 3.4 kDa molecular weight (polydispersity: 1.01; Nektar, Bradford, UK) was used to couple the peptides sequences with the PLL backbone. The following peptides were used for the synthesis of functionalized PLL-g-PEG polymers: the bioactive RGD-containing N-acetyl-GCRGYG**RGDSP**G-amide and the scrambled (bio-inactive) N-acetyl GCRGYGR<u>DG</u>SPG-amide (both purchased from Jerini, Berlin, Germany).

Characterization and Notation

Grafting ratio g and fraction of peptide-functionalized PEG-chains were determined by nuclear magnetic resonance spectroscopy (NMR, for details see [33]). Both the adsorption of the polymer and the degree of resistance of the polymeric adlayers to serum adsorption (always less than 5 ng/cm^2) were monitored *in situ* and quantitatively with optical waveguide lightmode spectroscopy (OWLS) [39, 41]. Grafting ratios (NMR) and adsorbed polymer masses (OWLS) allowed us to determine the surface densities of the immobilized peptide moieties. For simplicity, the peptide-functionalized polymers are named hereafter according to their peptide sequence as **RGD** for PLL-g-PEG/PEG-RGD, **R<u>DG</u>** for PLL-g-PEG/PEG-R<u>DG</u> and **PEG** for the unfunctionalized PLL-g-PEG.

Determination of Peptide Surface Density and Spacing of Bioligands

The following calculations were based on the assumption that cells were able to sense all the RGD-ligands present in the polymer. Although it is likely that a fraction of the ligands was hidden within the PEG-layer at a given time point, the dynamic structure of the PEG-brush system was expected to expose the majorities of ligands over time and make them available to cells. Peptide surface densities ρ_{ps} (Table 5.2) were varied by co-adsorption from mixed solutions of peptide-functionalized and unfunctionalized PLL-g-PEG and calculated using the following equation (see Tosatti

Table 5.1: Molecular weight, grafting ratio, peptide functionalization, polymer/protein adsorbed mass and peptide surface density for all polymers used in this study.

	PEG	RDG	RGD[a]	RGD A[b]
Molecular weight PLL [kDa]	15.9	15.9	15.9	15.9
Molecular weight lysine unit [kDa]	0.128	0.128	0.128	0.128
Molecular weight peptide [kDa]	-	1.222	1.222	1.222
Molecular weight entire polymer [kDa]	91.1	72.4	79.4	76
Grafting ratio g [-][c]	3.3	4.5	4	4.6
Peptide-functionalized PEG-chains [%][c]	-	1.7	1.7	8.6
Polymer adsorbed mass [ng/cm^2][d]	110 ± 15	110 ± 15	110 ± 15	110 ± 15
Protein adsorbed mass [ng/cm^2][d]	< 5	< 5	< 5	< 5
Peptide surface density ρ_{ps} [pmol/cm^2][e]	0	0.7134	0.7313	3.3614

[a]RGD concentration for epithelial cells and fibroblast experiments.

[b]RGD stock concentration for osteoblast experiments on different RGD-peptide densities (see Table 5.2).

[c]Measured with NMR technique.

[d]Measured with OWLS technique.

[e]Calculated for smooth topographies (see Equation 5.1).

et al. [33] for details):

$$\rho_{ps} = \frac{MW(PLL)}{MW(Lys)g} \frac{m_a}{MW(Pol)} P \qquad (5.1)$$

where *MW(PLL)*, *MW(Lys)*, and *MW(Pol)* denote the molecular weight of the PLL backbone, the lysine unit and the whole polymer, respectively, g is the grafting ratio, m_a the mass of polymer adsorbed on a smooth titanium surface and P the fraction

(%) of functionalized PEG side chains. The effective peptide density on SLA surfaces in theory is much higher, since the surface area is 6.5 times higher compared to a smooth surface [42, 43] and therefore, the peptide concentration should be multiplied by the same factor. However, when considering the dimensions (0.5–2 μm) of the topographical features provided by the acid-etching treatment of the SLA surface, it can be assumed that the majority of those small cavities cannot be sensed by entire cells, at most by the filopodia. Therefore, the number of cells attached to a SLA topography is likely to be primarily determined by the coarser, hemisphere-like structures (20–50 μm dimension) that are the result of the sand-blasting step during the manufacture of the SLA discs. The geometric surface area ratio of a surface with a "perfectly" blasted (densely packed hemispherical pits) and a smooth one can be expressed as

$$ratio_{surfacearea} = \frac{Area_{hemisphere}}{Area_{circle}} = \frac{2\pi r^2}{\pi r^2} = 2 \qquad (5.2)$$

As a consequence, it can be assumed that the number of cells attached to a SLA surface in comparison with a smooth surface is maximal a factor 2 higher. The theoretical peptide-peptide distance d_{p-p} on "smooth" surfaces assuming a hexagonal distribution of the peptide ligands was calculated as follows:

$$d_{p-p} = \sqrt{\frac{2}{\sqrt{3}} \frac{1}{\rho_{ps} A}} \qquad (5.3)$$

A refers to Avogadro's number A=6.022 x 10^{23} mol^{-1} and ρps to the peptide surface density (see Equation 5.1). This formula was also used for estimating the distances between the bioligands on SLA surfaces, since these values were small (nm-range; see Table 5.2) in comparison with the micro-features of SLA.

Table 5.2: Fraction of RGD-functionalization, RGD-peptide surface densities and peptide-peptide distances for all RGD concentrations used in this study.

	Fraction of RGD peptide-functionalized PEG side chains	RGD peptide surface density	Peptide-peptide distance
Short name	P [%]	ρ_{ps} [pmol/cm^2][d]	$d_{p\text{-}p}$ [nm][e]
RGD A[a]	8.6	3.3614	8
RGD B[b]	1.72	0.6723	17
RGD C[b]	0.344	0.1345	38
RGD D[b]	0.0688	0.0269	84
RGD E[b]	0.0138	0.0054	189
RGD F[b]	0.0028	0.0011	422
RGD G[b]	0.0006	0.0002	944
RGD[c]	1.7	0.7313	16

[a]RGD stock concentration for osteoblast experiments.

[b]RGD concentrations for osteoblast experiments, obtained by dilution of RGD Awith unfunctionalized PLL-*g*-PEG solutions.

[c]RGD concentration for epithelial cells and fibroblast experiments.

[d]Calculated for smooth topographies (see Equation 5.1).

[e]Calculated for smooth topographies (see Equation 5.3).

5.2.3   Cell Cultures

Porcine Epithelial Cells (EC)

Porcine epithelial cells were obtained from porcine periodontal ligaments and subcultured as described by Brunette *et al.* [44]. Isolated cells were plated on tissue culture dishes in a minimum essential medium (α-MEM; Stemcell, Vancouver, BC, Canada) supplemented with antibiotics (100 mg/ml penicillin G, Sigma-Aldrich, Oakville, Ont., Canada; 50 mg/ml gentamicin, Sigma-Aldrich; 3 mg/ml amphoteracin B, Gibco, Grand Island, NY, USA) and 15% of fetal calf serum (Medicorp, Rexdale, Ont., Canada).

Swiss Balb/c 3T3 Fibroblasts (FB)

Balb/c 3T3 fibroblastic cells were maintained according to the method of Elvin and Evans [45]. Stock cultures were recovered from liquid nitrogen and plated at 300,000 cells per 25 cm^2 plastic flask in Dulbecco's modified Eagles medium (DMEM) with 10% fetal calf serum (both purchased from Invitrogen, Basel, Switzerland) without antibiotics.

Rat Calvarial Osteoblasts (OB)

Osteogenic cells were obtained from newborn rat calvariae, isolated and subcultured as published by Hasegawa *et al.* [46] and Chehroudi *et al.* [47]. Frontal, parietal and occipital bone were dissected, rinsed in phosphate buffered saline (PBS; Sigma-Aldrich, Oakville, Ont., Canada), placed in α-MEM, supplemented with antibiotics (same mixture as described above for epithelial cells) and 15% of fetal calf serum (Cansera, Rexdale, Ont., Canada). The minced tissue was digested with a mixture of clostridial collagenase and trypsin (both purchased from Sigma-Aldrich, Oakville, Ont., Canada) and then plated in tissue culture flasks.

5.2.4   Experimental Design

Formation of Polymeric Adlayer

Frozen samples of PLL-g-PEG and peptide-functionalized PLL-g-PEG were warmed
up to room temperature, dissolved in 10mM PBS at pH 7.4 (to reach a final
concentration of 1 mg/ml) and used to prepare solutions of different concentra-
tions of peptide-functionalized PLL-g-PEG [36, 48]. Prior to surface modification,
the substrates were cleaned and sterilized in an oxygen plasma (Harrick Plasma
Cleaner/Sterilizer PDC-32G, Ossining, NY, USA) for 2 min, placed in a 24 well
plate, coated with a concentration of 250 ml/cm^2 of the desired polymer solution
and incubated for 30 min while gently shaken at room temperature. The substrates
were rinsed twice with PBS for each 5 min to remove loosely bound polymer and
subsequently seeded with the desired cell type.

Cell Incubation

Cells were removed with trypsin solution, diluted with the suitable media and seeded
at a concentration of 10^4 cells/cm^2. The whole set of surfaces with attached cells
was incubated for 24 h at 37 °C in a humidified atmosphere of 95% air and 5% CO_2.

Cell Membrane Staining

Cells were washed with warm PBS and fixed in 4% formaldehyde (Fisher Scientific,
Nepean, Ont., Canada) in PBS. Cell membrane was stained using 10mM FITC
(Sigma-Aldrich, Oakville, Ont., Canada) at 37 °C for 2 h followed by 3 washes with
PBS.

Microtubule Staining

Samples were rinsed with warm PBS and fixed with ice-cooled acetone (Fisher Sci-
entific, Nepean, Ont., Canada) at 20 C. Cells were permeabilized using 0.5% Triton
X-100 (Fisher Scientific, Nepean, Ont., Canada) in PBS and unspecific binding
blocked with 1% BSA/PBS (Sigma-Aldrich, Oakville, Ont., Canada). Samples were
incubated with the primary antibody (1:200 dilution in 0.1% BSA/PBS; Mouse anti

human btubulin, clone no. KMX-1; Chemicon Temecula, CA, USA) for 90 min at room temperature followed by an incubation with the secondary antibody (1:200 dilution in 0.1% BSA/PBS; Alexa 546 goat anti-mouse IgG; Invitrogen, Burlington, Ont., Canada) for one hour at room temperature. Antibodies were stabilized with 4% formaldehyde/PBS and washed extensively with PBS [49].

Vinculin Staining

Cells were washed with warm PBS and fixed in 4% formaldehyde/PBS. Samples were permeabilized using 0.5% Triton X-100/PBS and unspecific binding blocked with 1% BSA/PBS. Cells were incubated with the primary antibody (1:400 dilution in 0.1% BSA/PBS; Monoclonal antivinculin antibody produced in mouse; Sigma-Aldrich, Oakville, Ont., Canada) for 90 min at room temperature, followed by an incubation with the secondary antibody (1:200 dilution in 0.1% BSA/PBS; Alexa 546 goat anti-mouse IgG; Invitrogen, Burlington, Ont., Canada) for one hour at room temperature. Antibodies were stabilized with 4% formaldehyde/PBS and washed extensively with PBS [49].

5.2.5   Observation Methods

An epi-fluorescence microscope (Axioskop 2 MOT, Zeiss, Oberkochen, Germany) with a wavelength of λ_{max}=488nm was used to determine cell number and cell shape investigations. A filter with a wavelength of λ_{max}=546nm was chosen to observe microtubules and vinculin expression. In order to determine cell number, five random images of each surface topography (smooth and SLA) were taken for each sample. More than 30 single cells were randomly chosen to evaluate cell morphology. All images were analyzed with ImageJ software (Version 1.32i for Mac OS X).

5.2.6   Morphology

Cell morphology was described, by measuring the footprint area of the cell on the surface after attachment and using a shape factor. The shape factor Φ was expressed as

$$\Phi = \frac{4\pi A}{p^2} \tag{5.4}$$

where A is the footprint area and p the perimeter of the cell. Circular objects have the greatest area-to-perimeter ratio, and a shape factor of 1 represents a perfect circle. As an example, a thin thread-like object would have the lowest shape factor approaching 0. The footprint area for cells on smooth surfaces was easily defined and measured, whereas cells on rough surface topographies had a complex footprint. In this study, the biggest outline of a cell was projected to obtain a "footprint" on (rough) SLA surfaces. Although this assumption might underestimate the "real" footprint of a cell, it is still a fair and efficient way in defining cell shape for comparative purposes in a complex 3D environment. One way to overcome this underestimation could be 3D reconstruction of each single cell as done for example by Wieland *et al.* [11]. The limitation of such a technique, however, becomes clear when investigating less-spread, spherical cells, where the adhesion outline is shaded by the projected one (e.g., cells on ridges), and therefore highly difficult to identify correctly.

5.2.7   Statistical Analysis

Comparisons between measurement series were made using nonparametric tests (SPSS 11.4 for Mac OS X) because variances were not homogeneous and observed values were not distributed normally even after appropriate transformations. All mean values are shown $\pm$SE (standard error). We set our level of significance at 0.05.

5.3   Results

In this section, only significant differences between important chemistries, namely between bioactive surfaces (TiO_2 and RGD at high surface concentrations) and bioinactive surfaces (PEG and PLL-g-PEG/PEG-R<u>DG</u>), are listed. For detailed (significant) information about other pair comparisons (especially in the case of osteoblasts at low RGD concentrations) see Tables 5.3 and 5.4.

Table 5.3: Significant differences for multiple comparisons between pairs of smooth surface chemistries in cell number, footprint area and shape factor for osteoblasts, fibroblasts and epithelial cells (Tamhane test, p<0.05).

	Epithelial Cells	Fibroblasts	Osteoblasts
Number	all except	TiO_2 vs. RDG	TiO_2 vs. PEG, RDG, G-C
	TiO_2 vs. RGD		PEG, RDG vs. D-A
Footprint area	all except	all except	TiO_2 vs. PEG, RDG, G-D
	TiO_2 vs. RGD	TiO_2 vs. RGD	PEG, RDG vs. C-A
	PEG vs. RDG	PEG vs. RDG	
Shape factor	all except	all except	TiO_2 vs. G, C
	RDG vs. RGD	TiO_2 vs. RGD	PEG vs. C, A
		PEG vs. RDG	

Table 5.4: Significant differences for multiple comparisons between pairs of SLA surface chemistries in cell number, footprint area and shape factor for osteoblasts, fibroblasts and epithelial cells (Tamhane test, $p<0.05$).

	Epithelial Cells	Fibroblasts	Osteoblasts
	all except		TiO_2 vs. PEG, R<u>DG</u>, G-C
Number	TiO_2 vs. RGD	n. s.	PEG, R<u>DG</u> vs. E-A
	PEG vs. RGD		
	TiO_2 vs. PEG	TiO_2	TiO_2 vs.
Footprint area	PEG vs. RGD	vs.	PEG, R<u>DG</u>, G, F, D, C
	R<u>DG</u> vs. RGD	PEG, R<u>DG</u>	PEG vs. E, B, A
	TiO_2		TiO_2 vs. PEG, R<u>DG</u>
Shape factor	vs.	n. s.	PEG, R<u>DG</u> vs. E, B, A
	PEG, R<u>DG</u>, RGD		

5.3.1   Cell Number

Influence of Surface Topography

Significantly more epithelial cells attached on SLA surfaces with PEG than on smooth surfaces with PEG (Mann–Whitney: U=355.5, p=0.036; Figure 5.2a), whereas on RDG the opposite trend was observed (U=114.0, p<0.001). Although mean numbers of attached fibroblasts for all surface chemistries were higher on smooth than on SLA topographies (Figure 5.2b), a significant difference was only
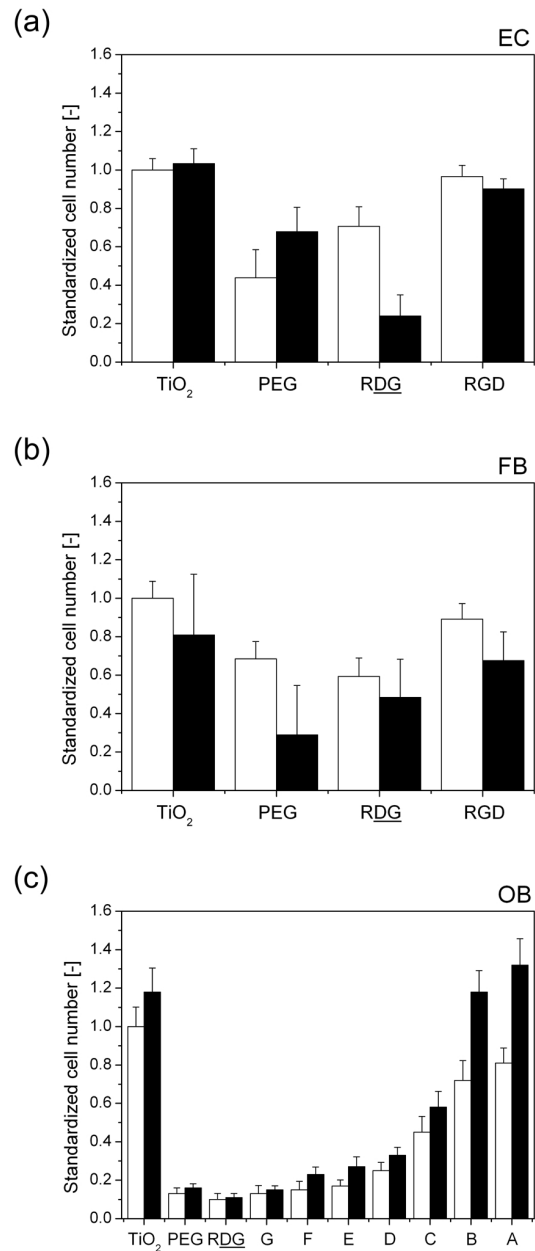
Figure 5.2: Cell number (standardized for smooth TiO_2 surfaces) for epithelial cells (a), fibroblasts (b) and osteoblasts (c). White columns refer to cells on the smooth surfaces and black to cells on the rough SLA topographies. The control surfaces were titanium (**TiO_2**), PLL-g-PEG (**PEG**) and PLL-g-PEG/PEG-R$\underline{DG}$ (**R$\underline{DG}$**). **RGD** concentrations in (a) and (b) are comparable with RGD concentration B in (c). See Tables 5.1 and 5.2 for further details.

found between the SLA and the smooth PEG-surface (U=17.0, p=0.001). Comparisons between the numbers of osteoblasts attached to surfaces with the same chemistry showed that a higher number of osteoblasts adhered to SLA topographies than to smooth topographies (Figure 5.2c). Differences were significant for all RGD (G–A) and PEG surfaces (p=0.02), although mean values on TiO_2 and R$\underline{DG}$ were also clearly higher on SLA than on smooth surfaces.

Influence of Surface (Bio)chemistry

Cell attachment between surface chemistries was significantly different on smooth (Kruskal–Wallis: EC: χ^2_3=44.44, p<0.001; FB: χ^2_3=10.74, p=0.013; OB: χ^2_9=294.34, p<0.001) and SLA topographies (EC: χ^2_3=68.79, p<0.001; FB: χ^2_3=44.44, p=0.013; OB: χ^2_9=326.89, p<0.001). In general, more epithelial cells, fibroblasts and osteoblasts were attached to the bioactive surfaces TiO_2 and RGD (D–A for osteoblasts) compared to the bioinactive surfaces PEG and R$\underline{DG}$, independent of topography (Figure 5.2a-c). In the specific case of osteoblasts, where a higher diversity of RGD concentrations was investigated, a direct relationship was found between mean osteoblast cell numbers and RGD-peptide surface densities for smooth (Pearson correlation: R=0.787, p=0.036, n=7; Figure 5.5a) and SLA topographies (R=0.809, p=0.027). Nonsignificant interaction was found (Two-way ANOVA: $F_{(3,351)}$=0.283, p=0.838) between surface chemistries (RGD D–A) and topographies (smooth and SLA) on the number of osteoblasts attached (Figure 5.5a).

5.3.2   Cell Footprint Area

Influence of Surface Topography

Footprint areas for all cell types were significantly larger on smooth than on SLA topographies (p<0.001; Figure 5.3a–c) for all surface chemistries.

Influence of Surface (Bio)chemistry

Significant differences for cell footprint areas between surface chemistries were found on smooth (Kruskal–Wallis: EC: χ^2_3=66.22, p<0.001; FB: χ^2_3=59.06, p<0.001; OB: χ^2_9=153.76, p<0.001) and SLA topographies (EC: χ^2_3=27.11, p<0.001; FB:

Figure 5.3: Cell footprint area for epithelial cells (a), fibroblasts (b) and osteoblasts (c). White columns refer to cells on the smooth surfaces (with left y-axis) and black to cells on the rough SLA topographies (with right y-axis). The control surfaces were titanium (**TiO$_2$**), PLL-g-PEG (**PEG**) and PLL-g-PEG/PEG-R<u>DG</u> (**R<u>DG</u>**). **RGD** concentrations in (a) and in (b) are comparable with RGD concentration B in (c). See Tables 5.1 and 5.2 for further details.

χ^2_3=31.38, p<0.001; OB: χ^2_9=191.44, p<0.001). Footprint areas of epithelial cells, fibroblasts and osteoblasts were consistently larger on bioactive surfaces TiO$_2$ and RGD (B–A for osteoblasts) compared to bio-inactive surfaces PEG and PLL-g-PEG/PEG-R<u>DG</u>, independent of topography type (Figure 5.3a–c). A direct relationship was found between the mean osteoblast cell footprint areas and RGD-peptide surface densities for smooth (Pearson correlation: R=0.859, p=0.013, n=7; Figure 5.5b) and SLA topographies (R=0.850, p=0.015, n=7).

5.3.3   Cell Shape Factor

Influence of Surface Topography

Similar epithelial cell shape factors on smooth and SLA topographies were found for all surface chemistries except for PEG (Mann–Whitney: U=595, p=0.001; Figure 5.4a). In contrast, fibroblast shape factors differed on all surface chemistries (p<0.02; Figure 5.4b) except on PLL-g-PEG/PEG-R<u>DG</u>. In the case of osteoblasts, significantly higher shape factors were found on all SLA topographies compared to smooth topographies (p<0.05; Figure 5.4c).

Influence of Surface (Bio)chemistry

There were significant differences in cell shape factors between surface chemistries on smooth (Kruskal–Wallis: EC: χ^2_3=54.42, p<0.001; FB: χ^2_3=37.90, p<0.001; OB: χ^2_9=75.74, p<0.001) and SLA topographies (EC: χ^2_3=42.33, p<0.001; FB: χ^2_3=34.44, p<0.001; OB: χ^2_9=234.08, p<0.001). Mean shape factors of fibroblasts and osteoblasts were smaller on bioactive surfaces TiO$_2$ and RGD (B–A for osteoblasts) compared to bio-inactive surfaces PEG and PLL-g-PEG/PEG-R<u>DG</u>, independent of topography type (Figure 5.4b–c). In contrast, mean shape factors of epithelial cells were higher on TiO$_2$ than on all the other surface chemistries (Figure 5.4a). No relationship was found between osteoblast shape factors and RGD-peptide surface densities for both topographies (Figure 5.5c).
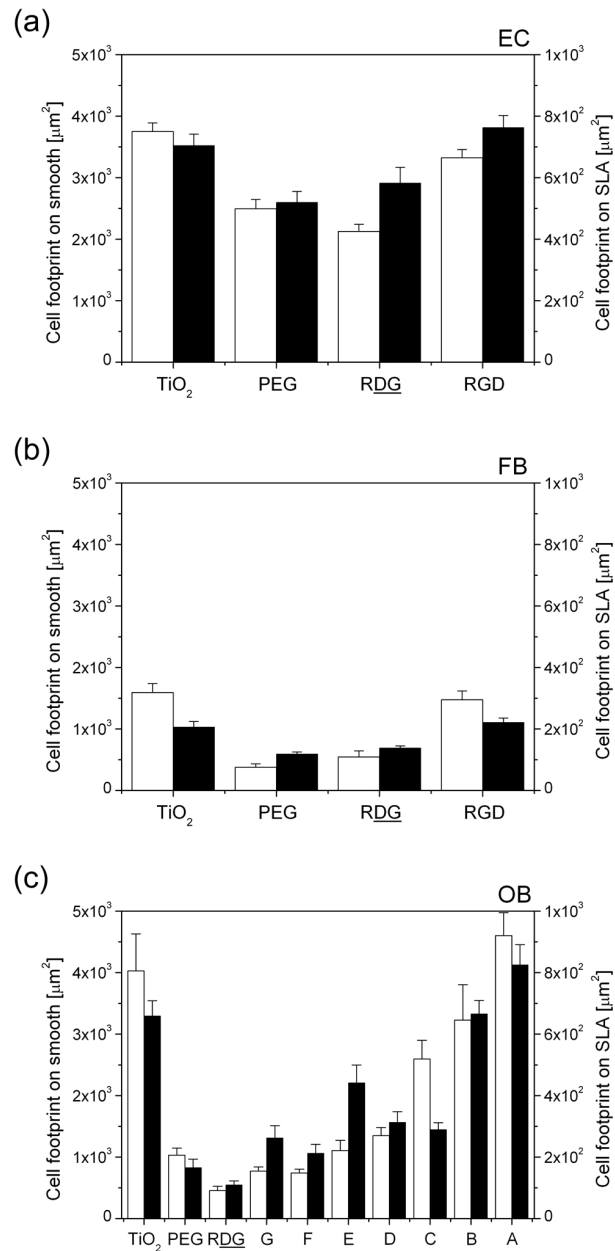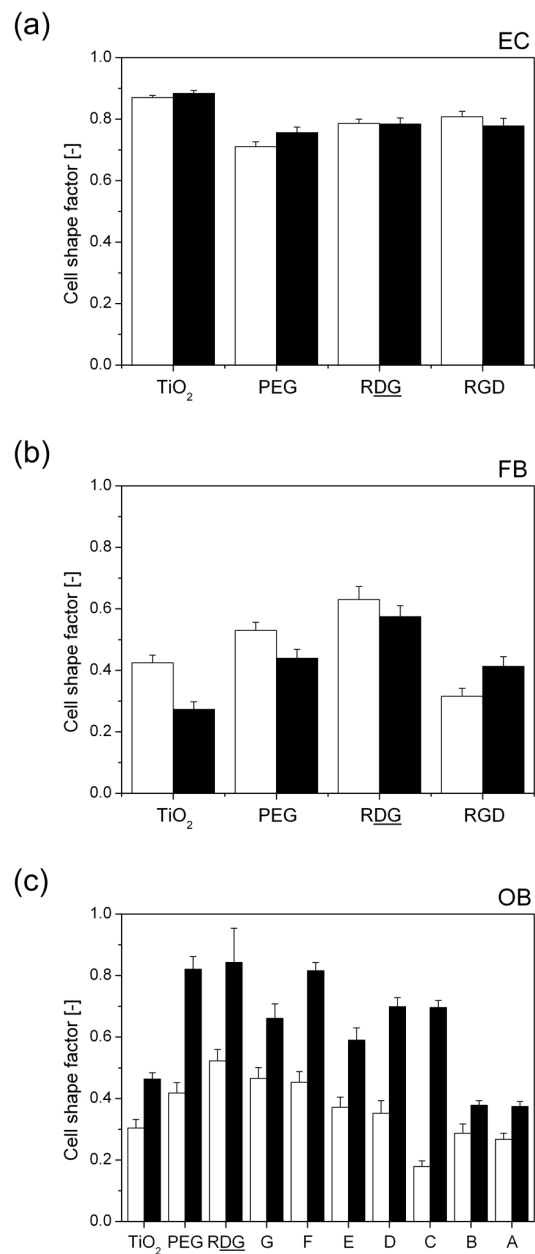
Figure 5.4: Cell shape factor for epithelial cells (a), fibroblasts (b) and osteoblasts (c). White columns refer to cells on the smooth surfaces and black to cells on the rough SLA topographies. The control surfaces were titanium ($\mathbf{TiO_2}$), PLL-g-PEG (**PEG**) and PLL-g-PEG/PEG-R$\underline{\mathrm{DG}}$ (**R$\underline{\mathrm{DG}}$**). **RGD** concentrations in (a) and (b) are comparable with RGD concentration B in (c). See Tables 5.1 and 5.2 for further details.
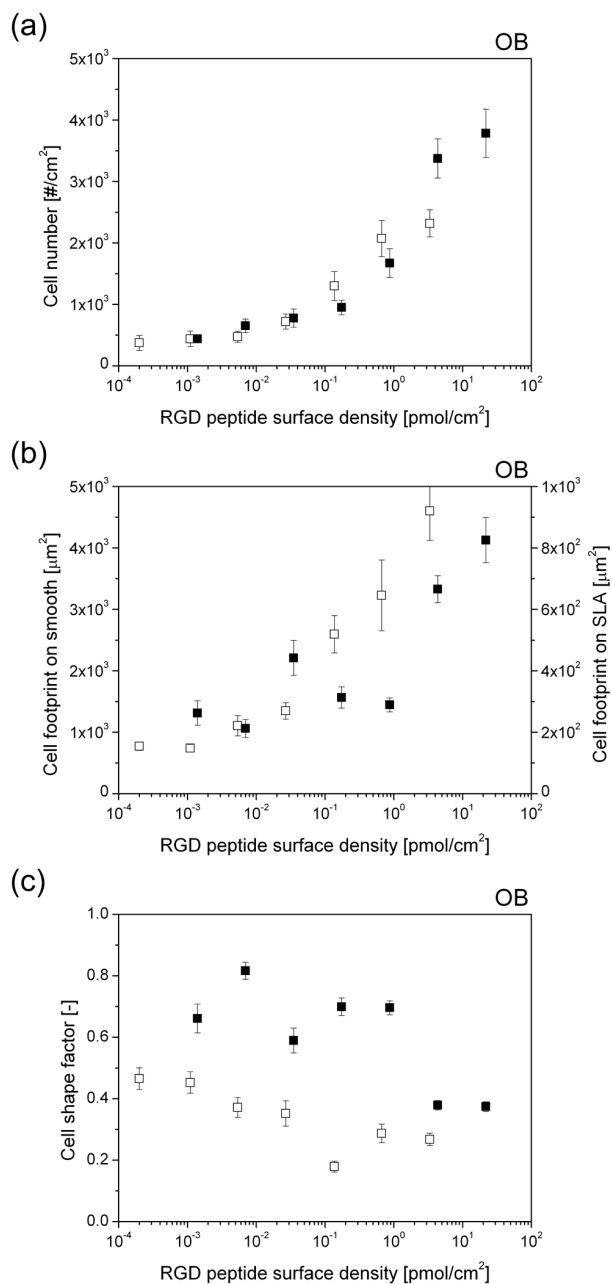
Figure 5.5: Cell number (a), footprint area (b) and shape factor (c) of osteoblasts at different RGD-peptide surface densities (see Table 5.2 for exact peptide densities). White squares refer to cells on the smooth surfaces and black squares to cells on the SLA topographies. Footprint area values in (b) for smooth and rough SLA topographies correspond to the left and right y-axis, respectively.

5.3.4 Osteoblast Microtubules

Microtubule systems of osteoblasts were more expanded on smooth surfaces than those on SLA surfaces (Figure 5.6). Microtubules on TiO_2 and on RGD concentrations A and B were widely distributed within the cells, whereas on RGD concentrations C and D microtubules were found to be concentrated in bundles. Microtubules were not observed clearly in osteoblasts cultured on PEG because these cells were small and spherical.

5.3.5 Vinculin Expression in Eptithelial Cells and Osteoblasts

Focal adhesion sites were qualitatively analyzed for epithelial cells and osteoblasts only. Vinculin expression in epithelial cells on SLA topographies was found on TiO_2 and RGD, except on bio-inactive PEG and R<u>DG</u> (Figure 5.7). Epithelial cells plated on smooth PEG and R<u>DG</u> surfaces showed a non-homogeneous vinculin distribution. Prominent vinculin staining was found on cell-to-cell contacts in comparison to the cell-to-substrate contacts. Vinculin was distinguished in osteoblasts on all SLA topographies except on PEG (Figure 5.8). On smooth surfaces, osteoblasts growing on RGD concentration A, showed the most abundant vinculin staining followed by osteoblasts on TiO_2 and osteoblasts on RGD concentrations B and C. No vinculin staining was visible in osteoblasts on smooth substrates coated with PEG and RGD concentration D.

5.4 Discussion

Our findings have demonstrated that surface topography and chemistry directly influenced the attachment and morphology of epithelial cells, fibroblasts and osteoblasts. In particular the use of the protein-resistant PLL-*g*-PEG system as a background allowed a more direct and powerful control of cell responses than an uncoated or physicochemically modified surface (e.g., hydrophobic/ hydrophilic; see for example [50]). In general, a higher cell attachment and spreading rate was observed on the bioactive surface RGD than on bio-inactive PEG and R<u>DG</u> substrates. This was in agreement with findings of other groups that used similar approaches

Figure 5.6: Microtubule staining of osteoblasts on **RGD**-peptide modified (concentrations A–D) smooth (left) and SLA (right) topographies. Titanium (**TiO₂**) and unfunctionalized PLL-*g*-PEG (**PEG**) coating served as control surfaces. Scale bar of 50 μm (as shown in image SLA-PEG) is the same for all images.
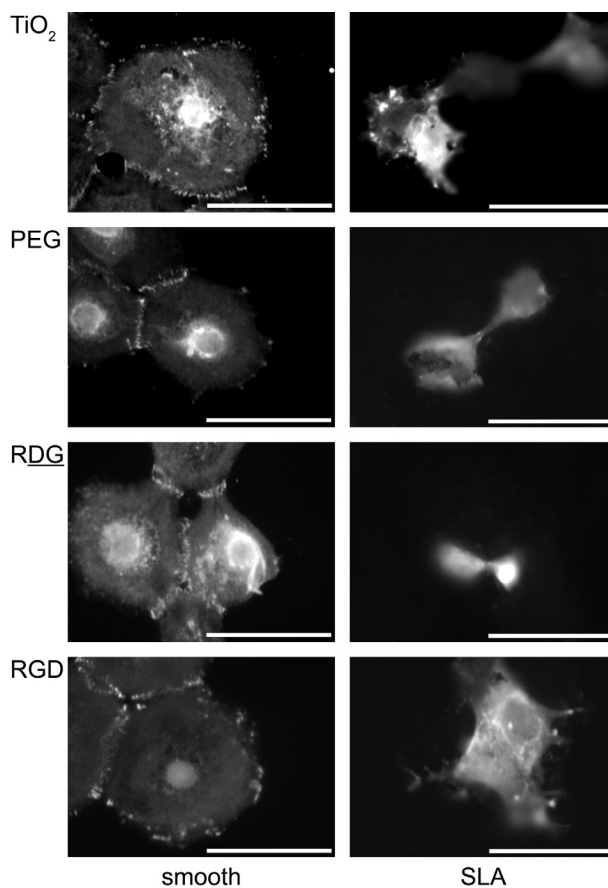
Figure 5.7: Vinculin staining of epithelial cells on **RGD**-peptide modified smooth (left) and SLA (right) topographies. Titanium (**TiO$_2$**) and unfunctionalized PLL-g-PEG (**PEG**) coating served as control surfaces. Size of the scale bar is 50 μm for all images.

(bio-functionalized PEGylated surfaces) for the control of cell attachment [35, 51]. These (non-fouling) immobilization systems have the clear advantage of enabling the influence of a given biofunctional group to be assessed compared to those where non-specific protein adsorption from the culture medium interferes with or dominates cell–surface interaction.
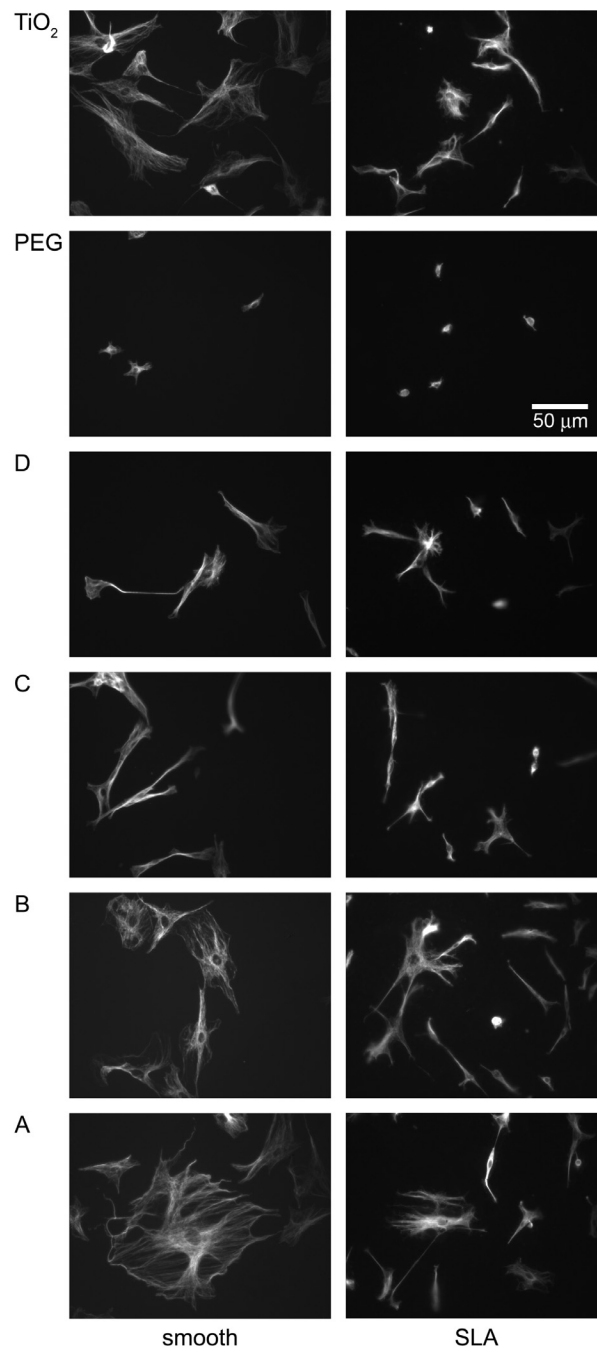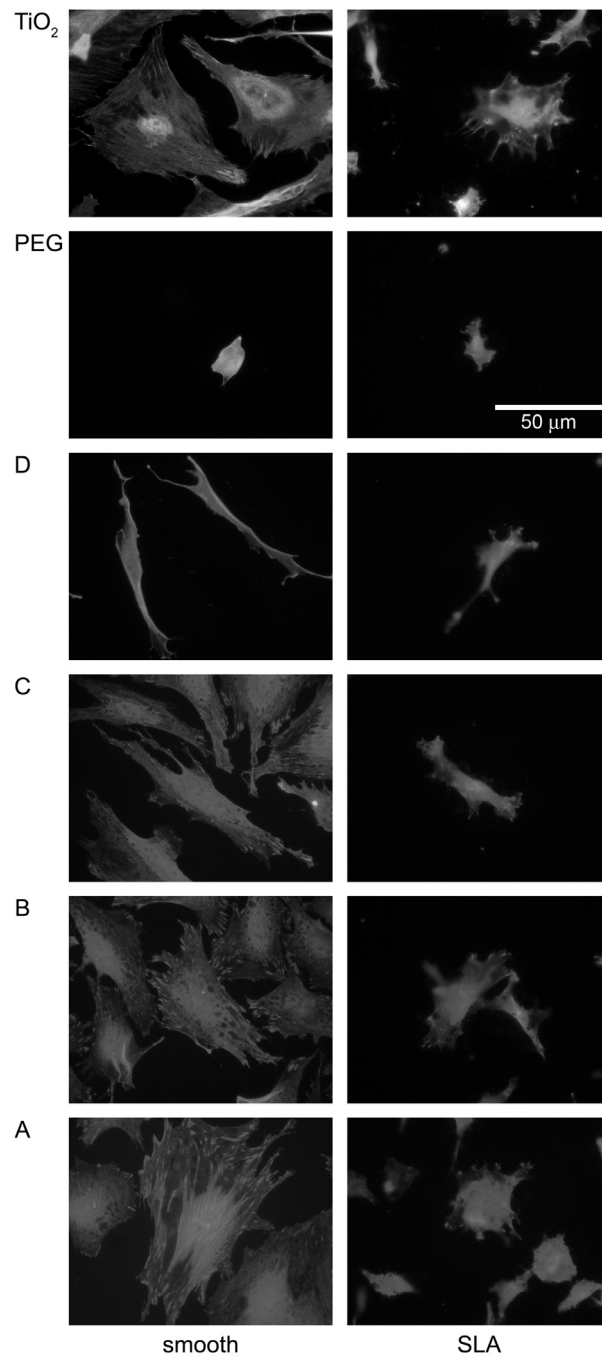
Figure 5.8: Vinculin staining of osteoblasts on **RGD**-peptide modified (concentrations A–D) smooth (left) and SLA (right) topographies. Titanium (**TiO$_2$**) and unfunctionalized PLL-g-PEG (**PEG**) coating served as control surfaces. Scale bar of 50 μm (as shown in image SLA-PEG) is the same for all images.

5.4.1   Cell Behavior on Smooth vs. Rough SLA Topographies

Our results indicate that cell adhesion of fibroblasts and osteoblasts can be influenced via surface roughness, independent of surface chemistry (Figure 5.2b–c). More fibroblasts were found on smooth compared to SLA surfaces, whereas for osteoblasts the opposite tendency was observed. In addition, osteoblast attachment was approximately 1.5 times higher on SLA than on smooth (Figure 5.2c), thus indicating that the small features produced by acid-etching did not seem to influence osteoblast adhesion (see Equation 5.2). Epithelial cell attachment did not follow a regular pattern (Figure 5.2a). Our results showed large variations due to cell clusters indicating a cell–cell contact phenomena, similar to that described in other studies [52–54]. Footprint areas for all cell types on SLA topographies were reduced approximately 5-fold compared to smooth topographies (Figure 5.3). This reduction in cell footprint areas seems to be the result of the specific surface area of the SLA surface (effective surface area divided by projected area), which has been estimated to be 6.5 cm^2/cm^2 by Contu *et al.* [42, 43]. When the effect of topographies was analyzed, osteoblasts demonstrated a significantly higher cell shape factor (more spherical) on SLA surfaces than on smooth surfaces (Figure 5.4c). The opposite response was observed for fibroblasts on TiO$_2$, PEG and R$\underline{DG}$. However, when the effect of bioligands is considered, fibroblasts on RGD surfaces were found to be more circular on rough surfaces than on smooth surfaces (Figure 5.4b). The antagonistic behavior observed in fibroblasts under these two conditions may indicate the lack of an additive effect of topography and surfaces chemistry on those cells. Epithelial cells were circular (high shape factor) on all surfaces, and this shape was independent of type of topography (Figure 5.4a).

5.4.2   Presentation of RGD-containing Peptides on an Inert, Protein-resistant Background

As expected, fewer epithelial cells, fibroblasts and osteoblasts were attached on bioinactive PEG and R$\underline{DG}$ in comparison to TiO$_2$ and RGD. Although PEG and R$\underline{DG}$ are protein-resistant surfaces (<5 ng/cm^2 as shown by OWLS technique) and do not contain any bioligands, a few cells were always found on these substrates. The few attached cells probably are the result of small defects in the PEG-brushes that lead

to local, unspecific protein-adsorption and hence cell adhesion. The introduction of the bioactive RGD-containing PLL-g-PEG polymer with a RGD concentration $\geqslant$0.67 pmol/cm^2 resulted in the restoration of cell adhesion (for all cell types in this study) to a level comparable to the one found on TiO$_2$ surfaces. Peptide surface density $\approx$0.027 pmol/cm^2 (corresponding to a calculated ligand-ligand distance of $\geqslant$84 nm, see Equation 5.3) was found to be the lower limit for producing significantly increased osteoblast adhesion in comparison to the bio-inactive surfaces PEG and RDG (see Figure 5.5a). A distance of <84 and >38 nm between the RGD ligands (see Table 5.2) resulted in limited osteoblast attachment and spreading on smooth surfaces. This finding is consistent with the results of Arnold $et\ al.$ [55], which studied MC3T3-osteoblasts on nano-patterned RGD-thiol functionalized Au-dots on smooth silicon substrates with a PEG background. Osteoblasts attached to SLA surfaces with low RGD densities $\leqslant$0.13 pmol/cm^2 seem to be more influenced by topography (were spherical and less spread) than chemistry. However, on higher peptide surface concentrations ($\geqslant$0.67 pmol/cm^2), the osteoblasts started to bridge over the "larger" cavities (20–50 μm; from the blasting process) and showed a more spread cell shape. The major axis of those cells was measured to be $\geqslant$39 μm. On non-adhesive surface chemistries (PEG and RDG), all cell types investigated in this study were found to be less spread, showing a smaller footprint area than on adhesive surface chemistries. When considering the cell shape factor, which is another marker used to quantify cell spreading, we observed that fibroblasts and osteoblasts on PEG, RDG and on low RGD-peptide surface densities ($\leqslant$0.13 pmol/cm^2) were more circular (less spread) than those on TiO$_2$ or on high RGD-peptide surface densities ($\geqslant$0.67 pmol/cm^2). Epithelial cells were spherical on all surfaces, although they were less spread on bio-inactive surfaces than on bioactive, indicating that the contact of neighbor cells may induce spreading [53] (Figure 5.7). This suggests, that the bio-inactive surface decreased the degree of cell–surface interactions. Osteoblast attachment and footprint areas increased with higher RGD-peptide surface density (Figure 5.5a–b). However, Tosatti $et\ al.$ [36] have shown with MG63 osteoblast-like cells on non-adhesive SLA surfaces (as PEG and RDG) that there was a higher degree of differentiation (as assessed by TGF-β1 and PGE$_2$) than on TiO$_2$ or RGD (peptide surface density >0.05 pmol/cm^2). This leads to the speculation that engineering of a surface, which maximizes osteoblast adhesion and spreading (e.g., through high RGD-peptide surface densities) might not be the optimal way for bone-contacting implants and that a surface which attaches osteoblasts in a

less-spread, more spherical shape (as observed on low-concentrated RGD surfaces) may be more favorable in terms of early differentiation. An alternative approach to create a surface that is more suitable for bone-contacting implants (e.g., dental implants) is the use of other, osteoblast-specific sequences such as KRSR [56, 57] or FHRRIKA [26, 51]. On the other hand, the RGD sequence could become a useful component for the design of new biomaterial surfaces when applied in combination with KRSR or FHRRIKA peptides [58].

5.4.3   Cell Organization and Focal Adhesion Sites

Maintenance of cell shape has been shown to depend on an intact microtubule system (see for example [59]). Our findings demonstrated that surface topography had an influence on microtubule architecture. Microtubule systems in osteoblasts on smooth surfaces were more isotropically distributed than those found on SLA surfaces (Figure 5.6). Osteoblasts on TiO_2 and on RGD surfaces with concentrations $\geqslant 0.67$ pmol/cm^2 expressed a widely distributed microtubule system, while microtubules of osteoblasts on RGD concentrations >0.03 pmol/cm^2 and <0.67 pmol/cm^2 were found to prefer a bipolar orientation, giving to the cell a more elongated shape. Cells on the bio-inactive PEG surface were found circular and small in footprint, making impossible to analyze the microtubule system. Epithelial cells expressed higher amounts of vinculin on smooth compared to rough surfaces with the same chemistry (Figure 5.7). Differences in vinculin expression were also observed on clusters of epithelial cells attached on PEG and RDG surfaces. A higher density of focal adhesion sites was found at the cell-to-cell interface in comparison to areas where no contact between cells occurred. This effect was less pronounced on TiO_2 or RGD substrates and can be explained with the rationale that on the bio-inactive surfaces the epithelial cells were forced to interact with each other. Furthermore, as a consequence of cell-clusters, we found a higher amount of cell-to-cell contacts on PEG and PLL-g-PEG/PEG-RDG surfaces than on TiO_2 or RGD, where the epithelial cells tended to be more isolated from each other. Vinculin expression in osteoblasts was not detected on RGD surfaces with surface densities $\leqslant 0.03$ pmol/cm^2, implying that no focal contacts were formed on these RGD concentrations (corresponding to an average peptide–peptide distance of 84 nm). However, there was some cell spreading observed despite of the absence of focal contacts (Figure 5.8). Spreading without pronounced focal contacts has been observed by Hubbell *et al.* [60] for

Human Foreskin Fibroblasts (HFF) on **GRGD**Y peptide modified glass substrates (corresponding to a ligand–ligand distance of <140 nm) indicating another mode of attachment.

5.5 Conclusion

Our study on cell attachment to surfaces with controlled surface topographies and (bio)chemistries demonstrated that surface roughness directly influenced cell attachment and cell footprint areas of fibroblasts and osteoblasts but not of epithelial cells under the cell culturing conditions used in this study. The presence or absence of cell–cell contacts seemed to have a more important influence on the behavior of epithelial cells. Surface chemistry was found to determine both the number of cells attached and the size of footprint areas for all cell types investigated in this study. In particular, the coating with the non-fouling PLL-g-PEG polymer reduced cell attachment and footprint areas drastically whereas the immobilization of the RGD-peptide sequence at surface densities $\geqslant 0.67$ pmol/cm^2 restored cell attachment and footprint areas to levels typically found on (unmodified) titanium surfaces. No synergy (interaction) between RGD-peptide surface density and surface topography was observed for osteoblasts neither in terms of attachment nor footprint area. However, there was a significant effect of RGD-peptide densities on the numbers and the footprint areas of osteoblasts attached to these surfaces.

Bibliography

[1] Scacchi, M. The development of the ITI (R) DENTAL IMPLANT SYSTEM - Part 1: A review of the literature. *Clinical Oral Implants Research*, **11**, 8–21, 2000.

[2] Rezania, A., Thomas, C. H., Branger, A. B., Waters, C. M. and Healy, K. E. The detachment strength and morphology of bone cells contacting materials modified with a peptide sequence found within bone sialoprotein. *Journal of Biomedical Materials Research*, **37**(1), 9–19, 1997.

[3] Ito, Y., Kajihara, M. and Imanishi, Y. Materials for Enhancing Cell-Adhesion by Immobilization of Cell-Adhesive Peptide. *Journal of Biomedical Materials Research*, **25**(11), 1325–1337, 1991.

[4] Puleo, D. A. and Nanci, A. Understanding and controlling the bone-implant interface. *Biomaterials*, **20**(23-24), 2311–2321, 1999.

[5] Jaeger, N. and Brunette, D. M. Production of microfabricated surfaces and their effects on cell behavior. In Brunette, D. M., Tengvall, P., Textor, M. and Thomsen, P., editors, *Titanium in Medicine*, pages 343–374. Springer-Verlag, Berlin Heidelberg, 2001.

[6] Brunette, D. M., Kenner, G. S. and Gould, T. R. L. Grooved Titanium Surfaces Orient Growth and Migration of Cells from Human Gingival Explants. *Journal of Dental Research*, **62**(10), 1045–1048, 1983.

[7] Sykaras, N., Iacopino, A. M., Marker, V. A., Triplett, R. G. and Woody, R. D. Implant materials, designs, and surface topographies: Their effect on osseointegration. A literature review. *International Journal of Oral Maxillofacial Implants*, **15**(5), 675–690, 2000.

[8] Wennerberg, A., Albrektsson, T. and Andersson, B. Design and surface characteristics of 13 commercially available oral implant systems. *Int J Oral Maxillofac Implants*, **8**, 622–633, 1993.

[9] Wieland, M. *Experimental determination and quantitative evaluation of the surface composition and topography of medical implant surfaces and their influence on osteoblastic cell-surface interactions*. Ph.D. Thesis No. 13247, Swiss Federal Institute of Technology Zurich, 1999.

[10] Wieland, M., Textor, M., Spencer, N. D. and Brunette, D. M. Measurement and Evaluation of the Chemical Composition and Topography of Titanium Implant Surface. In Davies, J. E., editor, *Bone Engineering*. Em Squared Inc., 2000.

[11] Wieland, M., Chehroudi, B., Textor, M. and Brunette, D. M. Use of Ti-coated replicas to investigate the effects on fibroblast shape of surfaces with varying roughness and constant chemical composition. *Journal of Biomedical Materials Research*, **60**(3), 434–444, 2002.

[12] Wieland, M., Textor, M., Spencer, N. D. and Brunette, D. M. Wavelength-dependent roughness: A quantitative approach to characterizing the topography of rough titanium surfaces. *International Journal of Oral Maxillofacial Implants*, **16**(2), 163–181, 2001.

[13] Albrektsson, T., Branemark, P. I., Hansson, H. A. and Lindstrom, J. Osseointegrated Titanium Implants - Requirements for Ensuring a Long-Lasting, Direct Bone-to-Implant Anchorage in Man. *Acta Orthopaedica Scandinavica*, **52**(2), 155–170, 1981.

[14] Brunette, D. M., Tengvall, P., Textor, M. and Thomsen, P. *Titanium in Medicine*. Springer-Verlag, Berlin Heidelberg, 2001.

[15] Buser, D. Titanium for dental applications (II). In Brunette, D. M., Tengvall, P., Textor, M. and Thomsen, P., editors, *Titanium in Medicine*, pages 875–888. Springer-Verlag, Berlin Heidelberg, 2001.

[16] Boyan, B. D., Dean, D. D., Lohmann, C. H., Cochran, D. L., Sylvia, V. L. and Schwartz, Z. The titanium-bone cell interface in vitro: the role of the surface in promoting osteointegration. In Brunette, D. M., Tengvall, P., Textor, M. and Thomsen, P., editors, *Titanium in Medicine*, pages 561–586. Springer-Verlag, Berlin Heidelberg, 2001.

[17] Scacchi, M., Merz, B. R. and Schar, A. R. The development of the ITI (R) DENTAL IMPLANT SYSTEM - Part 2. 1998-2000: Steps into the next millennium. *Clinical Oral Implants Research*, **11**, 22–32, 2000.

[18] Bornstein, M. M., Lussi, A., Schmid, B., Belser, U. C. and Buser, D. Early loading of nonsubmerged titanium implants with a sandblasted and acid-etched (SLA) surface: 3-year results of a prospective study in partially edentulous

patients. *International Journal of Oral Maxillofacial Implants*, **18**(5), 659–666, 2003.

[19] Cochran, D. L., Buser, D., ten Bruggenkate, C. M., Weingart, D., Taylor, T. M., Bernard, J. P., Peters, F. and Simpson, J. P. The use of reduced healing times on ITI (R) implants with a sandblasted and acid-etched (SLA) surface: Early results from clinical trials on ITI (R) SLA implants. *Clinical Oral Implants Research*, **13**(2), 144–153, 2002.

[20] Roccuzzo, M., Bunino, M., Prioglio, F. and Bianchi, S. D. Early loading of sandblasted and acid-etched (SLA) implants: A prospective split-mouth comparative study - One-year results. *Clinical Oral Implants Research*, **12**(6), 572–578, 2001.

[21] Boyan, B. D., Lohmann, C. H., Dean, D. D., Sylvia, V. L., Cochran, D. L. and Schwartz, Z. Mechanisms involved in osteoblast response to implant surface morphology. *Annual Review of Materials Research*, **31**, 357–371, 2001.

[22] Baharloo, B., Textor, M. and Brunette, D. M. Substratum roughness alters the growth, area, and focal adhesions of epithelial cells, and their proximity to titanium surfaces. *Journal Of Biomedical Materials Research Part A*, **74A**(1), 12–22, 2005.

[23] Chehroudi, B., Soorany, E., Black, N., Weston, L. and Brunette, D. M. Computer-Assisted 3-Dimensional Reconstruction Of Epithelial-Cells Attached To Percutaneous Implants. *Journal Of Biomedical Materials Research*, **29**(3), 371–379, 1995.

[24] Bains, R., Furness, P. N. and Critchley, D. R. A quantitative immunofluorescence study of glomerular cell adhesion proteins in proteinuric states. *Journal Of Pathology*, **183**(3), 272–280, 1997.

[25] Healy, K. E., Harbers, G. M., Barber, T. A. and Sumner, D. R. Osteoblast Interactions with Engineered Surfaces. In Davies, J., editor, *Bone Engineering*, pages 268–281. EMSSquared Inc., Toronto, 2000.

[26] Rezania, A. and Healy, K. E. Biomimetic peptide surfaces that regulate adhesion, spreading, cytoskeletal organization, and mineralization of the matrix deposited by osteoblast-like cells. *Biotechnology Progress*, **15**(1), 19–32, 1999.

[27] Garcia, A. J., Collard, D. M., Keselowsky, B. G., Cutler, S. M., Gallant, N. D., Byers, B. A. and Stephansson, S. N. Engineering of Integrin-Specific Biomimetic Surfaces to Control Cell Adhesion and Function. In Dillow, A. K. and Lowman, A. M., editors, *Biomimetic Materials and Design*, pages 29–53. Dekker, New York, 2002.

[28] Pierschbacher, M. D. and Ruoslahti, E. Cell Attachment Activity of Fibronectin Can Be Duplicated by Small Synthetic Fragments of the Molecule. *Nature*, **309**(5963), 30–33, 1984.

[29] Ruoslahti, E. RGD and other recognition sequences for integrins. *Annual Review of Cell and Developmental Biology*, **12**, 697–715, 1996.

[30] Hersel, U., Dahmen, C. and Kessler, H. RGD modified polymers: biomaterials for stimulated cell adhesion and beyond. *Biomaterials*, **24**(24), 4385–4415, 2003.

[31] Huang, N. P., Michel, R., Voros, J., Textor, M., Hofer, R., Rossi, A., Elbert, D. L., Hubbell, J. A. and Spencer, N. D. Poly(L-lysine)-g-poly(ethylene glycol) layers on metal oxide surfaces: Surface-analytical characterization and resistance to serum and fibrinogen adsorption. *Langmuir*, **17**(2), 489–498, 2001.

[32] Kenausis, G. L., Voros, J., Elbert, D. L., Huang, N. P., Hofer, R., Ruiz-Taylor, L., Textor, M., Hubbell, J. A. and Spencer, N. D. Poly(L-lysine)-g-poly(ethylene glycol) layers on metal oxide surfaces: Attachment mechanism and effects of polymer architecture on resistance to protein adsorption. *Journal of Physical Chemistry B*, **104**(14), 3298–3309, 2000.

[33] Tosatti, S., De Paul, S. M., Askendal, A., VandeVondele, S., Hubbell, J. A., Tengvall, P. and Textor, M. Peptide functionalized poly(L-lysine)-g-poly(ethylene glycol) on titanium: resistance to protein adsorption in full heparinized human blood plasma. *Biomaterials*, **24**(27), 4949–4958, 2003.

[34] Morra, M. On the molecular basis of fouling resistance. *Journal of Biomaterials Science-Polymer Edition*, **11**(6), 547–569, 2000.

[35] Dalsin, J. L., Lin, L. J., Tosatti, S., Voros, J., Textor, M. and Messersmith, P. B. Protein resistance of titanium oxide surfaces modified by biologically inspired mPEG-DOPA. *Langmuir*, **21**(2), 640–646, 2005.

[36] Tosatti, S., Schwartz, Z., Campbell, C., Cochran, D. L., VandeVondele, S., Hubbell, J. A., Denzer, A., Simpson, J., Wieland, M., Lohmann, C. H., Textor, M. and Boyan, B. D. RGD-containing Peptide GCRGYGRGDSPG Reduces Enhancement of Osteoblast Differentiation by Poly(L-lysine graft-poly(ethylene glycol) Coated Titanium Surfaces. *accepted in Journal of Biomedical Materials Research*, **68A**(3), 458–472, 2004.

[37] Pasche, S., Textor, M., Meagher, L., Spencer, N. D. and Griesser, H. J. Relationship between interfacial forces measured by colloid-probe atomic force microscopy and protein resistance of poly(ethylene glycol)-grafted poly(L-lysine) adlayers on niobia surfaces. *Langmuir*, **21**(14), 6508–6520, 2005.

[38] VandeVondele, S., Voros, J. and Hubbell, J. A. RGD-Grafted poly-l-lysine-graft-(polyethylene glycol) copolymers block non-specific protein adsorption while promoting cell adhesion. *Biotechnology and Bioengineering*, **82**(7), 784–790, 2003.

[39] Pasche, S., De Paul, S. M., Voros, J., Spencer, N. D. and Textor, M. Poly(L-lysine)-graft-poly(ethylene glycol) assembled monolayers on niobium oxide surfaces: A quantitative study of the influence of polymer interfacial architecture on resistance to protein adsorption by ToF-SIMS and in situ OWLS. *Langmuir*, **19**(22), 9216–9225, 2003.

[40] Tosatti, S., Michel, R., Textor, M. and Spencer, N. D. Self-assembled monolayers of dodecyl and hydroxy-dodecyl phosphates on both smooth and rough titanium and titanium oxide surfaces. *Langmuir*, **18**(9), 3537–3548, 2002.

[41] Voros, J., Ramsden, J. J., Csucs, G., Szendro, I., De Paul, S. M., Textor, M. and Spencer, N. D. Optical grating coupler biosensors. *Biomaterials*, **23**(17), 3699–3710, 2002.

[42] Contu, F., Elsener, B. and Bohni, H. Characterization of implant materials in fetal bovine serum and sodium sulfate by electrochemical impedance spectroscopy. II. Coarsely sandblasted samples. *Journal of Biomedical Materials Research Part A*, **67A**(1), 246–254, 2003.

[43] Contu, F., Elsener, B. and Bohni, H. Characterization of implant materials in fetal bovine serum and sodium sulfate by electrochemical impedance spec-

troscopy. I. Mechanically polished samples. *Journal of Biomedical Materials Research*, **62**(3), 412–421, 2002.

[44] Brunette, D. M., Melcher, A. H. and Moe, H. K. Culture and Origin of Epithelium-Like and Fibroblast-Like Cells from Porcine Periodontal-Ligament Explants and Cell-Suspensions. *Archives of Oral Biology*, **21**(7), 393–400, 1976.

[45] Elvin, P. and Evans, C. W. The Adhesiveness of Normal and Sv40-Transformed Balb/C 3t3- Cells - Effects of Culture Density and Shear Rate. *European Journal of Cancer Clinical Oncology*, **18**(7), 669–675, 1982.

[46] Hasegawa, S., Sato, S., Saito, S., Suzuki, Y. and Brunette, D. M. Mechanical Stretching Increases the Number of Cultured Bone- Cells Synthesizing DNA and Alters Their Pattern of Protein- Synthesis. *Calcified Tissue International*, **37**(4), 431–436, 1985.

[47] Chehroudi, B., Ratkay, J. and Brunette, D. M. The Role of Implant Surface Geometry on Mineralization Invivo and Invitro - a Transmission and Scanning Electron-Microscopic Study. *Cells and Materials*, **2**(2), 89–104, 1992.

[48] Huang, N. P., Voros, J., De Paul, S. M., Textor, M. and Spencer, N. D. Biotin-derivatized poly(L-lysine)-g-poly(ethylene glycol): A novel polymeric interface for bioaffinity sensing. *Langmuir*, **18**(1), 220–230, 2002.

[49] Hamilton, D. W. and Brunette, D. M. "Gap guidance" of fibroblasts and epithelial cells by discontinuous edged surfaces. *Experimental Cell Research*, **309**(2), 429–437, 2005.

[50] Textor, M., Tosatti, S., Wieland, M. and Brunette, D. M. Use of Molecular Assembly Techniques For Tailoring the Chemical Properties On Smooth and Rough Titanium Surfaces. In Ellingsen, J. and Lyngstadaas, S., editors, *Bio-Implant Interface: Improving Biomaterials and Tissue Reaction*. CRC Press, 2003.

[51] Healy, K. E., Rezania, A. and Stile, R. A. Designing biomaterials to direct biological responses. In *Bioartificial Organs Ii: Technology, Medicine, and Materials*, volume 875 of *Annals of the New York Academy of Sciences*, pages 24–35. NEW YORK ACAD SCIENCES, New York, 1999.

[52] Middleton, C. A. Effects Of Cell-Cell Contact On Spreading Of Pigmented Retina Epithelial-Cells In Culture. *Experimental Cell Research*, **109**(2), 349–359, 1977.

[53] Middleton, C. A. Contact-Induced Spreading Is A New Phenomenon Depending On Cell-Cell Contact. *Nature*, **259**(5541), 311–313, 1976.

[54] Oakley, C. and Brunette, D. M. Response of single, pairs, and clusters of epithelial cells to substratum topography. *Biochemistry and Cell Biology-Biochimie Et Biologie Cellulaire*, **73**(7-8), 473–489, 1995.

[55] Arnold, M., Cavalcanti-Adam, E. A., Glass, R., Blummel, J., Eck, W., Kantlehner, M., Kessler, H. and Spatz, J. P. Activation of integrin function by nanopatterned adhesive interfaces. *Chemphyschem*, **5**(3), 383–388, 2004.

[56] Dettin, M., Conconi, M. T., Gambaretto, R., Pasquato, A., Folin, M., Di Bello, C. and Parnigotto, P. P. Novel osteoblast-adhesive peptides for dental/orthopedic biomaterials. *Journal of Biomedical Materials Research*, **60**(3), 466–471, 2002.

[57] Hasenbein, M. E., Andersen, T. T. and Bizios, R. Micropatterned surfaces modified with select peptides promote exclusive interactions with osteoblasts. *Biomaterials*, **23**(19), 3937–3942, 2002.

[58] Schaffner, P. and Dard, M. M. Structure and function of RGD peptides involved in bone biology. *Cellular and Molecular Life Sciences*, **60**(1), 119–132, 2003.

[59] Rodionov, V. I., Gyoeva, F. K., Tanaka, E., Bershadsky, A. D., Vasiliev, J. M. and Gelfand, V. I. Microtubule-Dependent Control Of Cell-Shape And Pseudopodial Activity Is Inhibited By The Antibody To Kinesin Motor Domain. *Journal Of Cell Biology*, **123**(6), 1811–1820, 1993.

[60] Massia, S. P. and Hubbell, J. A. An Rgd Spacing of 440nm Is Sufficient for Integrin Alpha-V- Beta-3-Mediated Fibroblast Spreading and 140nm for Focal Contact and Stress Fiber Formation. *Journal of Cell Biology*, **114**(5), 1089–1100, 1991.

6

Comparison of the Response of Cultured Osteoblasts and Osteoblasts Outgrown from Rat Calvarial Bone Chips, to Non-fouling KRSR and FHRRIKA-peptide Modified Rough Titanium Surfaces

Martin Schuler, Douglas W. Hamilton, Tobias P. Kunzler, Christoph M. Sprecher, Michael de Wild, Donald M. Brunette, Marcus Textor, Samuele G.P. Tosatti

Mimicking proteins found in the extracellular matrix (ECM) using specific peptide sequences is a relatively new strategy for the design of biomimetic surfaces that could be used for a new generation of implants. We investigated osteoblast and fibroblast proliferation to novel consensus heparin-binding peptides sequences KRSR and FHRIKKA that were immobilized onto rough titanium dental implant surfaces using a poly(L-lysine)-graft-poly(ethylene glycol) (PLL-g-PEG) molecular assembly

system, which enabled due to its non-fouling properties, a detailed study of the specific cell-peptide interactions even in the presence of serum. Cell-binding peptide sequence RGD in combination with KRSR or FHRRIKA was used to examine a possible enhanced effect on osteoblast attachment and proliferation. Bare titanium and bio-inactive surfaces (i.e., unfunctionalized PLL-g-PEG and scrambled K̲S̲SR, R̲FHARIK and R̲D̲G) were used as control substrates. In addition, freshly harvested bone chips from newborn rat calvariae were placed onto similar functionally modified rough titanium substrates and the size and pattern of osteoblast outgrowths studied. Our findings demonstrated that the difference in osteoblast and fibroblast attachment was rather influenced by surface topography than by KRSR and FHRRIKA. On the other hand, in comparison with the control surfaces, osteoblast outgrowths from rat calvarial bone chips covered a significantly larger area on RGD, KRSR and FHRRIKA after 8 days and also migrated in an isotropic way unlike cells on the bio-inactive substrates. Furthermore, the stimulatory effect of RGD on both osteoblast attachment and migration pattern could be enhanced when applied in combination with KRSR.

Keywords: surface topography, primary rat calvarial osteoblasts, human gingival fibroblasts, bone chip, cell outgrowth, biomimetic modification.

6.1   Introduction

There is increasing interest in immobilizing on implants specific peptide sequences that mimic proteins found within the extracellular matrix (ECM) to enhance tissue integration [1, 2]. Such bioligands have the ability to bind to the cells via specific cell surface receptors. A frequently used peptide sequence is RGD (arginine-glycine-aspartic acid) [3] that has been identified on a loop on the tenth domain of fibronectin (FN III-10) [4]. RGD is recognized by nearly half of the over 20 known α/β integrins, a family of receptors present in most cell types [5]. However, integrin-RGD interaction is only one of the mechanisms involved in osteoblast adhesion; another is the interaction between cellular transmembrane heparan sulfate proteoglycans and heparin-binding sites on ECM proteins [6, 7]. Two recently identified peptides sequences that interact with transmembrane proteoglycans are KRSR and FHRRIKA. KRSR represents a sequence found in five different bone-related adhesive proteins, such as, fibronectin, vitronectin, bone sialoprotein, thrombospondin and osteopon-

tin [8], whereas FHRRIKA was derived from bone sialoprotein alone [9]. It has been reported in various studies that the KRSR motif is selective for osteoblast attachment to surfaces, but not for either endothelial cells [10] and fibroblasts [11]. Dee *et al.* have also demonstrated cell attachment on KRSR-modified surfaces with similar levels as usually found on RGD-modified ones [8]. The combination of two different peptide sequences, as for example RGD and FHRRIKA, could result in possible enhanced effects [9, 12]. Moreover, it has been reported in different studies that a more "complete" cell response was obtained by providing the cell with both a cell-binding and a heparin-binding domain of fibronectin as implied through cell attachment and spreading, formation of discrete focal contacts and an organized cytoskeletal assembly [6, 13].

Our concept of immobilizing peptide sequences was based on self-assembling adlayers of poly(L-lysine)-*graft*-poly(ethylene glycol) (PLL-*g*-PEG). These adlayers form a dense PEG brush that render negatively charged biomaterial surfaces (e.g., titanium dioxide) resistant to non-specific protein adsorption (typically less than 5 ng/cm^2 upon serum or blood plasma exposure) [14, 15]. The peptide sequence itself is covalently coupled to a fraction of the PEG-chains via vinyl sulfone-cysteine chemistry [14, 16, 17]. This principle of creating a "silent" (non-fouling [18]) background gives the possibility to study cell receptor-peptide interactions even in the presence of serum or blood plasma. Although this fact is already strongly recognized as a prerequisite in the biosensor field, it is applied less commonly in cell studies for implant applications [19].

The goal of our study was to determine rat calvarial osteoblast response to the novel peptide sequences KRSR and FHRRIKA using the PLL-*g*-PEG immobilization system on particle-blasted and acid-etched commercially pure titanium substrates (SLA CP Ti). Human gingival fibroblasts served as control cell type. Furthermore, a possible synergistic effect was investigated when KRSR- or FHRRIKA-modified PLL-*g*-PEG was co-adsorbed in combination with various concentrations of RGD-functionalized PLL-*g*-PEG . Osteoblast and fibroblast attachment was observed after 7 days. In addition, freshly harvested bone chips obtained from newborn rat calvariae were placed onto PEGylated surfaces containing peptides (as above) and patterns of outgrown osteoblasts were investigated after 4, 6, 8 and 10 days. Both parts of the experiment were analyzed using fluorescence microscopy.

6.2   Materials and Methods

6.2.1   Substrates

CP titanium discs with the dental implant surface SLA (manufactured by Institut Straumann AG, Basel, CH) were ultrasonically cleaned in 2-propanol (Sigma-Aldrich, Buchs, CH) for 2 x 10 min, dried immediately in a steam of N_2 (PanGas, Zurich, CH; 0.22 μm filtered) and wrapped with aluminum foil until further use.

6.2.2   Polymers

Synthesis and Notation

Peptide-functionalized and unfunctionalized PLL-g-PEG polymers were synthesized similarly to previously published protocols [14–17]. In brief, peptides and NHS-PEG-VS (Mw≈3.4 kDa, polydispersity: 1.01; Nektar, Bradford, UK) were reacted for 5 min in a salt buffer solution containing 10 mM HEPES (N-(2-hydroxyethyl)-piperazine-N'-2-ethanesulfonic acid; Sigma-Aldrich, Buchs, CH) at pH 8.4. PLL hydrobromide (polydispersity: 1.4; Sigma-Aldrich, Buchs, CH) was dissolved in HEPES and added to the reaction. After one hour mPEG-SPA (Mw≈2 kDa; polydispersity: 1.02; Sigma-Aldrich, Buchs, CH) was dissolved in HEPES and added to the final mixture that was stirred for 24 hours at room temperature. 50 μl of β-mercaptoethanol (Fluka, Buchs, CH) was used for quenching and prior to freeze-drying, the mixture was dialyzed against deionized water for 48 hours. Polymers resulted in a white powder and were kept frozen at -20 °C before use.

The following amino acid sequences were used for the synthesis of peptide-functionalized PLL-g-PEG polmyers: the cell binding Ac-GCRGYG**RGD**SPG-NH$_2$ (-R<u>DG</u>-) peptide (both purchased from Jerini, Berlin, GER) and the two heparin-binding Ac-GCRGYG**KRSR**G-NH$_2$ (-K<u>S</u>SR-) and Ac-GCRGYG**FHRRIKA**G-NH$_2$ (-<u>RFHARIK</u>-) peptides (all purchased from JPT Peptide Technologies GmbH, Berlin, GER). The (scrambled) sequences in brackets were used as negative control peptides.

For convenience, the peptide-functionalized polymers were named hereafter according to their peptide sequence (PLL-g-PEG/PEG-RGD as **RGD**; PLL-g-PEG/PEG-R<u>DG</u> as **R<u>DG</u>**; PLL-g-PEG/PEG-KRSR as **KRSR**; PLL-g-PEG/PEG-K<u>S</u>SR

as **K$\underline{\text{S}}$SR**; PLL-g-PEG/PEG-FHRRIKA as **FHRRIKA**; PLL-g-PEG/PEG-RFHARIK as **RFHARIK**) and the unfunctionalized PLL-g-PEG as **PEG**. Furthermore, surfaces coated with these polymers were separated into bio-active and bio-inactive surfaces as explained in Table 6.1.

Table 6.1: Notation used for bio-active and bio-inactive surfaces. Abbreviations are explained in section 6.2.2.

bio-active	bio-inactive
Ti	PEG
RGD	R$\underline{\text{D}}$G
KRSR	K$\underline{\text{S}}$SR
FHRRIKA	RFHARIK
and mixtures thereof	

Characterization

The architecture of the polymers, determined through grafting ratio g and fraction P of peptide-functionalized PEG-chains, was characterized with nuclear magnetic resonance spectroscopy (NMR) [14]. The adsorbed polymer masses and their protein resistances were examined with *in situ* optical waveguide lightmode spectroscopy (OWLS) [15, 20] (Table 6.2). All polymers used were proven to be highly resistant against serum adsorption and masses <5ng/cm^2 were measured, what is in the range of the detection limit of the OWLS.

Peptide Surface Densities and Multi-peptide Surfaces

Peptide surface densities (Table 6.2) for the peptide-functionalized PLL-g-PEG polymers were determined as published elsewhere ([14, 17]). For comparison reasons between the different peptide surfaces, equimolar surfaces with a total peptide surface density of 3.0 pmol/cm^2 were used. When working with multi-peptide surfaces of KRSR/RGD or FHRRIKA/RGD, the following notation was given (Figure 6.2, Figure 6.4): e.g., **75KRSR/25RGD** that refers to 75% KRSR ($= 2.25$ pmol/cm^2) of the total peptide density of 3.0 pmol/cm^2, mixed with 25% RGD ($= 0.75$ pmol/cm^2),

whereas for the corresponding control surface containing only the peptide RGD but with the same concentration (0.75 pmol/cm^2), the notation was **75PEG/25RGD**.

Table 6.2: Molecular weight, grafting ratio, peptide functionalization, polymer/protein adsorption and peptide surface density for all polymers used in this paper.

	PEG	RGD	R<u>D</u>G	KRSR	K<u>S</u>SR	FHRRIKA	<u>RFHARIK</u>
Molecular weight PLL [kDa]	15.9	15.9	15.9	15.9	15.9	15.9	15.9
Molecular weight lysine unit [kDa]	0.128	0.128	0.128	0.128	0.128	0.128	0.128
Molecular weight peptide [kDa]	-	1.222	1.222	1.197	1.128	1.578	1.578
Molecular weight entire polymer [kDa]	99.1	69.4	70.5	66.4	64.1	70.8	71.9
Grafting ratio g [-][a]	3.3	5.9	5.6	6	6.4	6.1	5.9
Peptide-functionalized PEG-chains [%][a]	-	10.4	7.7	7.4	8.9	13.7	13.5
Polymer adsorption [ng/cm^2][b]	175	180	180	169	170	178	179
Protein adsorption [ng/cm^2][b]	< 5	< 5	< 5	< 5	< 5	< 5	< 5
Peptide surface density ρ_{ps} [pmol/cm^2][c]	-	6.2	3	4.2	5	7.7	7.7

[a]measured with NMR technique.

[b]measured with OWLS technique.

[c]Calculated for smooth topographies (see Schuler *et al.* [17]).

6.2.3 *In vitro* Preparation

Cell Cultures

Osteogenic cells were obtained from newborn rat calvariae, isolated and subcultered as published by Hasegawa *et al.* [21] and Chehroudi *et al.* [22]. Frontal, parietal and occipital bone were dissected and rinsed in α-MEM (Stemcell, Vancouver, BC, CAN). Minced tissue was digested twice for each 15 min with a mixture of clostridial collagenase/trypsin (3:1; both purchased from Sigma-Aldrich, Oakville, Ont., CAN) and the second digestion plated in tissue culture flasks using α-MEM supplemented with antibiotics (100 mg/ml penicillin G, Sigma-Aldrich, Oakville, Ont., CAN; 50 mg/ml gentamicin, Sigma-Aldrich; 3 mg/ml amphoteracin B, Gibco, Grand Island, NY, USA and 15% of fetal calf serum (Cansera, Rexdale, Ont., CAN). Fibroblasts were isolated from human gingival explants as reported by Brunette *et al.* [23] and cultured in tissue culture flasks using α-MEM containing 15% serum fetal clone III (Hyclone, Logan, UT, USA) and antibiotics (same mixture as described above for osteoblasts).
Both cell cultures were kept in a humidified atmosphere at 37 °C and 5% CO_2.

Bone Chips

Bone chips were harvested within 2 hours *post mortem* from newborn rat calvariae. Skin between ears was completely removed with a scalpel and calvarial bone exposed. Calvariae were excised with scissors, removed carefully with forceps and rinsed twice in warm α-MEM (without serum and antibiotics). Calvariae were kept in warm α-MEM until all calvariae were dissected. To remove the fibrous tissue, entire calvariae were digested in a trypsin/collagenase mix (same as above) for 2 x 15 min at 37 °C and 5% CO_2 and two washes with warm α-MEM in between and at the end. Bone chips (approximately 2 mm in diameter) were then punched from the calvariae bone using a canula and placed immediately onto the coated SLA CP titanium discs (see below for details).

6.2.4   Experimental Design

Formation of Polymeric Adlayer

Frozen samples of PLL-g-PEG and peptide-functionalized PLL-g-PEG were warmed to room temperature, dissolved in a salt buffer solution (denoted hereafter as HEPES2) containing 10 mM HEPES and 150 mM NaCl at pH 7.4 (to reach a final concentration of 0.5 mg/ml), filter sterilized (0.22 μm filter, Milian, Basel, CH) and used to prepare the designated peptide surface densities of exactly 3.0 pmol/cm^2. Titanium substrates were sterilized for 5 min using a glow-discharge unit, placed into 24-well plates and subsequently coated with 350 μl of the desired PLL-g-PEG polymer solutions. Substrates were washed twice with after 30 min and kept humid at all times.

Cell Incubation

Rat calvarial osteoblasts and human gingival fibroblasts were removed with trypsin solution, diluted with the suitable media and seeded onto the coated substrates at a concentration of each 10^4 cells/cm^2. The whole set of surfaces with attached cells was incubated for 7 days in a humidified atmosphere at 37 °C and 5% CO_2. Media was exchanged at day 3 and 5.

Placement of Bone Chip

HEPES2 buffer solution was removed and surfaces covered with 1 ml of α-MEM supplemented with a mixture of ascorbic acid (L-ascorbic acid phosphate magnesium salt n-hydrate; Wako Chemicals, VA, USA) and β-glycerophosphate (Sigma-Aldrich, Oakville, Ont., CAN). Bone chips were placed in the center of titanium discs. Four independent experiments for four different time points (4, 6, 8 and 10 days) were set up and incubated in a humidified atmosphere at 37 °C and 5% CO_2. After 4 days culture, media was replaced every second day without contacting the bone chips.

Fluorescent Labeling

Substrates from the cell culture assays containing rat calvarial osteoblasts or human gingival fibroblasts were washed with warm PBS and fixed in 4% formaldehyde

(Fisher Scientific, Nepean, Ont., CAN) in PBS for 15 minutes. Membranes were stained with 10 mM FITC (Sigma-Aldrich, Oakville, Ont., CAN) at 37 °C for 2 h, followed by 3 washes with PBS.

Samples from the bone chip experiments were washed once with warm α-MEM and fixed with 4% formaldehyde/PBS for 5 min, extensively washed with PBS and the nuclei stained with DAPI (Vectashield$^{\textregistered}$ Mounting media with DAPI, Vector Laboratories, Burlington, Ont., CAN) for fluorescence investigation.

6.2.5   Observation Methods

An epi-fluorescence microscope (Axioskop 2 MOT, Zeiss, Oberkochen, GER) was used to investigate both cell proliferation (osteoblasts and fibroblasts) and bone chips outgrowths. For cell number determination, 10 random positions were mapped with a 40x magnification. The bone chip experiments were investigated at 5x magnification and single images (with some overlap) from chips and outgrown osteoblasts were taken, saved in TIFF format and stitched with Adobe Photoshop CS2$^{\textregistered}$ (Version 9.0.1 for Mac OS X). Cell numbers of fibroblasts and osteoblasts as well as bone chips areas and areas covered by the migrated osteoblasts were analyzed using ImageJ software (Version 1.32i for Mac OS X).

6.2.6   Analysis of Bone Chip Experiment

Osteoblasts migration and proliferation from the bone chips built up a "fried-egg"-like image with the bone chip forming the "egg yolk" and the cell outgrowths the "white". Areas of osteoblast outgrowths and calvarial bone chips were determined (since all bone chips were slightly different in size) and the ratio γ thereof calculated for obtaining a "standardized" measure for the outgrowth of osteoblasts:

$$\gamma = \frac{Area_{migratedosteoblasts}}{Area_{bonechip}} \tag{6.1}$$

6.2.7   Statistical Analysis

Comparisons between measurement series were made using non-parametric tests (SPSS 11.4 for Mac OS X) because variances were not homogenous and observed

values were not distributed normally even after appropriate transformations. All mean values are shown $\pm$ SE (standard error). We set our level of significance at 0.05.

6.3   Results

6.3.1   Cell Proliferation

Osteoblasts vs.   Fibroblasts on Novel Peptide Surfaces KRSR and FHRRIKA

In general, more osteoblasts than fibroblasts attached to all the surfaces (p<0.001) except to the PEG-surface (Mann-Whitney: U=183.5, p=0.525). Multiple comparisons showed that significantly more osteoblasts (Tamhane: p<0.001) and more fibroblasts (p<0.001) attached on bare titanium and RGD-surfaces than on all bioinactive ones and the heparin-binding KRSR and FHRRIKA (Figure 6.1a, b). Although more osteoblasts were found on KRSR and FHRRIKA than on their control surfaces with scrambled peptide sequence, a significant difference was only found for FHRRIKA (p=0.02). Fibroblast attachment on both KRSR and FHRRIKA was not different from their control surfaces K<u>S</u>SR and <u>RFHARIK</u> (p>0.270).

Osteoblasts on Mixed KRSR/RGD and FHRRIKA/RGD Surfaces

More osteoblasts were observed on bare titanium than on all the other surface chemistries (Figure 6.2a, b; Tamhane: p<0.001). Osteoblast attachment on scrambled R<u>DG</u> was similar to that observed on PEG and also found to be less than on all the other surfaces except on pure FHRRIKA (p=0.973). A tendency for higher osteoblast attachment on surfaces containing KRSR/RGD as well as FHRRIKA/RGD was found except for both "50/50" mixes. However, differences were only significant for all other KRSR/RGD mixes (Mann Whitney: p<0.011) but not for the RGD/FHRRIKA mixes (p>0.162). No differences in terms of osteoblast attachment between the KRSR/RGD surfaces and the corresponding ones containing FHRRIKA/RGD existed (p>0.066).
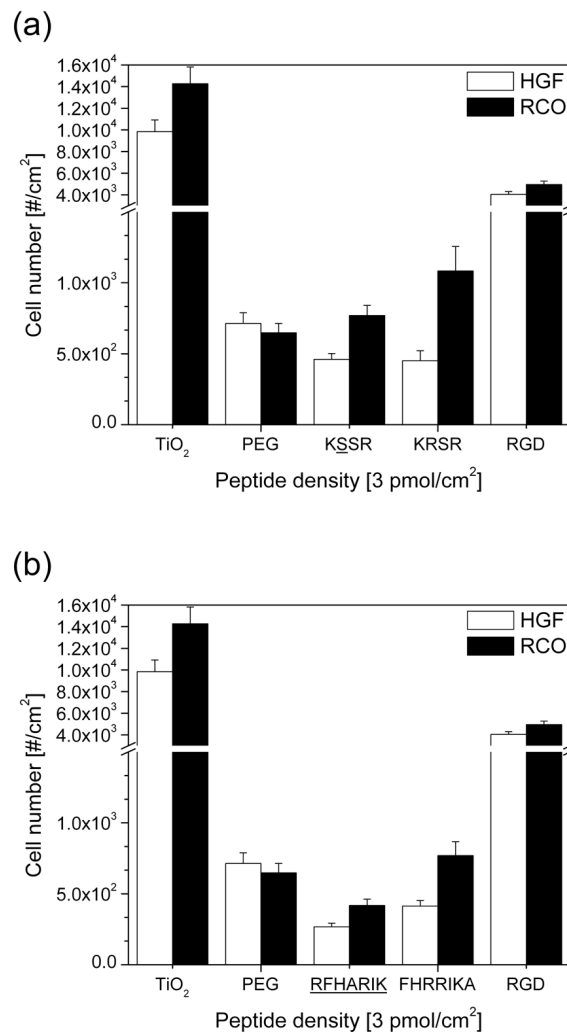
Figure 6.1: Cell number after 7 days in culture of rat calvar-ial osteoblasts (RCO) and human gingival fibroblasts (HGF) on (a) PLL-g-PEG/PEG-KRSR (**KRSR**) and (b) PLL-g-PEG/PEG-FHRRIKA (**FHRRIKA**) modifed SLA CP titanium surfaces. Bare ti-tanium (**TiO$_2$**), PLL-g-PEG (**PEG**), PLL-g-PEG/PEG-RGD (**RGD**), PLL-g-PEG/PEG-KSSR (**KSSR**) and PLL-g-PEG/PEG-RFHARIK (**RFHARIK**) were the control surfaces.
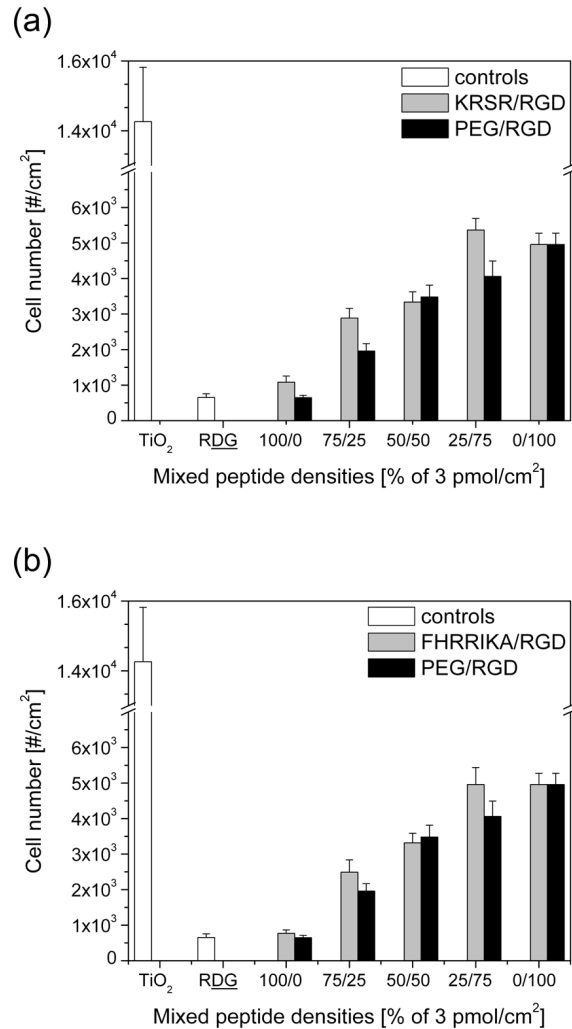
Figure 6.2: Cell number after 7 days in culture of rat calvarial osteoblasts (RCO) on (a) PLL-*g*-PEG/PEG-KRSR mixed with PLL-*g*-PEG/PEG-RGD (**KRSR/RGD**) and (b) PLL-*g*-PEG/PEG-FHRRIKA mixed with PLL-*g*-PEG/PEG-RGD (**FHRRIKA/RGD**) modified SLA CP titanium surfaces. Corresponding control surfaces were PLL-*g*-PEG mixed with PLL-*g*-PEG/PEG-RGD (**PEG/RGD**). Peptide concentrations (e.g., 75/25) are given in percentage (%) of the total mixed peptide surface densities (3.0 pmol/cm^2). Bare titanium (**TiO$_2$**) and scrambled PLL-*g*-PEG/PEG-R<u>DG</u> (**R<u>DG</u>**) modified surface are shown for comparison and complete the controls from Figure 6.1.

Rat Calvarial Bone Chips

None of the bone chips stuck (attached in a way that avoided displacement) to any SLA CP Ti disc independent from surface chemistry after 4 days of incubation, although there were few osteoblasts grown out of the bone on all surface chemistries. No significant differences for osteoblast migration were found between surface chemistries (Kruskal Wallis: χ^2_{10}=18.24, p=0.051; Figure 6.4), however, most osteoblasts migrated from bone chips placed onto titanium, RGD, FHRRIKA and 75PEG/25RGD.

After 6 days, 70% of the bone chips on the bio-active surfaces attached and osteoblasts migrated migrated out from all sides (Figure 6.3). Approximately 30% of the bone chips adhered to the bio-inactive surfaces, although cells which migrated from the bone chip covered a smaller area than cells found on all the other surfaces. Significant differences were found for cell migration area vs. bone chip area between surface chemistries (Kruskal Wallis: χ^2_{10}=18.34, p=0.050; Figure 6.4). Mean values for the ratios found on titanium and RGD were higher than the ones on their control surfaces. Cells observed on the two RGD-containing mixes, on the other hand, did not migrate as far as the ones found on their control surface 75PEG/25RGD. Additionally, osteoblasts on all bio-inactive surfaces were also the only ones observed to not migrate out in an isotropic way (Figure 6.3).

All bone chips on the bio-active surfaces stuck after 8 days, whereas on the bio-inactive ones still 30% did not attach completely. The ratios of cell migration area vs. bone chip area were found to be significantly different between surface chemistries (Kruskal Wallis: χ^2_{10}=25.76, p=0.004; Figure 6.4). Mean values found on all pure bio-active surfaces showed the same pattern as for titanium and RGD at day 6 in comparison with their controls. Furthermore, cells observed on 75KRSR/25PEG did cover a larger area than the ones on the 75PEG/25RGD surface.

After 10 days, all bone chips stuck on all surface chemistries and osteoblasts started to migrate in all directions even on the bio-inactive surfaces. Significant differences for the area covered by osteoblasts between surface chemistries existed (Kruskal Wallis: χ^2_{10}=23.09, p=0.010; Figure 6.4). Mean values were higher for all bio-active surfaces in comparison with their corresponding inactive control surfaces.
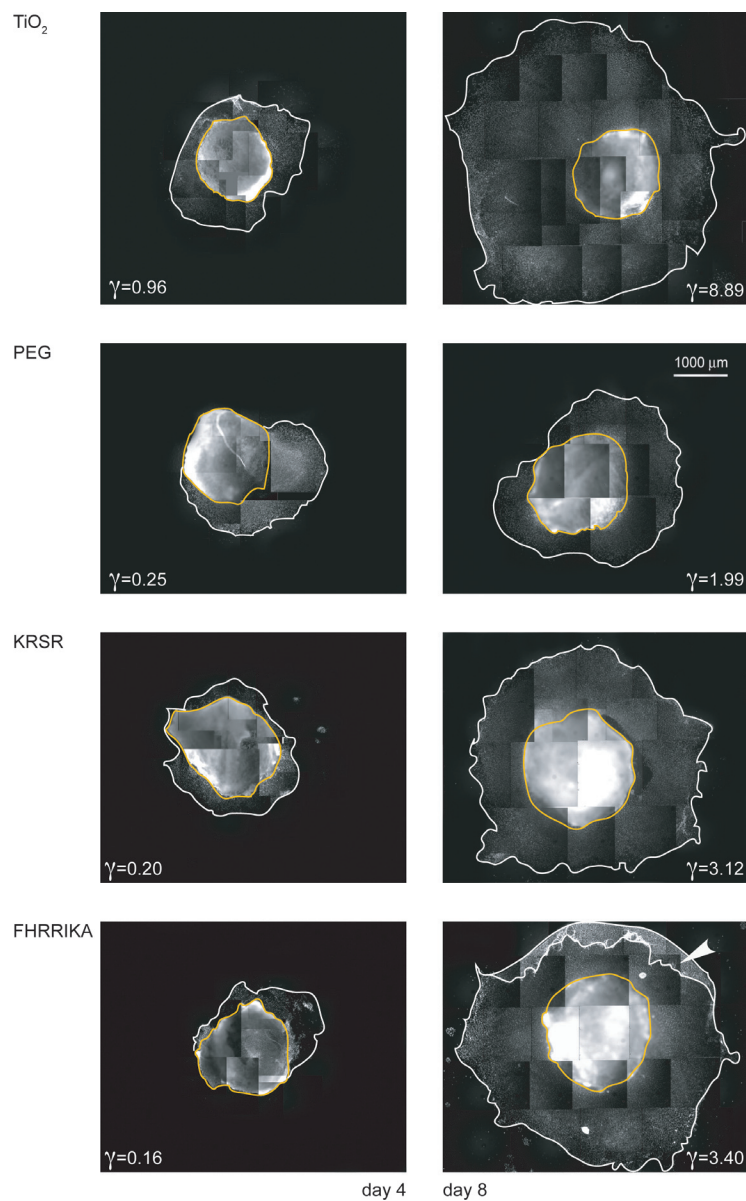
Figure 6.3: Fluorescent images showing bone chips from rat calvariae surrounded with outgrown cells (nuclei were stained for DAPI). All substrates were SLA CP titanium discs with the following surface modifications: (a) bare titanium surface ($\mathbf{TiO_2}$), (b) PLL-g-PEG (**PEG**), (c) PLL-g-PEG/PEG-KRSR (**KRSR**), (d) PLL-g-PEG/PEG-FHRRIKA (**FHRRIKA**). The peptide surface densities were 3.0 pmol/cm^2. γ describes the ratio between outgrown rat calvarial osteoblasts (surrounded with white) and bone chip area (surrounded with yellow). The arrow in the FHRRIKA image refers to a flipped-over area of migrated osteoblasts (see text for more details).

(a)

(b)

(c)
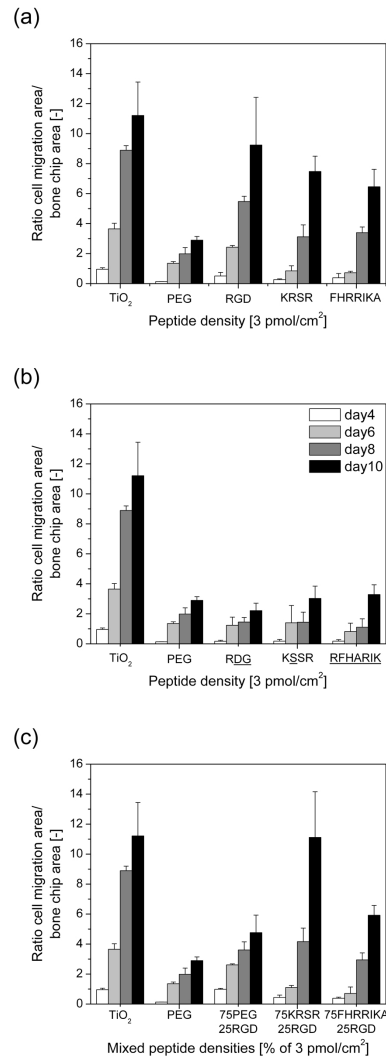
Figure 6.4: Ratio γ between the area covered by outgrown rat calvarial osteoblasts and the bone chip area after 4 different time periods (see label in (b) for details). All substrates were SLA CP titanium discs with the following surface modifications: (a) Pure PLL-g-PEG/PEG-KRSR (**KRSR**) and PLL-g-PEG/PEG-FHRRIKA (**FHRRIKA**). (b) PLL-g-PEG polymers with scrambled peptides R<u>DG</u>, K<u>S</u>SR and <u>RFHARIK</u> (negative controls). (c) Three parts (75%) of PLL-g-PEG polymers containing KRSR or FHRRIKA mixed with one part (25%) RGD-modified PLL-g-PEG to reach a total peptide surface density of 3.0 pmol/cm^2. The 75PLL-g-PEG/25PLL-g-PEG/PEG-RGD surface served here as control for the enhanced effect. Bare titanium (**TiO$_2$**) and unfunctionalized PLL-g-PEG (**PEG**) served as control surfaces and are plot in all three graphs for comparison.

6.4   Discussion

6.4.1   Osteoblast and Fibroblast Response to KRSR and FHRRIKA Surfaces

Our findings indicated that rat calvarial osteoblast and human gingival fibroblast cell numbers were influenced through surface chemistry. A PEGylation of the titanium surface drastically reduced attachment of both osteoblasts and fibroblasts, whereas the introduction of the RGD-peptide ($3.0\,\mathrm{pmol/cm^2}$) restored cell numbers to similar values found on bare titanium. These observations after seven days of culture showed the same tendency as previously published data [17] based on earlier incubation times. In general, more osteoblasts than fibroblasts were found on all surface chemistries (except for PEG) thus demonstrating the preference of osteoblasts [24, 25] to proliferate more than fibroblasts [26] on rough substrata like SLA over a time period of 7 days. Osteoblast attachment on KRSR and FHRRIKA did not reach the levels found on RGD or bare titanium, although they were found to be higher than the values obtained on the bio-inactive surfaces. An increase of osteoblast attachment on KRSR surfaces in comparison with RGD by approximately 5% and an increase by approximately 30% in comparison with control KSSR surfaces were found by Dee *et al.* [8]. In our case, however, an increase of osteoblast attachment by 40% on KRSR in comparison with KSSR was observed, but a decrease of a factor 4.6 in respect to RGD was measured. One explanation for these differences could be the lower peptide density used in our experiments ($3.0\,\mathrm{pmol/cm^2}$ instead of Dee's $80\,\mathrm{pmol/cm^2}$) and our use of a non-fouling strategy to immobilize our biomolecules, so that we could explicitly study the peptide-cell surface receptor interaction without interference of non-specific factors. Unlike some other studies that have reported cell selectivity for osteoblasts when using KRSR-peptide [10, 11], our results indicated that the difference in osteoblast vs. fibroblast attachment was rather influenced by surface topography (more osteoblasts than fibroblasts on SLA) than by chemistry. However, fibroblast attachment on both KRSR and FHRRIKA was not different from their control surfaces KSSR and RFHARIK unlike osteoblast attachment on FHRRIKA that was higher in comparison with RFHARIK.
The co-adsorption of RGD and KRSR- or FHRRIKA-containing PLL-*g*-PEG polymer surfaces showed an increase of osteoblast attachment in comparison with surfaces that had the same concentration of RGD only, indicating an enhanced effect

similar to the one reported by others [8, 9, 12]. Although mean values were higher on both FHRRIKA and KRSR-containing RGD-mixes (except for the 50/50 surfaces), the effect was weaker (and not significant for FHRRIKA) than expected. On the other hand, Harbers *et al.* reported no enhanced effect of FHRRIKA and RGD using non-fouling interpenetrating polymer networks (IPNs) [27]. A possible explanation would be that the immobilization of RGD and KRSR (or FHRRIKA) in this somewhat random way does not represent exactly defined distances of cell-binding and heparin-binding sites as found for example in fibronectin [6, 13]. This could be overcome through designing a new peptide that would include both the cell-binding and the heparin-binding pattern in the same sequence with the "native" spatial spacing.

6.4.2   Bone Chips and Osteoblast Migration

Bone chip attachment and osteoblast outgrowths (size of areas and migration patterns) were mediated through surface chemistries. Bone chips cultured on the bio-inactive surfaces needed up to 10 days to completely adhere and osteoblasts from those cells did not migrate isotropically until day 10. The fact that bone chip attachment und subsequent osteoblast migration was slowed on bio-inactive compared to bio-active but was still possible, can be most likely explained that some small surface defects in the PEG-coating always existed [17] and that at these positions some osteoblasts had the chance to attach over time on the SLA CP titanium surface. Once they made contact with the surface, it may have been possible for the cells to proliferate possibly by displacing/degrading the PEG-coating as they encountered it, allowing further colonization of the substrate. This situation was completely different from osteoblasts in culture, which do not have a proliferation "machinery" in form of a bone chip and therefore can not proliferate that much on a PEGylated surface.

Bone chip attachment on bio-active surfaces was always more efficient and by day 8 all chips were well adhered to these surfaces. Additionally, osteoblasts on bio-active surfaces started to migrate in an isotropic way as early as day 6. Even on pure heparin-binding peptides KRSR and FHRRIKA, osteoblast migration demonstrated this same effect, indicating that cell migration could also be mediated through transmembrane proteoglycan receptors. This observation is further supported that during preparation of the samples for microscope investigation, a tendency of the osteoblast

outgrowths to flip over together in form of a "sheet" (see arrow in Figure 6.3) was observed, showing that these osteoblasts were linked to each other and suggesting that they were "floating" over the peptide-functionalized PLL-*g*-PEG coating rather than being directly bound to the titanium surface. In contrast, osteoblasts migrating from underneath the bone chip (towards the titanium surface) were probably facing closer an *in vivo* situation than the outgrown osteoblasts that more likely can be compared to standard *in vitro* cell culture assays. Furthermore, the earlier attachment of the bone chips on bio-active surfaces in comparison with the controls might also be an indicator that these polymers had a shorter life-time than the ones that were not functionalized (or carried a scrambled sequence). *In vitro* stability of PLL-*g*-PEG polymer surfaces was investigated by Vande Vondele *et al.* and it was shown that these adlayers were still showing anti-fouling properties as assessed with fibroblast proliferation data after 10 days exposure time to phosphate buffer solution or serum and were comparable to freshly prepared PLL-*g*-PEG coatings [16]. Even less is know about stability of PLL-*g*-PEG in an *in vivo* environment as somewhat the coating underneath the bone chip was experiencing. A recent study has reported enhanced bone apposition only during early stages (2 weeks) of bone regeneration on PEGylated SLA CP titanium implant surfaces using a minipig model indicating a limited life-time (<2 weeks) of PLL-*g*-PEG [28].

An enhanced effect in osteoblast migration was visible when mixing RGD with KRSR and FHRRIKA, respectively. It can be hypothesized that osteoblasts were stimulated by both the heparin-binding peptides and RGD to migrate over the surface since some studies have reported that crosstalk between integrins and proteoglycans (syndecans) is taking place during cell adhesion and attachment or even is required for cell spreading [29–31].

6.4.3   Comparison of Cell Proliferation Assay vs. Bone Chip Experiment

Osteoblasts outgrown from calvarial bone chips interacted to a greater extent with the novel peptide sequences KRSR and FHRRIKA than osteoblasts from cell culture did. Although the two types of osteoblasts were obtained from the same type of rats employing a similar protocol, the cells in the culture experiments have usually undergone several passages involving exposure to trypsin/EDTA, whereas the osteoblasts that migrated from bone chips were not exposed to trypsin/EDTA. In this respect,

it has been described by Chung *et al.* [32] that serial passage of MC3T3-E1 cells (derived from newborn mouse calvaria) altered among other parameters cell morphology, cell proliferation, ALP activity, Osteocalcin secretion and responsiveness to TGF-β and BMP-2. Additionally, various authors have reported that exposure of cultured cells to trypsin and/or chelating agents such as EDTA or EGTA resulted in changes of cell surface morphology and nuclear morphology [33–35]. Although it seems that these changes are mostly reversible and the cells regain a "normal" surface structure 24 hours after cell seeding on a substrate [36, 37], little is known about how trypsinization alters cell adhesion at early times and how these alterations modify cell behavior later.

6.5   Conclusions

Outgrowths from bone chips can be considered as closer to the *in vivo* condition than standard *in vitro* osteoblast culture assays because the cells have never been exposed to trypsin or EDTA. Osteoblast outgrowths differed from osteoblast cell cultures in showing attachment to KRSR- and FHRRIKA-coated surfaces. That result introduces the possibility that coating titanium implant surfaces with the peptides KRSR and FHRRIKA using PLL-*g*-PEG chemistry may enhance osteoconduction on implants. It might be also possible that these coatings show a preference for a certain osteoblast phenotype, thus promoting a subpopulation of osteoblasts to proliferate. This could open new windows for cell differentiation assays, where the potential of having somewhat more selected cell types is of interest. However, it must be noted that surfaces coated with only KRSR or FHRRIKA do not reach the efficiency of the RGD peptide surfaces in promoting cell attachment at equal peptide surface densities. Nevertheless, the possibility of addressing in a single coating several cell surface receptors found in osteoblasts might be a useful approach for developing novel biomaterial surfaces. In particular, a co-adsorption of RGD and KRSR may be a useful strategy to further improve the surface (bio)chemistry of an implant used in bone-contact applications.

Bibliography

[1] Dee, K. C. and Bizios, R. Mini-review: Proactive biomaterials and bone tissue engineering. *Biotechnology and Bioengineering*, **50**(4), 438–442, 1996.

[2] Schuler, M., Trentin, D., Textor, M. and Tosatti, S. Biomedical Interfaces: Titanium Surface Technology for Implants and Cell Carriers. *nanomedicine*, **1**(4), 449–463, 2006.

[3] Pierschbacher, M. D. and Ruoslahti, E. Cell Attachment Activity of Fibronectin Can Be Duplicated by Small Synthetic Fragments of the Molecule. *Nature*, **309**(5963), 30–33, 1984.

[4] Main, A. L., Harvey, T. S., Baron, M., Boyd, J. and Campbell, I. D. The 3-Dimensional Structure of the 10th Type-Iii Module of Fibronectin - an Insight into Rgd-Mediated Interactions. *Cell*, **71**(4), 671–678, 1992.

[5] Ruoslahti, E. RGD and other recognition sequences for integrins. *Annual Review of Cell and Developmental Biology*, **12**, 697–715, 1996.

[6] Dalton, B. A., McFarland, C. D., Underwood, P. A. and Steele, J. G. Role of the Heparin-Binding Domain of Fibronectin in Attachment and Spreading of Human Bone-Derived Cells. *Journal of Cell Science*, **108**, 2083–2092, 1995.

[7] Underwood, P. A., Dalton, B. A., Steele, J. G., Bennett, F. A. and Strike, P. Antifibronectin Antibodies That Modify Heparin Binding and Cell-Adhesion - Evidence for a New Cell Binding-Site in the Heparin Binding Region. *Journal of Cell Science*, **102**, 833–845, 1992.

[8] Dee, K. C., Andersen, T. T. and Bizios, R. Design and function of novel osteoblast-adhesive peptides for chemical modification of biomaterials. *Journal of Biomedical Materials Research*, **40**(3), 371–377, 1998.

[9] Rezania, A. and Healy, K. E. Biomimetic peptide surfaces that regulate adhesion, spreading, cytoskeletal organization, and mineralization of the matrix deposited by osteoblast-like cells. *Biotechnology Progress*, **15**(1), 19–32, 1999.

[10] Dettin, M., Conconi, M. T., Gambaretto, R., Pasquato, A., Folin, M., Di Bello, C. and Parnigotto, P. P. Novel osteoblast-adhesive peptides for

dental/orthopedic biomaterials. *Journal of Biomedical Materials Research*, **60**(3), 466–471, 2002.

[11] Hasenbein, M. E., Andersen, T. T. and Bizios, R. Micropatterned surfaces modified with select peptides promote exclusive interactions with osteoblasts. *Biomaterials*, **23**(19), 3937–3942, 2002.

[12] Rezania, A. and Healy, K. E. Integrin subunits responsible for adhesion of human osteoblast- like cells to biomimetic peptide surfaces. *Journal of Orthopaedic Research*, **17**(4), 615–623, 1999.

[13] Woods, A., Couchman, J. R., Johansson, S. and Hook, M. Adhesion and Cytoskeletal Organization of Fibroblasts in Response to Fibronectin Fragments. *Embo Journal*, **5**(4), 665–670, 1986.

[14] Tosatti, S., De Paul, S. M., Askendal, A., VandeVondele, S., Hubbell, J. A., Tengvall, P. and Textor, M. Peptide functionalized poly(L-lysine)-g-poly(ethylene glycol) on titanium: resistance to protein adsorption in full heparinized human blood plasma. *Biomaterials*, **24**(27), 4949–4958, 2003.

[15] Pasche, S., De Paul, S. M., Voros, J., Spencer, N. D. and Textor, M. Poly(L-lysine)-graft-poly(ethylene glycol) assembled monolayers on niobium oxide surfaces: A quantitative study of the influence of polymer interfacial architecture on resistance to protein adsorption by ToF-SIMS and in situ OWLS. *Langmuir*, **19**(22), 9216–9225, 2003.

[16] VandeVondele, S., Voros, J. and Hubbell, J. A. RGD-Grafted poly-l-lysine-graft-(polyethylene glycol) copolymers block non-specific protein adsorption while promoting cell adhesion. *Biotechnology and Bioengineering*, **82**(7), 784–790, 2003.

[17] Schuler, M., Owen, G., Hamilton, D. W., de Wild, M., Textor, M., Brunette, D. M. and Tosatti, S. Biomimetic modification of titanium dental implant model surfaces using the RGDSP-peptide sequence: A cell morphology study. *Biomaterials*, **27**(21), 4003–4015, 2006.

[18] Morra, M. On the molecular basis of fouling resistance. *Journal of Biomaterials Science-Polymer Edition*, **11**(6), 547–569, 2000.

[19] Textor, M., Tosatti, S., Wieland, M. and Brunette, D. M. Use of Molecular Assembly Techniques For Tailoring the Chemical Properties On Smooth and Rough Titanium Surfaces. In Ellingsen, J. and Lyngstadaas, S., editors, *Bio-Implant Interface: Improving Biomaterials and Tissue Reaction.* CRC Press, 2003.

[20] Voros, J., Ramsden, J. J., Csucs, G., Szendro, I., De Paul, S. M., Textor, M. and Spencer, N. D. Optical grating coupler biosensors. *Biomaterials*, **23**(17), 3699–3710, 2002.

[21] Hasegawa, S., Sato, S., Saito, S., Suzuki, Y. and Brunette, D. M. Mechanical Stretching Increases the Number of Cultured Bone- Cells Synthesizing DNA and Alters Their Pattern of Protein- Synthesis. *Calcified Tissue International*, **37**(4), 431–436, 1985.

[22] Chehroudi, B., Gould, T. R. L. and Brunette, D. M. The Role of Connective-Tissue in Inhibiting Epithelial Downgrowth on Titanium-Coated Percutaneous Implants. *Journal of Biomedical Materials Research*, **26**(4), 493–515, 1992.

[23] Brunette, D. M., Melcher, A. H. and Moe, H. K. Culture and Origin of Epithelium-Like and Fibroblast-Like Cells from Porcine Periodontal-Ligament Explants and Cell-Suspensions. *Archives of Oral Biology*, **21**(7), 393–400, 1976.

[24] Bowers, K. T., Keller, J. C., Wick, D. G. and Randolph, B. A. Optimization of Surface-Morphology for Osteoblast Attachment. *Journal of Dental Research*, **69**, 370–370, 1990.

[25] Lincks, J., Boyan, B. D., Blanchard, C. R., Lohmann, C. H., Liu, Y., Cochran, D. L., Dean, D. D. and Schwartz, Z. Response of MG63 osteoblast-like cells to titanium and titanium alloy is dependent on surface roughness and composition. *Biomaterials*, **19**(23), 2219–2232, 1998.

[26] Cochran, D. L., Simpson, J., Weber, H. and Buser, D. Attachment and growth of periodontal cells on smooth and rough titanium. *International Journal of Oral Maxillofacial Implants*, , 289–297, 1994.

[27] Harbers, G. M. and Healy, K. E. The effect of ligand type and density on osteoblast adhesion, proliferation, and matrix mineralization. *Journal of Biomedical Materials Research Part A*, **75A**(4), 855–869, 2005.

[28] Germanier, Y., Tosatti, S., Broggini, N., Textor, M. and Buser, D. Enhanced bone apposition around biofunctionalized sandblasted and acid-etched titanium implant surfaces - A histomorphometric study in miniature pigs. *Clinical Oral Implants Research*, **17**(3), 251–257, 2006.

[29] Schaffner, P. and Dard, M. M. Structure and function of RGD peptides involved in bone biology. *Cellular and Molecular Life Sciences*, **60**(1), 119–132, 2003.

[30] Beauvais, D. M. and Rapraeger, A. C. Syndecan-1-mediated cell spreading requires signaling by alpha(v)beta(3) integrins in human breast carcinoma cells. *Experimental Cell Research*, **286**(2), 219–232, 2003.

[31] Couchman, J. R. and Woods, A. Syndecan-4 and integrins: combinatorial signaling in cell adhesion. *Journal of Cell Science*, **112**(20), 3415–3420, 1999.

[32] Chung, C. Y., Iida-Klein, A., Wyatt, L. E., Rudkin, G. H., Ishida, K., Yamaguchi, D. T. and Miller, T. A. Serial passage of MC3T3-E1 cells alters osteoblastic function and responsiveness to transforming growth factor-beta 1 and bone morphogenetic protein-2. *Biochemical and Biophysical Research Communications*, **265**(1), 246–251, 1999.

[33] Furcht, L. T. and Wendelschafercrabb, G. Trypsin-Induced Coordinate Alterations in Cell-Shape, Cytoskeleton, and Intrinsic Membrane Structure of Contact-Inhibited Cells. *Experimental Cell Research*, **114**(1), 1–14, 1978.

[34] Ukena, T. E. and Karnovsky, M. J. Role of Microvilli in Agglutination of Cells by Concanavalin-A. *Experimental Cell Research*, **106**(2), 309–325, 1977.

[35] Collard, J. G. and Temmink, J. H. M. Surface Morphology and Agglutinability with Concanavalin-a in Normal and Transformed Murine Fibroblasts. *Journal of Cell Biology*, **68**(1), 101–112, 1976.

[36] Thyberg, J. and Moskalewski, S. Influence of Proteolytic-Enzymes and Calcium-Binding Agents on Nuclear and Cell-Surface Topography. *Cell and Tissue Research*, **237**(3), 587–593, 1984.

[37] Moskalewski, S. and Thyberg, J. Reversible Changes in Nuclear and Cell-Surface Topography in Cells Exposed to Collagenase and Edta. *Cell and Tissue Research*, **220**(1), 51–60, 1981.

7

Differentiation Assays of MG63 Osteoblast-like Cells on KRSR- and RGD-peptide Modified Titanium Surfaces

The work described in this chapter has been done in collaboration with the following people: Brian Bell, Prof. Zvi Schwartz, Prof. Barbara D. Boyan (all Georgia Institute of Technology, Atlanta, USA), Dr. Michael de Wild (Institut Straumann AG, Basel, CH), Prof. Marcus Textor and Dr. Samuele Tosatti.

7.1   Introduction

In the previous chapter, we have demonstrated that osteoblast outgrowths from rat calvariae bone chips attached to PLL-g-PEG/PEG-KRSR and PLL-g-PEG/PEG-FHRRIKA coated SLA titanium surfaces, supporting the hypothesis that coating titanium implant surfaces with these peptides using PLL-g-PEG chemistry may enhance osteoconduction on implants. It was also shown that a co-adsorption of RGD- and KRSR-functionalized PLL-g-PEG polymers may be a favorable approach for implant surfaces in bone-contact applications. However, a successful osseointegration entails more than the control of cell migration and proliferation, and for a better understanding of the roles that the novel peptides KRSR and FHRRIKA might have on osteoblasts, further experiments like cell differentiation assays are necessary.
Due to the large number of substrates typically needed in a cell differentiation assay,

we decided to focus on the more promising KRSR-peptide. This decision was based on studies conducted by Dee *et al.*, where it was shown that high KRSR-peptide surface concentrations (approximately 80 pmol/cm^2) resulted in osteoblast attachment comparable to that of RGD-modified surfaces [1]. For the cell differentiation assays we synthesized a PLL-*g*-PEG/PEG-KRSR polymer with a high percentage of the PEG chains (76%) functionalized with the KRSR peptide resulting in 20 pmol/cm^2 KRSR surface density (to be compared with 3 pmol/cm^2 as used in Chapter 6). With this type and the RGD-modified polymer the following surfaces were prepared for subsequent cell culture studies:

i) Surfaces with different concentrations of PLL-*g*-PEG/PEG-KRSR to investigate a potential KRSR surface concentration dependence (5, 10, 15 and 20 pmol/cm^2), and ii) surfaces with different ratios of PLL-*g*-PEG/PEG-RGD and PLL-*g*-PEG/PEG-KRSR to investigate a potential synergistic effect of the KRSR and RGD peptide. The amount of PLL-*g*-PEG/PEG-RGD was kept constant at two different peptide densities (0.05 pmol/cm^2 and 1.26 pmol/cm^2) to allow a comparison with a previous study [2]. Differentiation assays were performed using MG63 osteoblast-like cells and cell numbers, alkaline phosphatase activity, osteocalcin, total transforming growth factor β1 and prostaglandin E$_2$ were determined after 8 days of culture.

7.2   Materials and Methods

7.2.1   Polymers and Notation

Peptide-functionalized and unfunctionalized PLL-*g*-PEG polymers were synthesized according to the protocols described in Chapter 3. The following 4 polymers were used (named hereafter according to their peptide sequences): peptide-functionalized polymers PLL-*g*-PEG/PEG-RGD (**RGD**), PLL-*g*-PEG/PEG-KRSR (**KRSR**), PLL-*g*-PEG/PEG-KSSR (**KSSR**) and unfunctionalized PLL-*g*-PEG (**PEG**) (see Table 7.1 for detailed information). KRSR peptide surface density varied between 5, 10, 15 and 20 pmol/cm^2; KSSR (scrambled control peptide) was set to 10 pmol/cm^2, and RGD was used with 0.05 pmol/cm^2 and 1.26 pmol/cm^2. Different concentrations of peptide-functionalized PLL-*g*-PEG polymers were obtained by mixing with unfunctionalized PLL-*g*-PEG. When working with multi-peptide
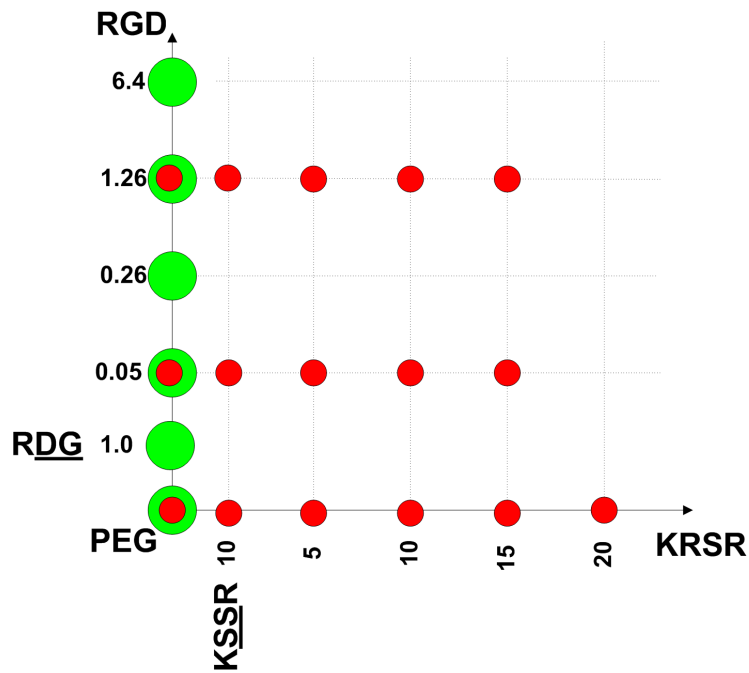
Figure 7.1: Experimental design of this study (red) showing peptide surface densities of PLL-g-PEG/PEG-RGD, PLL-g-PEG/PEG-KRSR and combinations thereof in comparison to similar PLL-g-PEG/PEG-RGD surfaces (green) used in a previously published study [2]. Note: all peptide surface concentrations are given in pmol/cm^2.

surfaces, the following notation was given: e.g., **0.05RGD/10KSSR** that refers to a mix of 0.05 pmol/cm^2 RGD and 10 pmol/cm^2 KSSR with a total peptide density of 10.05 pmol/cm^2 on the surface. Concentrations of single peptide surfaces were also visible from their notations: e.g., **15KRSR** that corresponds to 15 pmol/cm^2.

7.2.2 Experimental Design

SLA CP Ti discs were cleaned and sterilized in oxygen plasma for 5 minutes, placed in 24 well plates and immediately coated with the desired PLL-g-PEG polymer solutions for 30 min at room temperature. Substrates were rinsed twice with HEPES2 buffer solution. MG63 osteoblast-like cells were cultured and seeded in Dulbecco's Modified Eagle Medium (DMEM) supplemented with 10% FCS and 1% penicillin/streptomycin at a concentration of 9'000 cells/cm^2. The whole set with

Table 7.1: Molecular weight, grafting ratio, peptide functionalization, polymer/protein adsorption and peptide surface density for all polymers used in this study.

	PEG	RGD	KRSR	KSSR
Molecular weight PLL [kDa]	15.9	15.9	15.9	15.9
Molecular weight lysine unit [kDa]	0.128	0.128	0.128	0.128
Molecular weight peptide [kDa]	-	1.222	1.197	1.128
Molecular weight entire polymer [kDa]	99.1	69.4	75	63.2
Grafting ratio g [-][a]	3.3	4	9.3	9.7
Peptide-functionalized PEG-chains [%][a]	-	8	76.3	50.1
Polymer adsorption [ng/cm^2][b]	175	175	135	143
Protein adsorption [ng/cm^2][b]	< 5	< 5	< 5	< 5
Peptide surface density ρ_{ps} [pmol/cm^2]	-	5.1	20	15.8

[a]measured with NMR technique.

[b]measured with OWLS technique.

attached cells was incubated in a humidified atmosphere with 5% CO_2 at 37 °C. Media was exchanged at day 3, 5 and 7. Assays were conducted at day 8 (one day post confluence). MG63 osteoblast-like cell numbers and cell markers (Alkaline phosphatase activity, osteocalcin, total TGF-β1 and prostaglandin E_2) were determined as previously published [2, 3].

7.3 Results and Discussion

Alkaline phosphatase activity was investigated since it is usually upregulated when the extracellular matrix is being prepared for calcification. Osteocalcin was measured as an indicator of osteoblast differentiation. Transforming growth factor $\beta 1$ and prostaglandin E_2 were determined as indicators of local factors that are involved in wound healing and osteogenesis (formation of bone) [4]. All data are shown as mean values $\pm$ SE.

7.3.1 Cell Number

MG63 cell number was lower on PEG compared to bare titanium and TCPS. Similar cell numbers as on PEG were found for cells on pure KSSR and low RGD combined with KSSR, whereas the 1.26RGD/10KSSR mix showed higher cell numbers than on PEG. Addition of KRSR alone did not increase the number of cells for any concentration examined. Cell number was also unaffected or lowered by low levels of RGD (0.05 pmol/cm^2), but at higher concentrations (1.26 pmol/cm^2), RGD did result in slightly increased numbers of cells.

7.3.2 Alkaline Phosphatase

All PLL-g-PEG modified surfaces (independent from type and degree of functionalization) caused an increase of alkaline phosphatase activity in comparison to bare titanium or TCPS. Highest values for ALP activity were found for PEG, KSSR, 0.05RGD, 0.05RGD/10KSSR as well as for 0.05RGD/10KRSR surfaces. As the RGD content increased, there was evidence for a cooperative effect between RGD and KRSR with respect to ALP activity, although the level was still lower than for the PEG surfaces.

7.3.3 Osteocalcin

Osteocalcin production of MG63 osteoblast-like cells was higher on all PLL-g-PEG modified surfaces (independent from type and degree of functionalization) in comparison to bare titanium or TCPS. Addition of peptides to PLL-g-PEG resulted

(a)

(b)

Figure 7.2: Cell number of MG63 osteoblast-like cells cultured for 8 days on PLL-*g*-PEG modified CP Ti SLA surfaces. The control surfaces are shown in the upper panel: "Plastic" (Tissue culture polystyrene), "SLA" (bare Ti) and "SLA-PEG" (PLL-*g*-PEGmodified only) and the three RGD/KSSR-containing surfaces. The lower panel "0.05RGD" and "1.26RGD" shows the results of the experiments with a constant RGD peptide density (0.05 and 1.26 pmol/cm^2, respectively) and varied KRSR-peptide densities (5, 10, 15 pmol/cm^2) whereas "0RGD" refers to the assays with only KRSR at different surface densities (5, 10, 15, 20 pmol/cm^2).

(a)

(b)
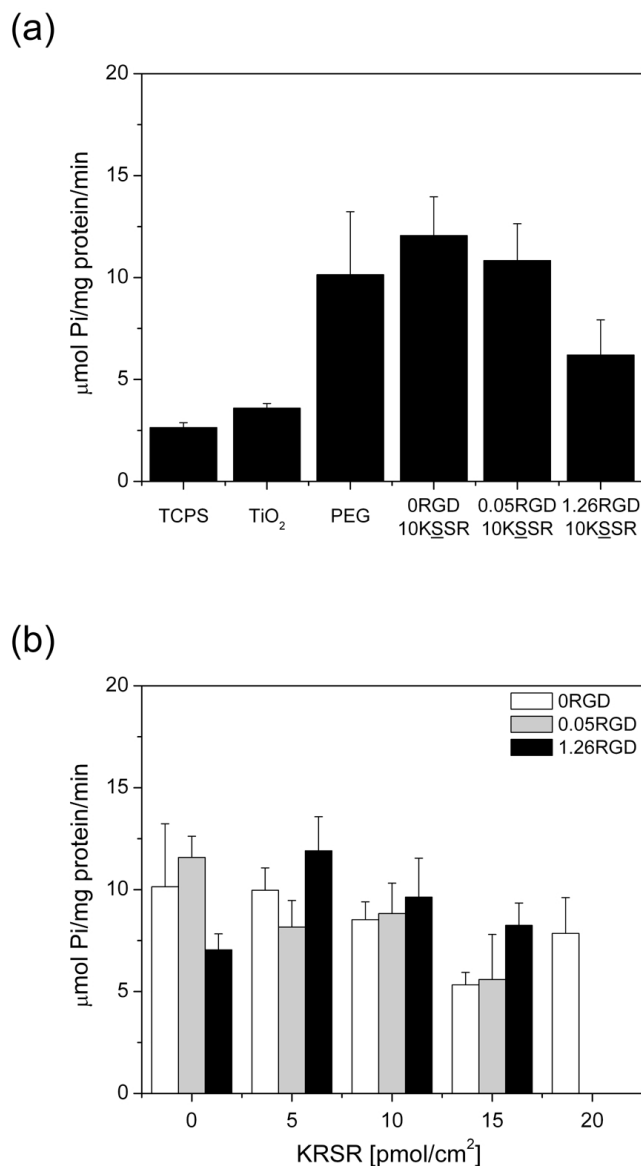
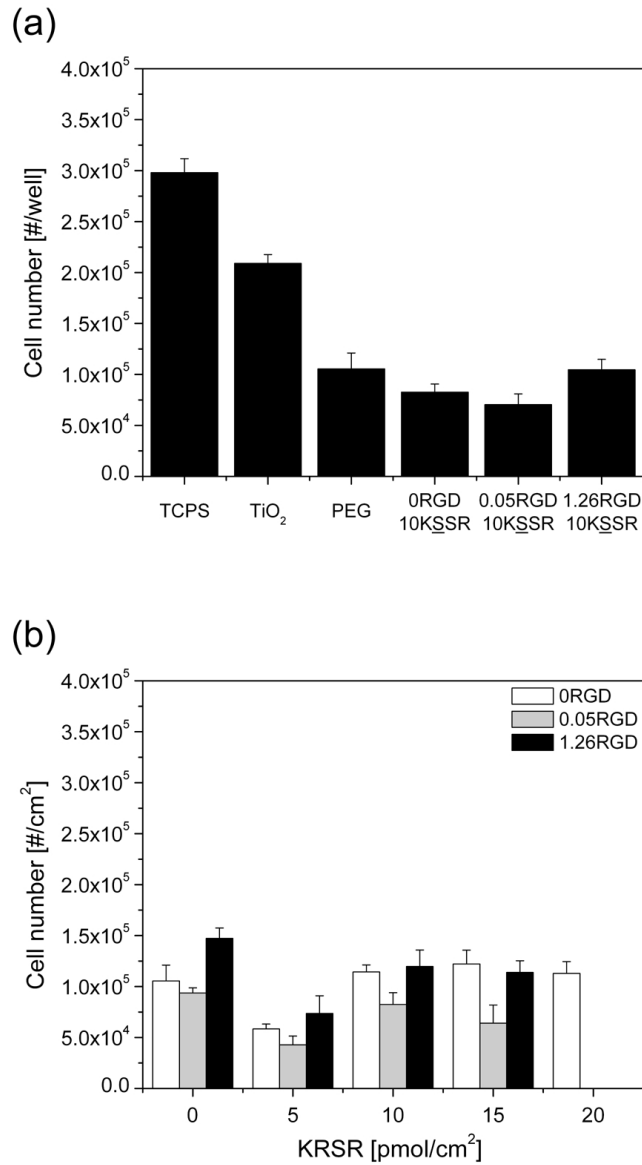Figure 7.3: Alkaline phosphatase activity of MG63 osteoblast-like cells cultured for 8 days on PLL-*g*-PEG modified CP Ti SLA surfaces. The control surfaces are shown in the upper panel: "Plastic" (Tissue culture polystyrene), "SLA" (bare Ti) and "SLA-PEG" (PLL-*g*-PEGmodified only) and the three RGD/KSSR-containing surfaces. The lower panel "0.05RGD" and "1.26RGD" shows the results of the experiments with a constant RGD peptide density (0.05 and 1.26 pmol/cm^2, respectively) and varied KRSR peptide densities (5, 10, 15 pmol/cm^2) whereas "0RGD" refers to the assays with only KRSR at different surface densities (5, 10, 15, 20 pmol/cm^2).

(a)

(b)
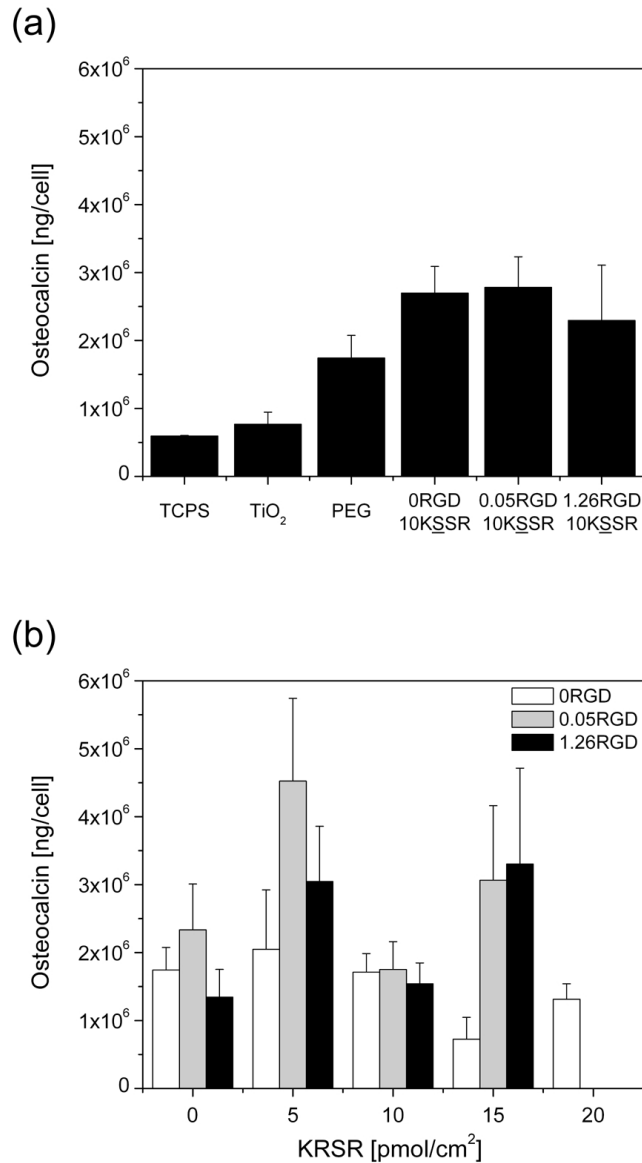
Figure 7.4: Osteocalcin production of MG63 osteoblast-like cells cultured for 8 days on PLL-g-PEG modified CP Ti SLA surfaces. The control surfaces are shown in the upper panel: "Plastic" (Tissue culture polystyrene), "SLA" (bare Ti) and "SLA-PEG" (PLL-g-PEGmodified only) and the three RGD/KSSR-containing surfaces. The lower panel "0.05RGD" and "1.26RGD" shows the results of the experiments with a constant RGD peptide density (0.05 and 1.26 pmol/cm^2, respectively) and varied KRSR peptide densities (5, 10, 15 pmol/cm^2) whereas "0RGD" refers to the assays with only KRSR at different surface densities (5, 10, 15, 20 pmol/cm^2).

in increased osteocalcin levels (except for 15KRSR and 20KRSR) in comparison to titanium. RGD caused a further increase when combined with 5KRSR and 15KRSR.

7.3.4 Transforming Growth Factor β1

Transforming growth factor β1 showed higher mean values for MG63 cells that were cultured on all PEGylated surfaces compared to titanium and TCPS. Highest values were found on KSSR, 0.05RGD and 0.05RGD/5KRSR. Increased RGD with higher KRSR ($>10\,\mathrm{pmol/cm^2}$) concentrations resulted in a decrease of TGF-β1 production.

7.3.5 Prostaglandin E$_2$

Prostaglandin E$_2$ levels in the conditioned media were higher on all PLL-g-PEG modified surfaces (independent from type and degree of functionalization) in comparison to bare titanium or TCPS. This effect was further increased on 5KRSR and 0.05RGD/5KRSR.

7.4 Conclusions

According to the preliminary data presented in this chapter, the PLL-g-PEG coatings had a positive effect on ALP activity as well as on osteocalcin, total TGF-β1 and prostaglandin E$_2$ production. However, this upregulation on PEGylated surfaces holds for values per cell only, while the values per total culture vary much less. The introduction of the KRSR-peptide at different concentrations did not show any up (or down) regulation of these markers, neither did the co-adsorption of RGD and KRSR reveal a promising trend in showing an enhanced or even synergistic effect. Although additional studies would be required to obtain sufficient data for appropriate statistical analysis, it can be speculated that with this system and the peptide concentrations used, higher osteoblast differentiation is unlikely since the coresponding effects were in general weak and/or not present at all. These findings contrast with the results obtained from rat calvarial osteoblast outgrowths on KRSR surfaces presented in the previous chapter, where it was shown that cell outgrowth was stimulated on KRSR surfaces in comparison to the control surfaces PEG and KSSR. Still, it should be noted, that in the same study for rat calvarial osteoblasts in
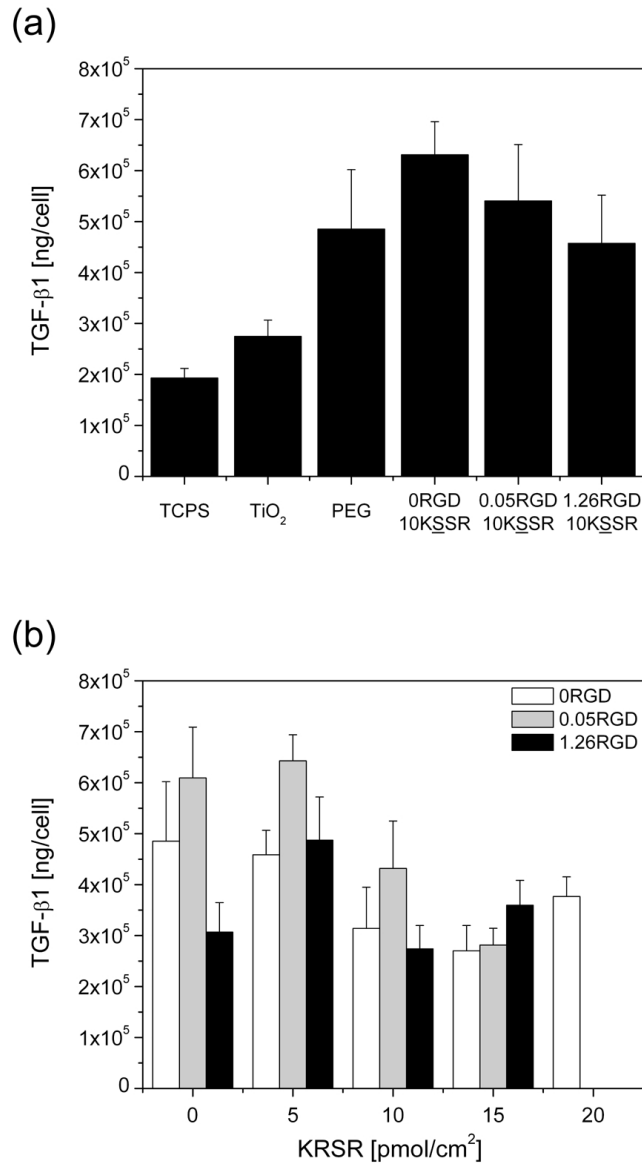
Figure 7.5: Transforming growth factor $\beta 1$ production of MG63 osteoblast-like cells cultured for 8 days on PLL-g-PEG modified CP Ti SLA surfaces. The control surfaces are shown in the upper panel: "Plastic" (Tissue culture polystyrene), "SLA" (bare Ti) and "SLA-PEG" (PLL-g-PEGmodified only) and the three RGD/KSSR-containing surfaces. The lower panel "0.05RGD" and "1.26RGD" shows the results of the experiments with a constant RGD peptide density (0.05 and 1.26 pmol/cm^2, respectively) and varied KRSR peptide densities (5, 10, 15 pmol/cm^2) whereas "0RGD" refers to the assays with only KRSR at different surface densities (5, 10, 15, 20 pmol/cm^2).

(a)

(b)
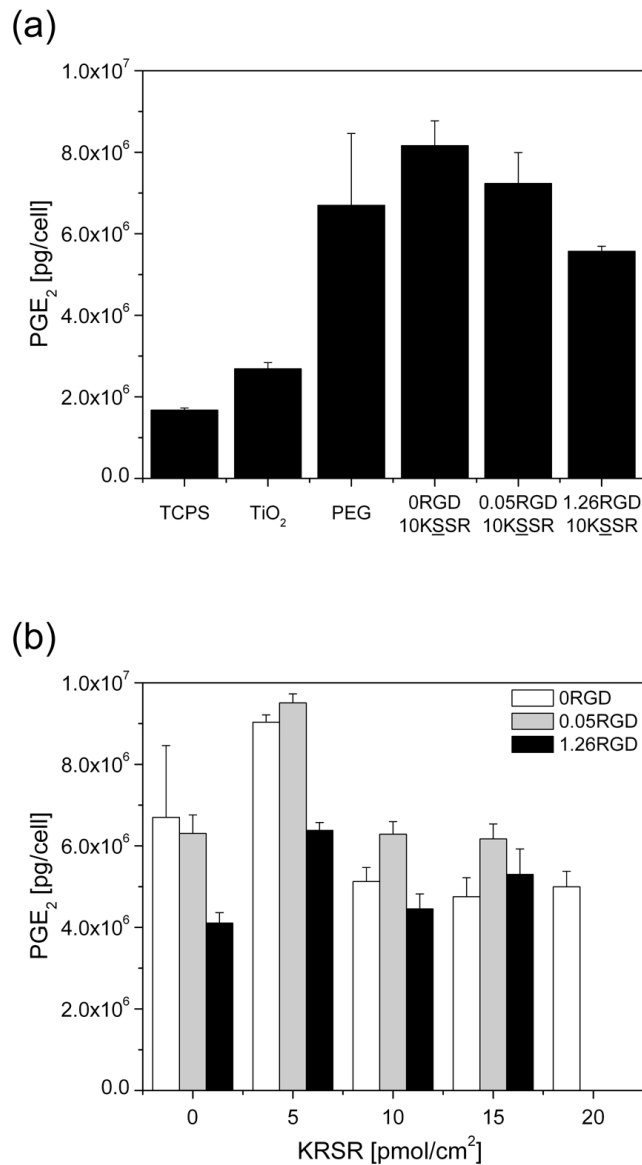
Figure 7.6: Prostaglandin E_2 expression of MG63 osteoblast-like cells cultured for 8 days on PLL-g-PEG modified CP Ti SLA surfaces. The control surfaces are shown in the upper panel: "Plastic" (Tissue culture polystyrene), "SLA" (bare Ti) and "SLA-PEG" (PLL-g-PEGmodified only) and the three RGD/KSSR-containing surfaces. The lower panel "0.05RGD" and "1.26RGD" shows the results of the experiments with a constant RGD peptide density (0.05 and 1.26 pmol/cm^2, respectively) and varied KRSR peptide densities (5, 10, 15 pmol/cm^2) whereas "0RGD" refers to the assays with only KRSR at different surface densities (5, 10, 15, 20 pmol/cm^2).

culture, the KRSR-effect was not that effective either, as assessed by cell attachment after 7 days. These results lead us to the conclusion that although KRSR is likely to have an osteoconductive effect (based on the bone chip outgrowth study, Chapter 6), this effect may not become evident in standard *in vitro* studies where at least a minimum number of single cells have to attach first – in order to be able to proliferate – before they can undergo differentiation. Thus, for a better understanding of the effect of KRSR on bone formation, *in vivo* studies are indispensable.

Bibliography

[1] Dee, K. C., Andersen, T. T. and Bizios, R. Design and function of novel osteoblast-adhesive peptides for chemical modification of biomaterials. *Journal of Biomedical Materials Research*, **40**(3), 371–377, 1998.

[2] Tosatti, S., Schwartz, Z., Campbell, C., Cochran, D. L., VandeVondele, S., Hubbell, J. A., Denzer, A., Simpson, J., Wieland, M., Lohmann, C. H., Textor, M. and Boyan, B. D. RGD-containing Peptide GCRGYGRGDSPG Reduces Enhancement of Osteoblast Differentiation by Poly(L-lysine graft-poly(ethylene glycol) Coated Titanium Surfaces. *accepted in Journal of Biomedical Materials Research*, **68A**(3), 458–472, 2004.

[3] Boyan, B. D., Dean, D. D., Lohmann, C. H., Cochran, D. L., Sylvia, V. L. and Schwartz, Z. The titanium-bone cell interface in vitro: the role of the surface in promoting osteointegration. In Brunette, D. M., Tengvall, P., Textor, M. and Thomsen, P., editors, *Titanium in Medicine*, pages 561–586. Springer-Verlag, Berlin Heidelberg, 2001.

[4] Tosatti, S. *Functionalized Titanium Surfaces for Biomedical Applications: Physico-chemical Characterization and Biological in vitro Evaluation*. Ph.D. Thesis No. 15095, Swiss Federal Institute of Technology Zurich, 2003.

8

Summary and Outlook

8.1 Epoxy Replica Technique

We have demonstrated that we were able to reproduce surface topographical features and surface compositions of a rough titanium metallic surface by the use of TiO_2-coated epoxy replicas. The chosen replica technique showed suitable replication of highly complex 3-D structures in the millimeter, micrometer and (partially) sub-micrometer range without controlled (constant) surface chemistry at the same time. Such replicas provide the possibility to observe exactly the same structures in different experiments, e.g., by applying a mechanical mark to the master. This advantage has the potential to open new windows in the observation of cell behavior on a randomly structured surface. In addition, the possibility to coat epoxy replica samples with practically any metal or metal oxide using physical vapor deposition (PVD) technique provides a perfect tool to investigate the effect of surface chemistry independently from surface topography on morphologically highly complex surfaces. We have also shown that the replica technique allows the straightforward fabrication of substrates with two different types of topography (e.g., smooth and SLA) on the same specimen, which not only is difficult but also extremely expensive to obtain with other surface engineering techniques. These dual-type topography substrates facilitate comparisons within a single culture dish, thus, eliminating dish-to-dish variation as well as saving material, time and costs compared to the usual method of evaluating surfaces in separate dishes.

8.2   Influence of Surface Topography on Cell Behavior

We have shown that cell attachment after 24 hours of 3T3 fibroblasts and rat calvarial osteoblasts can be influenced by surface topography independently from surface chemistry. More 3T3 fibroblasts were found on smooth than on SLA surfaces, whereas for rat calvarial osteoblasts the opposite tendency was observed. Additionally, rat calvarial osteoblast attachment was approximately a factor 1.5 higher on SLA than on smooth topography, thus indicating that the small features produced by acid-etching (and mainly responsible for the 6.5-fold increase of specific surface area of SLA compared to a smooth surface) did not seem to influence the adhesion process. Porcine epithelial cell attachment did not follow any regular pattern; here the presence of cell-cell contacts leading to cell clusters were more relevant for cell attachment. Footprint areas of 3T3 fibroblasts, rat calvarial osteoblasts and porcine epithelial cells were approximately 5-fold reduced on SLA compared to smooth surfaces, indicating a direct influence of the specific surface area of SLA ($6.5 \ cm^2/cm^2$). Rat calvarial osteoblasts were found to be more circular (higher cell shape factor) on SLA compared to smooth surfaces, whereas for 3T3 fibroblasts the opposite response was observed except for the RGD-peptide surface. This antagonistic behavior observed with 3T3 fibroblasts may indicate the lack of an additive effect of topography and surface chemistry on those cells. Porcine epithelial cells were circular on both surface topographies smooth and SLA.

8.3   Influence of Surface (Bio)chemistry on Cell Behavior

8.3.1   Cell-binding RGD-peptide Surfaces

Attachment and footprint areas of 3T3 fibroblasts, rat calvarial osteoblasts and porcine epithelial cells on bio-inactive surfaces PEG and RDG were drastically reduced after 24 hours in culture. Although these two surfaces were resistant to protein adsorption as shown by OWLS and did not contain any bioligands, a small number of cells did always adhere, probably due to small surface defects of the

PEG-brushes. The immobilization of the RGD-peptide sequence at surface densities $\geqslant$0.67 pmol/cm^2 restored 3T3 fibroblast, rat calvarial osteoblast and porcine epithelial cell attachment and footprint areas to levels typically found on (unmodified, i.e., protein-covered) titanium surfaces. A peptide surface density of $\approx$0.027 pmol/cm^2 (corresponding to a calculated ligand-ligand distance of $\approx$84 nm) was found to be the lower limit for producing a surface with significantly increased rat calvarial osteoblast attachment in comparison to bio-inactive surfaces PEG and R<u>DG</u>. In general, we found that rat calvarial osteoblast attachment and footprint areas increased with increased RGD-peptide surface density. However, no synergy (interaction) between RGD-peptide surface density and surface topography was observed for rat calvarial osteoblasts, neither in terms of attachment nor footprint area. 3T3 fibroblasts and rat calvarial osteoblasts on PEG, R<u>DG</u> and low RGD concentrations ($\leqslant$0.13 pmol/cm^2) were more circular than those on titanium or high RGD concentrations ($\geqslant$0.67 pmol/cm^2). Porcine epithelial cells were spherical on all surfaces.

Rat calvarial bone chip attachment and osteoblast outgrowths (size of area and migration pattern) were mediated through surface chemistries. Bone chips cultured on PEG surfaces needed up to 10 days to completely adhere, and osteoblasts from those chips did not migrate isotropically until day 10. On the other hand, bone chip attachment on RGD surfaces was always more efficient and at day 8, all chips were well adhered to these surfaces. Additionally, osteoblasts from bone chips on RGD surfaces started to migrate in an isotropic way as early as day 6.

It was reported in a study by Tosatti *et al.*, that MG63 osteoblast-like cells on nonadhesive SLA surfaces as PEG and low RGD surfaces ($<$0.05 pmol/cm^2) showed a higher degree of differentiation (as assessed by TGF-β1 and PGE$_2$ production) than MG63 cells on high RGD surfaces ($>$0.05 pmol/cm^2) [1]. This leads to the conclusion that modifying biomedical interfaces with RGD above a certain surface density might not be the optimal way for implants in bone-contact applications. However, it might be still useful to present RGD ligands at lower densities, or to coat areas of the implant that are in contact with other tissues as for example epithelium or fibrous tissue.

8.3.2 Heparin-binding KRSR- and FHRRIKA-peptide Surfaces

Rat calvarial osteoblast attachment on KRSR and FHRRIKA did not reach the levels found on RGD or bare titanium after 7 days in culture, although they were found to be higher than the values obtained on the bio-inactive surfaces PEG, KSSR and RFHARIK. An increase of 40% in rat calvarial osteoblast attachment on KRSR compared to KSSR (85% on FHRRIKA vs. RFHARIK), and a 4.6-fold decrease in respect to RGD was measured. Our results also indicated that the difference in rat calvarial osteoblast vs. human gingival fibroblast attachment was more significantly influenced by surface topography (more osteoblasts than fibroblasts on SLA) than by surface chemistry. However, human gingival fibroblast attachment on both KRSR and FHRRIKA was not different from their control surfaces KSSR and RFHARIK. Conversely, rat calvarial osteoblast attachment on FHRRIKA was higher in comparison to RFHARIK.

Osteoblast outgrowths from rat calvariae differed from rat calvarial osteoblast cell cultures by showing attachment to pure heparin-binding peptides KRSR and FHRRIKA coated surfaces. Additionally, osteoblast outgrowth and migration on KRSR and FHRRIKA started in an isotropic way as early as day 6, indicating that cell migration could also be mediated through transmembrane proteoglycan receptors. Furthermore, the earlier attachment of the bone chips on bio-active surfaces in comparison to the controls might indicate that these polymers had a shorter lifetime than the ones that were not functionalized (or carried a scrambled sequence). MG63 osteoblast-like cells on PLL-g-PEG coatings showed a positive effect on ALP activity as well as on osteocalcin, total TGF-β1 and prostaglandin E$_2$ production in comparison to cells on unmodified titanium surfaces. However, the introduction of the KRSR-peptide at different concentrations did not show any further upregulation of these markers.

Outgrowths from bone chips can be considered closer to the *in vivo* condition than standard *in vitro* osteoblast culture assays because the cells were exposed to trypsin or EDTA. Additionally, these outgrown cells had the support of a "proliferation machinery" in form of a bone chip, which is different from osteoblasts in culture (as rat calvarial osteoblasts and MG63 osteoblast-like cells). This might also be an explanation for the observation that outgrown osteoblasts proliferated in a higher rate than osteoblasts from culture on the heparin-binding surfaces KRSR and FHRRIKA.

Therefore, one may speculate that in a *in vivo* situation, bone formation on these new coatings KRSR and FHRRIKA might also be enhanced in comparison to PEG although MG63 osteoblast-like cell differentiation assays did not show any upregulation of osteoblastic markers as a function of KRSR.

8.3.3 Multi-peptide Surfaces of RGD/KRSR and RGD/FHRRIKA

Co-adsorption of RGD- and KRSR- or FHRRIKA-containing PLL-*g*-PEG polymer surfaces showed enhanced rat calvarial osteoblast attachment in comparison with surfaces that had the same concentration of RGD only, although this effect was not synergistic. An elevated outgrowth and migration of osteoblasts from rat calvarial bone chips was also visible on surfaces containing mixtures of RGD with KRSR and FHRRIKA, respectively. On the other hand, differentiation assays over 8 days using MG63 osteoblast-like cells did not show any promising trend or an enhanced or even synergistic effect on RGD/KRSR surfaces in comparison to PEGylated control surfaces (e.g., single RGD or RGD/KSSR). An enhanced effect through the combined immobilization of both a cell-binding and a heparin-binding domain has been shown by Rezania *et al.* where larger areas of mineralized ECM on RGD/FHRRIKA surfaces were found in comparison with single RGD or FHRRIKA surfaces after 21 days in culture [2]. The reason for the absence of any significant effect in this differentiation assay might be that the low MG63 osteoblast-like cell numbers on these surfaces, probably below a critical level, above which effective communication via cytokine crosstalk can be expected to occur. Another explanation is that using MG63 osteoblast-like cells (originating from an osteosarcoma) might not be the optimal model since it is generally assumed that osteoblast-like cell lines represent a certain maturation state along the differentiation pathway when a cell was transformed [3]. Thus, comparisons between tumor cells and normal cells often show multiple differences that could interfere with the phenomenon studied.

A co-adsorption of RGD and KRSR using PLL-*g*-PEG may still, in principle, be a useful strategy to further improve the surface (bio)chemistry of an implant used in bone-contact applications since it provides the potential of addressing, with a single coating, several cell surface receptors present at the surface of osteoblasts. Whether this is the case or not would require corresponding animal studies. Currently, an animal study based on a miniature pig model as published by Germanier *et al.* [4] is

in preparation. In addition to bone chamber implants [5], titanium removal torque implants [6], both having SLA surface topography, will be used and coated with different KRSR and RGD/KRSR mixtures using PLL-*g*-PEG chemistry.

8.4 Stability Aspects of PLL-*g*-PEG

Stability investigations using MG63 osteoblast-like cells have revealed that SLA CP Ti substrates coated with PLL-*g*-PEG have lost their protein-resistant properties when stored in dry state for 3 weeks resulting in higher numbers of attached cells in comparison to freshly PEGylated surfaces. However, this loss of non-fouling character can be avoided by rehydrating the PEG-brushes in HEPES2 buffer solution prior to *in vitro* studies. On the other hand, when PLL-*g*-PEG coated SLA CP Ti substrates were stored in HEPES2 buffer solution in the fridge at 4 °C, rat calvarial osteoblast assays on SLA CP Ti surfaces and OWLS measurements on titanium waveguide surfaces showed well preserved anti-fouling properties, even after 28 days. Still, it should be mentioned that for industrial applications of PLL-*g*-PEG , a shelf life of up to 5 years is required. Currently, some accelerated aging assays according to ASTM (norm F 1980-02) are in process with a large variety of possible combinations of PLL-*g*-PEG (dehydrated powder) and PLL-*g*-PEG solutions (dissolved in HEPES2, 0.9% NaCl/H_2O) as well as coated titanium substrates (dehydrated; stored under HEPES2 or 0.9% NaCl/H_2O). These investigations will reveal the optimal storage conditions of PLL-*g*-PEG and/or PLL-*g*-PEG coated titanium surfaces. Additionally, RGD-functionalized PLL-*g*-PEG will be tested similarly to test for preservation of bioactivity.

The stability of PLL-*g*-PEG polymer surfaces against serum-containing media was investigated by VandeVondele *et al.* [7]. Adlayers adsorbed onto tissue culture polystyrene (TCPS) were incubated with PBS or serum-containing media over 10 days and then seeded with cells. Cell proliferation was assessed with WST-1 and shown to be comparable with data obtained on freshly prepared corresponding PLL-*g*-PEG coatings. However, this finding does not answer a priori the stability of PLL-*g*-PEG coatings *in vivo*. Little is known and predictions are very uncertain. At the same time, the time during which such a (bio)chemical coating has to be stable and functional *in vivo* is also not known, but likely different for different applications. Would it be enough to be stable over a short time period of a couple of

days to "attract" certain cell types (or stop others from attachment) and to avoid inflammatory processes (or bacterial adhesion) or has the coating to be in place and active for weeks or even months to ensure cell differentiation and finally bone formation? A disadvantage associated with the use of adsorbed PLL-*g*-PEG coatings on surfaces might be the limited wear resistance and possible alteration and degradation over longer time periods due to biological activity. However, a damage or removal of such a coating when exposed to wear (as probably happens during implantation) can be reduced to some extent through the topographical features (especially the undercuts from the acid-etching process) of the SLA implant surface. Another possibility could be a covalent immobilization of PLL-*g*-PEG via a plasma polymer interlayer with surface aldehyde groups and reductive amination reaction as shown by Blattler *et al.* with SiO_2 wafer surfaces *et al.* [8].

8.5   Future Perspectives

For designing a dental implant surface to serve patients that have an impaired bone forming or wound healing capacity, like those suffering from osteoporosis or diabetes, a surface modification using only peptides is probably not sufficient. A surface with a therapeutic effect by additional functionalities such as growth factors might be required to rapidly stimulate the formation of the desired tissue at the interface. The role of such growth factors is the regulation of the process of bone growth and remodeling in a systemic or local way. Systemic hormones include, for example, growth hormone (GH)/insuline-like growth factor-1 (IGF-1), thyroid hormone, vitamin D, estrogens, androgens, selective estrogen receptor modifiers (SERMs)m, glucorticoids, and parathyroid hormone (PTH). Local factors are, among others, IGF-1, transforming growth factor beta (TGF-β), bone morphogenic proteins (BMPs), fibroblast growth factors (FGFs), parathyroid hormone related peptide (PTHrP), prostaglandins (PGs), platelet-derived growth factors (PDGF), and vascular endothelial growth factor (VEGF) [9].

8.5.1 Coupling of Growth Factors to Titanium Using PLL-*g*-PEG

We developed a protocol (see cartoon in Figure 8.1) to couple TG-modified growth factors (Transglutaminase substrate site) to PLL-*g*-PEG coated surfaces through the transglutaminase factor XIII. As model-growth factor TG-VEGF was linked to
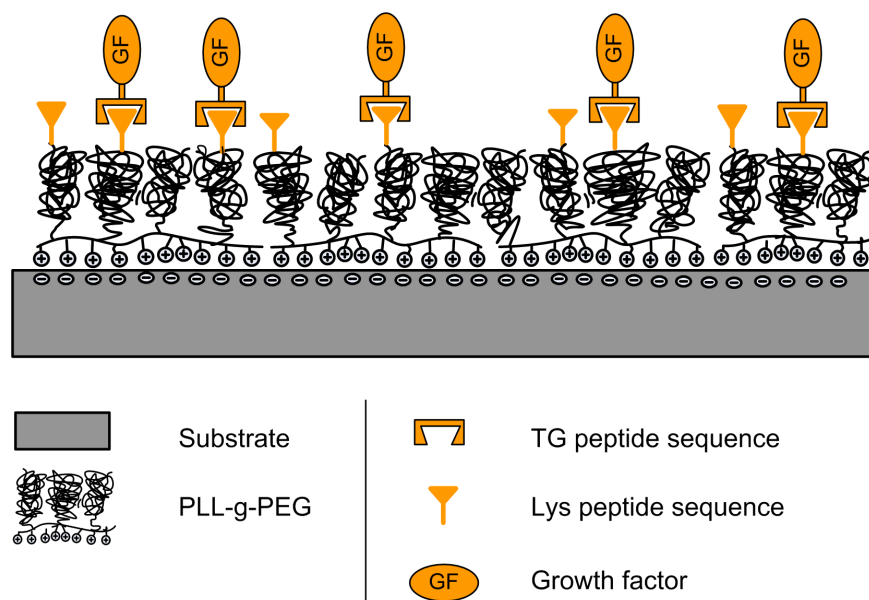

Figure 8.1: Schematic view of coupling transglutaminase (TG)-modified growth factors to PLL-*g*-PEG modified titanium surfaces.

PLL-*g*-PEG/PEG-Lyspep. Coupling between TG-VEGF and Lyspep was shown by SDS page gel (Figure 8.2) and Western Blot (Figure 8.3). Successful coupling of TG-VEGF to titanium surfaces coated with PLL-*g*-PEG/PEG-Lyspep was demonstrated by OWLS (see Figure 8.4). Future experiments include endothelial cell proliferation studies on these VEGF-modified titanium surfaces to investigate the effect of the coupled growth factor on cell behavior. In a later phase, it is expected to couple other growth factors (with TG-sites) to the titanium surface using PLL-*g*-PEG/PEG-Lyspep chemistry.

Lanes (from left to right):

1. Beads
2. PLL-*g*-PEG free
3. PLL-*g*-PEG from beads
4. PLL-*g*-PEG/PEG-Lys
5. PLL-*g*-PEG incubated with TG-VEGF
6. Supernatant of beads with
      PLL-*g*-PEG/PEG-Lys-TG-VEGF
7. Polymer from beads with
      PLL-*g*-PEG/PEG-Lys-TG-VEGF
8. Marker
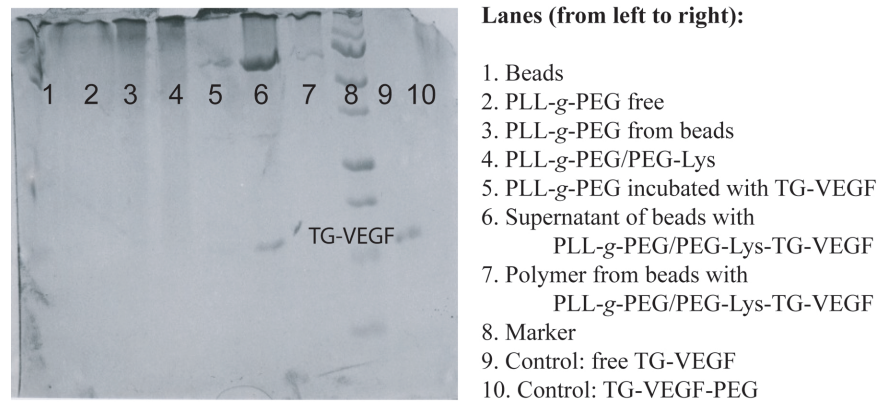9. Control: free TG-VEGF
10. Control: TG-VEGF-PEG

Figure 8.2: SDS page gel stained with coomassie showing TG-VEGF and other proteins. Coomassie stains unspecifically all proteins present in the gel. For specific and more sensitive detection of TG-VEGF, a western blot is usually needed (see Figure 8.3).

Lanes (from left to right):

1. PLL-*g*-PEG/PEG-Lys incubated with VEGF
2. PLL-*g*-PEG/PEG incubated with VEGF
3. PLL-*g*-PEG/PEG-Lys reacted with TG-VEGF;
      2 ug VEGF
4. PLL-*g*-PEG/PEG-Lys reacted with TG-VEGF;
      1 ug VEGF
5. Supernatant of reaction preparation
6. Marker
7. TG-VEGF control; 1 ul
8. TG-VEGF control; 5 ul
9. Control TG-VEGF reacted to PEG, purified
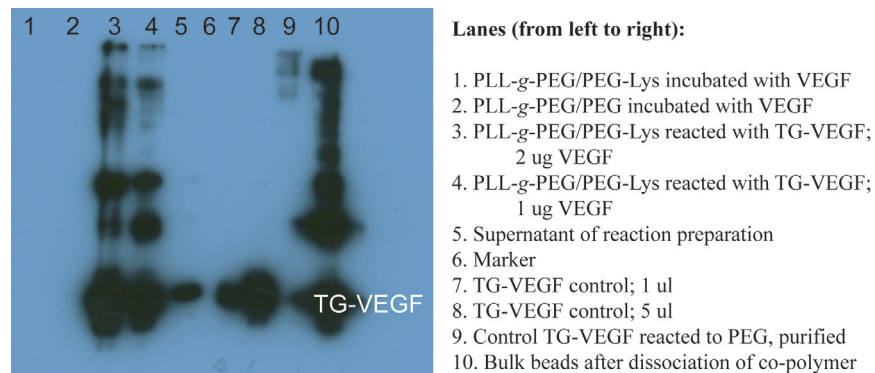10. Bulk beads after dissociation of co-polymer

Figure 8.3: Western Blot specific for TG-VEGF. Western blots are treated with antibodies against the desired protein, in this case VEGF, to detect it. By knowing the molecular weight of free TG-VEGF, a coupling to a higher molecular weight molecule through can be shown, as only bands containing VEGF are visible.
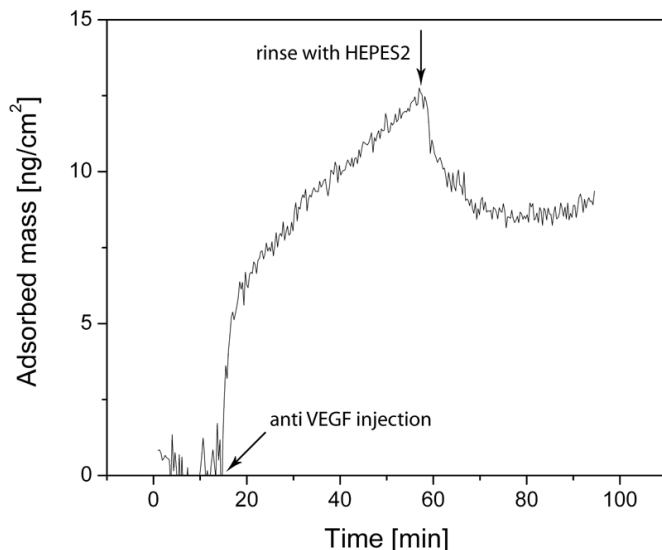
Figure 8.4: OWLS measurement of TG-VEGF coupled to PLL-*g*-PEG/PEG-Lyspep. TiO$_2$/waveguide was coated *ex situ* with PLL-*g*-PEG/PEG-Lyspep and coupled with TG-VEGF at 37°C. Subsequently, the modified waveguide was introduced into the OWLS instrument and after, reaching a stable baseline, antiVEGF antibody was injected.

8.5.2 Coupling of Drug Delivery System to Titanium Using PLL-*g*-PEG

A more sophisticated approach of immobilizing growth factors onto a titanium surfaces is the use of a drug delivery system (Figure 8.5). Preliminary studies have shown a successful coupling of model drug delivery carriers (polystyrene microspheres) to PLL-*g*-PEG. The protocol for coupling these carriers to PLL-*g*-PEG/PEG-Lyspep was similar to the one of TG-VEGF except that the coupling partner for PLL-*g*-PEG/PEG-Lyspep was PLL-*g*-PEG/PEG-TG. To prove the coupling of the microspheres to the surface, molecular assembly patterning by lift-off (MAPL) technique was used [10]. (Figure 8.6). Next steps include development of "real" drug delivery carriers and loading thereof as well as studies of drug release kinetics. Possible candidates for producing such delivery devices are poly(lactic-*co*-glycolic acid) (PLGA).
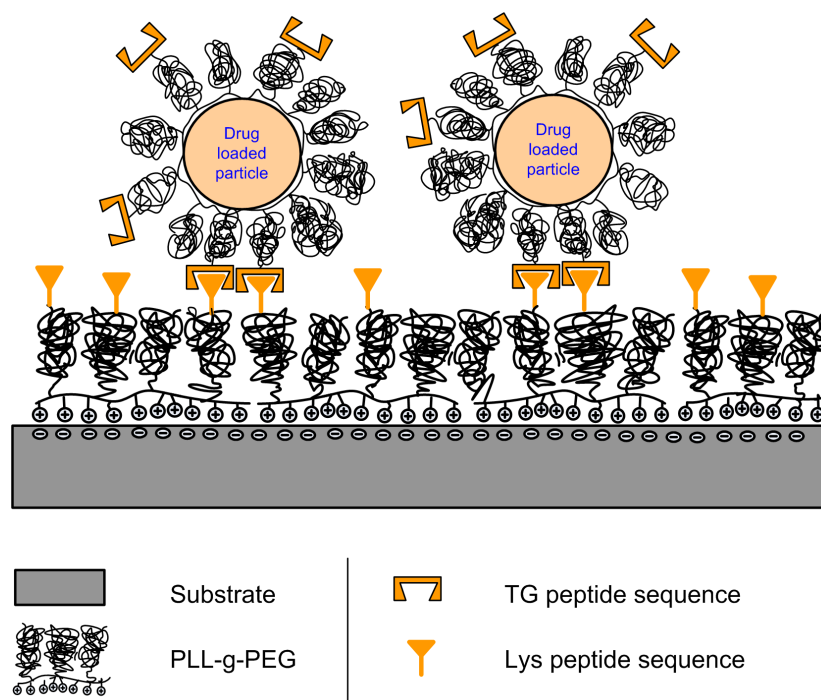
Figure 8.5: Cartoon of coupling drug loaded particles (e.g., poly(lactic-*co*-glycolic acid) (PLGA) beads) to the titanium surface using PLL-*g*-PEG chemistry. Titanium is coated with PLL-*g*-PEG/PEG-Lyspep that covalently binds to PLL-*g*-PEG/PEG-TG modified microspheres.

8.6 Final Remarks

This thesis focused on the development and screening of different (bio)chemical modification strategies of titanium dental implant surfaces using PLL-*g*-PEG chemistry. The important advantage of using PLL-*g*-PEG is its ability to render implant surfaces resistant to non-specific protein adsorption since it has been hypothesized that non-specific, uncontrolled protein adsorption to biomaterials is one of the factors inducing foreign body response, inflammatory processes and delayed healing in tissue [11]. Another advantage is its potential to drastically decreased bacteria adhesion to PEGylated surfaces even in the presence of RGD as shown with 4 different types of bacteria that are associated with (dental) implant infections: *S. aureus, S. epidermidis, Strep. Mutans and P. aeruginosa* [12, 13] (see Chapter 2). This is an interesting finding since implant-related infections are extremely difficult to treat and some of these bacteria are already resistant against standard antibiotics. Fur-
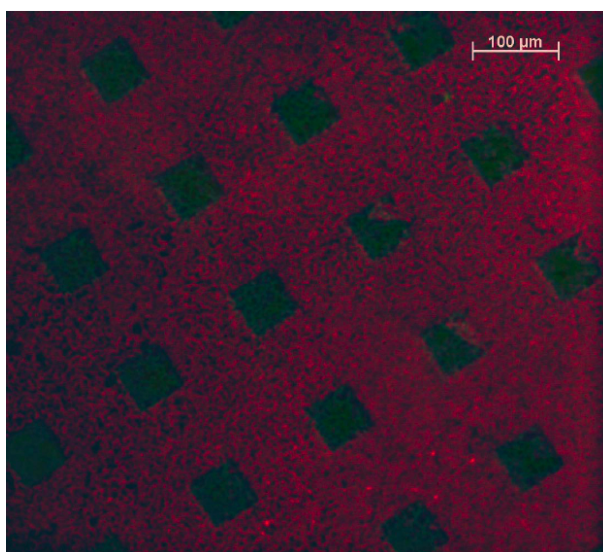
Figure 8.6: On a MAPL-patterned surface [10] PLL-*g*-PEG/PEG-FITC (fluorescein isothyocianate-labeled (green) PLL-*g*-PEG polymer) was deposited. After photoresist removal, PLL-*g*-PEG/PEG-Lyspep was deposited in the "empty" area (developed region) leading to a surface with a color contrast green vs. black. Model drug delivery carriers were subsequently coated with a mixture of PLL-*g*-PEG/PEG-TG and PLL-*g*-PEG/PEG-CY3 (Carbocyanin-3-labeled (red) PLL-*g*-PEG polymer). Microspheres were washed and resuspended in a reaction mixture containing the transglutaminase and then transferred to the MAPL surface. Since coupling is specific, red fluorescent areas were visible by fluorescence microscopy in the PLL-*g*-PEG/PEG-Lyspep coated area surrounding green fluorescence in the non-binding coated spots.

thermore, the possibility to link biomolecules and/or drug delivery carriers to the titanium surface using PLL-*g*-PEG chemistry by a simple adsorption process makes PLL-*g*-PEG a highly versatile immobilization system. With such a self-assembly system, there is no need for complex multistep surface functionalization procedures; furthermore, it is relatively straightforward to control quantitatively the density of the biological function as well as to assemble multiple types of ligands in defined concentration ratios.

In the future, one could imagine to produce multifunctional coatings designed specifically for a given patient by assembly of polymers that are functionalized with different bioligands such peptides, growth factors and/or drug delivery carriers. Whether PLL-*g*-PEG in the form of adsorbed monolayers, as used in this thesis, will be

the carrier material of the future for modifying implant surfaces or not, is speculative, since the used grafting-to polymer system is one out of dozens of other systems (e.g., grafting-from [14], polyelectrolyte multilayers [15], photochemically immobilized polymers [16], hydrogels [17] etc.). However, the results of this thesis demonstrate that in principle it should be possible to provide cells on the titanium surface with suitable attachment factors (e.g., peptides), growth factors, and other components using PLL-g-PEG chemistry to enhance osseointegration.

Bibliography

[1] Tosatti, S., Schwartz, Z., Campbell, C., Cochran, D. L., VandeVondele, S., Hubbell, J. A., Denzer, A., Simpson, J., Wieland, M., Lohmann, C. H., Textor, M. and Boyan, B. D. RGD-containing Peptide GCRGYGRGDSPG Reduces Enhancement of Osteoblast Differentiation by Poly(L-lysine graft-poly(ethylene glycol) Coated Titanium Surfaces. *accepted in Journal of Biomedical Materials Research*, **68A**(3), 458–472, 2004.

[2] Rezania, A. and Healy, K. E. Biomimetic peptide surfaces that regulate adhesion, spreading, cytoskeletal organization, and mineralization of the matrix deposited by osteoblast-like cells. *Biotechnology Progress*, **15**(1), 19–32, 1999.

[3] Brunette, D. M., Tengvall, P., Textor, M. and Thomsen, P. *Titanium in Medicine*. Springer-Verlag, Berlin Heidelberg, 2001.

[4] Germanier, Y., Tosatti, S., Broggini, N., Textor, M. and Buser, D. Enhanced bone apposition around biofunctionalized sandblasted and acid-etched titanium implant surfaces - A histomorphometric study in miniature pigs. *Clinical Oral Implants Research*, **17**(3), 251–257, 2006.

[5] Buser, D., Broggini, N., Wieland, M., Schenk, R. K., Denzer, A. J., Cochran, D. L., Hoffmann, B., Lussi, A. and Steinemann, S. G. Enhanced bone apposition to a chemically modified SLA titanium surface. *Journal of Dental Research*, **83**(7), 529–533, 2004.

[6] Ferguson, S. J., Broggini, N., Wieland, M., de Wild, M., Rupp, F., Geis-Gerstorfer, J., Cochran, D. L. and Buser, D. Biomechanical evaluation of the interfacial strength of a chemically modified sandblasted and acid-etched titanium surface. *Journal of Biomedical Materials Research Part A*, **78A**(2), 291–297, 2006.

[7] VandeVondele, S., Voros, J. and Hubbell, J. A. RGD-Grafted poly-l-lysine-graft-(polyethylene glycol) copolymers block non-specific protein adsorption while promoting cell adhesion. *Biotechnology and Bioengineering*, **82**(7), 784–790, 2003.

[8] Blattler, T. M., Pasche, S., Textor, M. and Griesser, H. J. High salt stability and protein resistance of poly(L-lysine)-g-poly(ethylene glycol) copolymers co-

valently immobilized via aldehyde plasma polymer interlayers on inorganic and polymeric substrates. *Langmuir*, **22**(13), 5760–5769, 2006.

[9] Bronner, F. and Farach-Carson, M. *Bone Formation. Topics in Bone Biology*, volume 1. Springer, 2004.

[10] Falconnet, D., Csucs, G., Grandin, H. M. and Textor, M. Surface engineering approaches to micropattern surfaces for cell-based assays. *Biomaterials*, **27**(16), 3044–3063, 2006.

[11] Ratner, B. D. A Perspective on Titanium Biocompatibility. In Brunette, D. M., Tengvall, P., Textor, M. and Thomsen, P., editors, *Titanium in Medicine*, pages 1–12. Springer-Verlag, Berlin Heidelberg, 2001.

[12] Harris, L. G., Tosatti, S., Wieland, M., Textor, M. and Richards, R. G. Staphylococcus aureus adhesion to titanium oxide surfaces coated with non-functionalized and peptide-functionalized poly(L-lysine)-grafted-poly(ethylene glycol) copolymers. *Biomaterials*, **25**(18), 4135–4148, 2004.

[13] Maddikeri, R., Tosatti, S., Schuler, M., Chessari, S., Textor, M., Richards, R. and Harrs, L. Effect of modifying titanium surfaces with PLL-g-PEG and RGD-functionalised PLL-g-PEG on bacterial adhesion. *Journal of Biomedical Materials Research, submitted*, , 2007.

[14] Siow, K. S., Britcher, L., Kumar, S. and Griesser, H. J. Plasma methods for the generation of chemically reactive surfaces for biomolecule immobilization and cell colonization - A review. *Plasma Processes and Polymers*, **3**(6-7), 392–418, 2006.

[15] Haynie, D. T. Physics of polypeptide multilayer films. *Journal of Biomedical Materials Research Part B-Applied Biomaterials*, **78B**(2), 243–252, 2006.

[16] Defife, K. M., Hagen, K. M., Clapper, D. L. and Anderson, J. M. Photochemically immobilized polymer coatings: effects on protein adsorption, cell adhesion, and leukocyte activation. *Journal of Biomaterials Science-Polymer Edition*, **10**(10), 1063–1074, 1999.

[17] Hoffman, A. S. Hydrogels for biomedical applications. *Advanced Drug Delivery Reviews*, **54**(1), 3–12, 2002.

Curriculum Vitae

Name:	Martin Schuler
Date of Birth:	18th of May, 1973
Citizenship:	Davos GR, Switzerland
Marital Status:	married, one son
Present Address:	Obere Weidstrasse 9
	CH-6343 Rotkreuz
E-mail:	martin.schuler@alumni.ethz.ch

Education

2003 - 2006 **Swiss Federal Institute of Technology, ETH Zürich**
Department of Materials, Laboratory for Surface Science and Technology, BioInterfaceGroup (Prof. Dr. Marcus Textor)
Doctoral student

1997 - 2003 **Swiss Federal Institute of Technology, ETH Zürich**
Department of Materials
Diploma in Material Science
Diploma Thesis entitled "Morphology and Motility of Osteoblast Cells on Peptide-Modified Titanium Surfaces" performed at ETH Zürich (Prof. Dr. Marcus Textor) and University of British Columbia, Vancouver, BC, Canada (Prof. Dr. Donald M. Brunette)

1993 - 1997 **Swiss Ski**
Professional cross country skier, member of the Swiss National Ski Team

1993 **Schweizerische Alpine Mittelschule, Davos, Switzerland**
"Gymnasium Typus C", focusing on mathematics and sciences

Working Experience

2006 - 2007	**Swiss Federal Institute of Technology, ETH Zürich**
	Department of Materials, Laboratory for Surface Science and Technology, BioInterfaceGroup (Prof. Dr. Marcus Textor)
	Postdoctoral Fellow (6 months)
2006	**Georgia Institute of Technology, Atlanta, GA, United States of America**
	Institute of Bioengineering and Bioscience (Prof. Dr. Barbara B. Boyan, Prof. Dr. Zvi Schwartz)
	Visiting Scholar (1 month)
2004	**University of British Columbia, Vancouver, BC, Canada**
	Department of Oral Biological and Medical Science (Prof. Dr. Donald M. Brunette)
	Visiting Scholar (6 months)
2001	**Philips Research Laboratories, Eindhoven, Netherlands**
	Polymers and Chemistry Group (Prof. Dr. Hans Hofstraat, Dr. Giovanni Nisato)
	Traineeship (5 months)
	Project: "Development of Transparent Conductor for Display Applications"
2001	**AO Research Institute, Davos, Switzerland**
	Joint Replacement Group (Dr. Markus Wimmer, Christoph Sprecher)
	Traineeship (5 months)
	Project: "Isolation and Characterization of CoCrMo Particles from Bovine Serum Obtained with a Pin-on-ball Experiment"

Publications

Journals

Comparison of the Response of Cultured Osteoblasts and Osteoblasts Outgrown from Rat Calvarial Bone Chips, to Non-fouling KRSR- and FHRRIKA-peptide Modified Rough Titanium Surfaces
Schuler M., Hamilton, D. W., Kunzler, T. P., Sprecher, C. M., de Wild M., Brunette D. M., Textor M., Tosatti S. G. P.
Biomaterials, submitted, 2007.

Fabrication of TiO$_2$-coated Epoxy Replicas with Identical Dual-type Surface Topographies Used in Cell Culture Assays
Schuler M., Kunzler, T. P., de Wild M., Sprecher, C. M., Textor M., Brunette D. M., Tosatti S. G. P.
Journal of Biomedical Materials Research Part A, submitted, 2007.

Biomedical Interfaces: Titanium Surface Technology for Implants and Cell Carriers
Schuler M., Trentin D., Textor M., Tosatti S. G. P.
nanomedicine, **1**(4), 449-463, 2006.

Biomimetic Modification of Titanium Dental Implant Model Surfaces Using the RGDSP-peptide Sequence: A Cell Morphology Study
Schuler M., Owen G. Rh., Hamilton D. W., de Wild M., Brunette D. M., Textor M., Tosatti S. G. P.
Biomaterials, **27**(21), 4003-4015, 2006.

Reduced Medical Infection Related Bacterial Strains Adhesion on Bio-active RGD Modified Titanium Surfaces: A First Step Towards Cell Selective Surfaces
Maddikeri R.R., Tosatti S. G. P., Chessari S., **Schuler M**., Textor M., Richards R. G., Harris L. G.
Journal of Biomedical Materials Research Part A, submitted, 2007.

Systematic Study of Cell Response to Roughness by means of Surface Morphology Gradients
Kunzler T. P., Drobek T., **Schuler M**., Spencer N. D.
Biomaterials, **28**(13), 2157-2182, 2007.

Fabrication of material-independent morphology gradients for high-throughput applications
Kunzler T. P., Sprecher, C. M., **Schuler M**., Drobek T., Spencer N. D.
Applied Surface Science, **253**(4), 2148-2153, 2006.

Influence of Substratum Topography and RGD-Peptide Density on Activation and Nuclear Translocation of Runx2, STAT3 and ERK 1/2 in Rat Calvarial Osteoblasts
Hamilton D. W., **Schuler M**.,de Wild M., Tosatti S. G. P., Textor M., Brunette D. M.
In preparation, 2007.

Response of Adult Human Articular Chondrocytes to a Non-fouling RGD-Peptide Modified Surface
Vonwil D., **Schuler M**., Barbero A., Strobel S., Textor M., Aebi U., Marti I.
In preparation, 2007.

Electronically Addressable Polyelectrolyte Thin Films as a Novel Platform for Cell Sheet Engineering
Guillaume-Gentil O., Akiyama Y., **Schuler M**., Tang C., Textor M., Yamato M., Okano T., Voros J.
In preparation, 2007.

Patents

Cell Selective Implant Surface with Controlled Release of Bioactive Agents
Schuler M., Trentin D., Tosatti S. G. P., de Wild M.
Patent No. 07405002.2-1219, date of filing January 5th, 2007.

Theses

Multifunctional Titanium Dental Implant Surface Based on Biochemically Modified
Molecular Assembly Systems
Schuler M.
ETH Zürich, PhD Thesis No. 16914, 2006.

Morphology and Motility of Osteoblast Cells on Peptide-modified Titanium Surfaces
Schuler M.
ETH Zürich, Diploma Thesis, 2003.

Stability of Self-assembled Alkane Phosphate-/Phosphonate Monolayers on Smooth
Titanium Oxide **Schuler M**.
ETH Zürich, Semester Thesis, 2002.

Plastizität von SiRu-Einkristallen
Schuler M.
ETH Zürich, Semester Thesis, 2002.

Presentations

Multifunctional Titanium Dental Implant Surface Based on Biochemically Modified Molecular Assembly Systems (*oral presentation*)
Schuler M., Tosatti S. G. P., Textor M.
Kolloquium D-MATL, June 21st, 2006, ETH Zürich, Switzerland.

A Novel Method for Testing Osteoblast Proliferation from Rat Calvarial Explants on Non-fouling Peptide-modified Titanium Surfaces (*poster*)
Schuler M., Tosatti S. G. P., Hamilton D. W., Sprecher C. M., de Wild M., Brunette D. M., Textor M.
Cells @ Interfaces, Toscana Workshop, October 22nd-28th, 2005, Florence, Italy.

Innovative Method for the Production of Similar TiO_2-coated Epoxy Replicas Used in Cell Culture Assays (*poster*)
Schuler M., Kunzler T. P., Sprecher C. M., de Wild M., Tosatti S. G. P., Textor M.
Biosurf VI, Tissue-Surface-Interaction, September 21st-23rd, 2005, Lausanne, Switzerland.

A Novel Experimental Setup for Testing Primary Osteoblasts on Non-fouling Peptide-modified Titanium Surfaces (*oral presentation; SSB student travel award*)
Schuler M., Tosatti S. G. P., Hamilton D. W., Sprecher C. M., de Wild M., Brunette D. M., Textor M.
19th European Society for Biomaterials Conference, September 11th-15th, Sorrento, Italy.

TiO_2-coated Epoxy Replicas with Identical Surface Topography for Cell Culture Experiments (*poster*)
Schuler M., Kunzler T. P., Sprecher C. M., de Wild M., Tosatti S. G. P., Textor M.
Excellence in Spine, ECM VI/SRN I Spinal Motion Segment: From Basic Science to Clinical Application, July 4th-7th, 2005, Davos, Switzerland.

Primary Osteoblasts Outgrown from Rat Calvarial Explants Form a "Fried-egg"-like Image on Non-fouling Peptide-modified Titanium Surfaces (*poster*)
Schuler M., Tosatti S. G. P., Hamilton D. W., Sprecher C. M., de Wild M., Brunette D. M., Textor M.
11th Swiss Society for Biomaterials Conference, June 1st, 2005, Mägenwil, Switzerland.

Peptide-functionalized Protein-resistant Adlayers on Titanium Surfaces: An Approach for Producing Cell-selective Biomaterial Surfaces (*oral presentation*)
Schuler M., Owen G. Rh., Tosatti S. G. P., Brunette D. M., Boyan B. D., Textor M.
10th Swiss Society for Biomaterials Conference, July 1st, 2004, Davos, Switzerland.

Peptide-functionalized Protein-resistant Adlayers on Titanium Surfaces: An Approach for Producing Cell-selective Biomaterial Surfaces (*oral presentation*)
Schuler M., Tosatti S. G. P., Owen G. Rh., Schwartz Z., Wieland M., Brunette D. M., Boyan B. D., Textor M.
7th World Biomaterial Congress, May 17th-21st, 2004, Sydney, Australia.

Expansion of Adult Human Articular Chondrocytes on a Protein Resistant RGD-peptide Modified Surface (*poster*)
Vonwil D., **Schuler M.**, Barber A., Strobel S., Textor M., Aebi U., Martin, I.
Gemeinsame Jahrestagung der Deutschen, Österreichischen und Schweizerischen Gesellschaft für Biomedizinische Technik, September 6th-9th 2006, ETH Zürich, Switzerland.

Response of Adult Human Articular Chondrocytes to a Non-fouling RGD-peptide Modified Surface (*oral presentation*).
Vonwil D., **Schuler M.**, Barber A., Strobel S., Textor M., Aebi U., Martin, I.
12th Swiss Society for Biomaterials Conference, May 10th, 2006, Grenchen, Switzerland.

Investigations on a Superhydrophobic Surface Structure (*oral presentation*).
Spori D., Drobek T., **Schuler M**., Morgenthaler S., Spencer N. D.
22nd Annual Meeting Swiss User Group Surfaces and Interfaces (SAOG), January 20th, 2006, Fribourg, Switzerland.

A Comparison of Time *in situ* and Metal Content in the Periprosthetic Tissue: A Study on 42 Retrieved Metal/Metal Articulation (*oral presentation*).
Sprecher C.M., **Schuler M**., Tager G., Wimmer M.A.
5th Combined Meeting of the Orthopaedic Research Societies of Canada, USA, Japan and Europe, Oct 10th-13th, 2004, Banff, Alberta, Canada.

Osteoblast Response to Peptide Functionalized Poly(L-lysine)-*graft*-poly(ethylene glycol) Coated Titanium Surfaces (*oral presentation*)
Tosatti S. G. P., Schwartz Z., Campbell C., **Schuler M**., Wieland M., Brunette D. M., Textor M., Boyan B. D.
European Congress and Exhibition on Advanced Materials and Processes, September 1st-9th, 2003, Lausanne, Switzerland.

Plastizität von SiRu-Einkristallen (*oral presentation*)
Wollgarten M., **Schuler M**., Krogh F., Fischer E., Kostorz G.
Spring Meeting of the German Physical Society, March 11th-15th, 2002, Regensburg, Germany.